BINDING AFFINITY OF EPITHELIAL SODIUM CHANNEL SUBUNITS AND PEPTIDES MEASURED THROUGH SURFACE PLASMON RESONANCE

by

Andres Gonzalez, B.S.

A thesis submitted to the Graduate Council of
Texas State University in partial fulfillment
of the requirements for the degree of
Master of Science
with a Major in Biochemistry
August 2014

Committee Members:

Rachell E. Booth

Wendi David

Steven T. Whitten

FAIR USE AND AUTHOR'S PERMISSION STATEMENT

Fair Use

Duplication Permission

DEDICATION

I would like to dedicate this thesis to my parents and my sister.

I love you!

ACKNOWLEDGEMENTS

I would like to thank Dr. Booth for her guidance throughout this project, and I would especially like to thank the patience she (and my other committee members) had to endure all the questions my curiosity threw at her. Thank you to my committee members Dr. David—for her counsel on surface plasmon resonance—and Dr. Whitten—for his direction on the concepts behind the formulaic evaluations of SPR's kinetic analysis. Even though we exchanged few words, I would also like to thank Dr. Kevin Lewis for providing me with the lab materials I required in order for me to complete this project. Of course, I would like to thank my family for their support throughout this endeavor. Lastly, I would like to thank Allison Noel, who was with me since the beginning of my project and withstood the hours I was tucked away in the laboratory running my experiments.

TABLE OF CONTENTS

Page

LIST OF TABLES

Table **Page**

LIST OF FIGURES

Figure **Page**

LIST OF ABBREVIATIONS

Abbreviation	Description
APS	Ammonium Persulfate
ASIC	Acid-Sensing Ion Channel
BCIP	5-bromo-4-chloro-3'-indolyphosphate
BME	β-mercaptoethanol
BNaC or BNC	Brain Sodium Channel
cASIC	Chicken ASIC
ENaC	Epithelial Sodium Channel
EDC	1-Ethyl-3-(3-dimethylaminopropyl)-carbodiimide
DEG	Degenerin
DTT	Dithiothreitol
Fc	Flow Cell
GST	Glutathione S-Transferase
hENaC	Human ENaC
IPTG	Isopropyl β-D-1-thiogalactopyranoside
MDEG	Mammalian Degenerins
MR	Mineralocorticoid Receptor
NBT	nitro-blue tetrazolium
Nedd4-2	Neural Precursor Cell Expressed Developmentally Down-Regulated Protein 4
NHS	N-hydroxysuccinimide
NMWL	Nominal Molecular Weight Limit
PKA	Protein Kinase A
PHA-1	Pseudohypoaldosteronism Type I
SGK	Serum and Glucocorticoid-Inducible Kinase
SPR	Surface Plasmon Resonance
TAE	Tris base, Acetic Acid, and EDTA
TBS	Tris Buffered Saline
TEMED	Tetramethylethylenediamine
TM	Transmembrane
V_2R	Basolateral Membrane Vasopressin Receptor

CHAPTER I

INTRODUCTION AND LITERATURE REVIEW

In the human body, salt levels play a crucial role in the regulation of blood pressure. Indeed, the living organism's body must be able to maintain the concentration of solutes within a narrow range of osmolality if the body is to preserve healthy blood pressure levels [12, 28, 32 – 35, 38, 39, 46]. This delicate balance is mainly achieved through appropriate fluid and salt excretion and intake. More specifically, the majority of this resorption and elimination of salts occurs within the kidney, where epithelial cells are able to allow the passage of ions via ion channels embedded within each cellular membrane. Fundamentally, ion channels are pore-forming proteins that allow the permeation of ions through lipid bilayers. Without these ion channels, cells would otherwise be unable to transport ions through the nonpolar region of the cellular plasma membrane. Over time, it has been concluded that cells possess a myriad of channel proteins, each of which is synthesized to permit a specific type of ion or molecule to traverse the plasma membrane. The epithelial sodium channel, ENaC, is currently being studied as a major participant in the regulation of ions within the majority of epithelial cells lining organs such as the kidney and salivary ducts. Primarily, ENaC is known as the rate-limiting step for the reabsorption and balance of Na^+ levels within the distal nephron [6 – 9, 15, 19, 26, 35, 36, 40, 43, 46].

ENaC, a multi-subunit, voltage-independent, amiloride-sensitive member of the ENaC/Degenerin (DEG) superfamily, allows the selective passage of the positively charged Na^+ ion [8, 26, 28, 33, 36 – 38, 41, 45]. Previous studies showed that it also

allows passage of Li^+ and K^+, but it does so to a lesser extent [15, 35]. First identified in the early 1990s, the ENaC/DEG family represented a new class of ion channels. These channels obtained their DEG classification when it was discovered that a mutation in the deg-1 gene (through a screening of the mechanosensory pathway of *Caenorhabditis elegans*) caused degeneration of touch sensory neurons [37]. At that time, cloning and isolation strategies allowed researchers to sequence the cDNA of one of ENaC's subunits (later labeled as the "a" subunit), and it was discovered that deg-1 and its other related genes had high identity with ENaC's "SCNN1a" ("Sodium Channel Nonneuronal") subunit gene [23]. In conjunction with other similar proteins, this group of related proteins came to also be known as "Mammalian Degenerins" (MDEG) and "Brain Sodium Channels" (BNaC or BNC), and when researchers became aware of the notion that extracellular protons stimulated these channels, they became what are now known as the "Acid-Sensing Ion Channels," or ASICs. There have been no reports of homologous prokaryotic proteins [38]. Ultimately, these proteins acquired their categorization through sequence, and thus structural and functional, similarities, and this homology became one of the fundamental aspects of how this project came to be (below) [8].

ENaC is expressed in various parts of epithelial tissue throughout the body [1, 9, 12, 19, 22, 27, 33, 36, 46]. Even though its primarily studied location resides within the kidney, it is also expressed in the colon where sodium reabsorption is governed by glucocorticoids [8, 38]. It remains unclear, however, how colonic ENaC participates in whole-body sodium homeostasis. ENaC has also been implicated as an important participant for salt-tasting within the taste buds [32]. In the lung, ENaC supports the maintenance of solutes at the air-liquid boundary. Additionally, it has been shown that

lung-localized ENaC is responsible for clearing the alveolar space from fluids [12]. In the sweat glands, ENaC helps balance what is excreted through sweat [27]. Similar to colonic ENaC, responsibility for whole-body sodium balance has not been shown to fall upon lung and sweat-glandular ENaCs.

Renal ENaC can be found at the Medulla-Cortex boundary where most of the nephrons, the kidney's basic functional unit, reside (**Figure 1**). Blood fluid solutes are exchanged in the region labeled "Renal Corpuscle" within the cortex-region of the nephron. These solutes then traverse the proximal convoluted tubule, travel through the Loop of Henle, and then arrive at the distal convoluted tubule, where ENaC resides and carries out its solute-balancing duties. **Figure 2** shows both the apical and basolateral membrane of the epithelial cells lining the lumen of distal convoluted tubule. Although it is not shown in the figure, ENaC is situated within the apical membrane where it makes contact with the fluid flowing through the lumen prior to its entering the collecting duct, which also contains ENaC. As sodium is brought into the cell, an electro-chemical gradient is established that causes sodium to be excreted on the basolateral side via the Na^+ K^+ ATPase pump [37 – 39, 45]. Additionally, this movement of Na^+ also establishes an osmotic gradient that causes water to proceed in the same direction within water permeable channels. Potassium leaves the cell on the apical side using channels that are specific to potassium, relieving the gradient established by the pump [35]. This basic mechanism is multiplied throughout the one million nephrons within each kidney, and when one factors in all the nephrons residing within both kidneys, it is easy to see how this is an important part of regulating salt levels within the body.

Members of the ENaC/DEG ion channel superfamily share common structural

A)

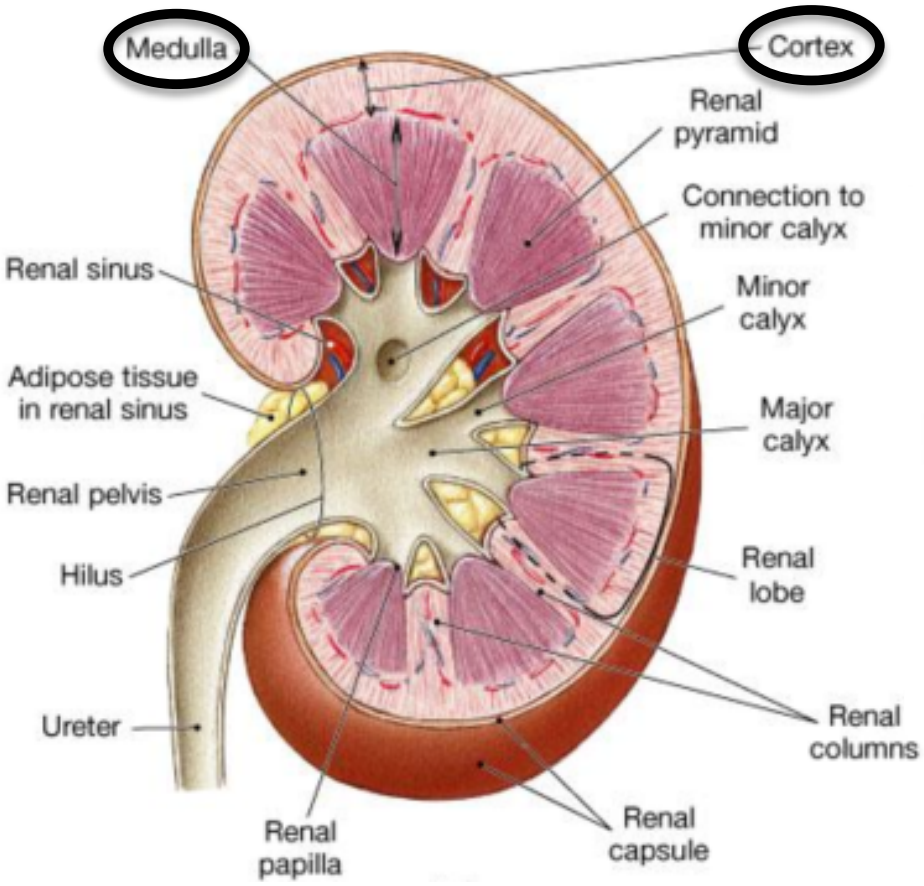

Reprinted from http://www4.ncsu.edu/~kmpigfor/zoo/KidneyAnatomy.html

Figure 1. The Kidney And The Nephron. A) Shown above is a figure depicting the location of a nephron within the kidney, and most of the approximately 1 million nephrons in a human kidney are located in the outer region of the organ known as the cortex. B) Shown on the following page is a typical nephron, the main functional unit of the kidney. Blood fluid solutes are exchanged in the region labeled "Renal Corpuscle" within the cortex. These solutes then traverse the Proximal Convoluted Tubule, travel through the Loop of Henle, and then arrive at the Distal Convoluted tubule. It is here where ENaC resides and carries out its solute-balancing duties.

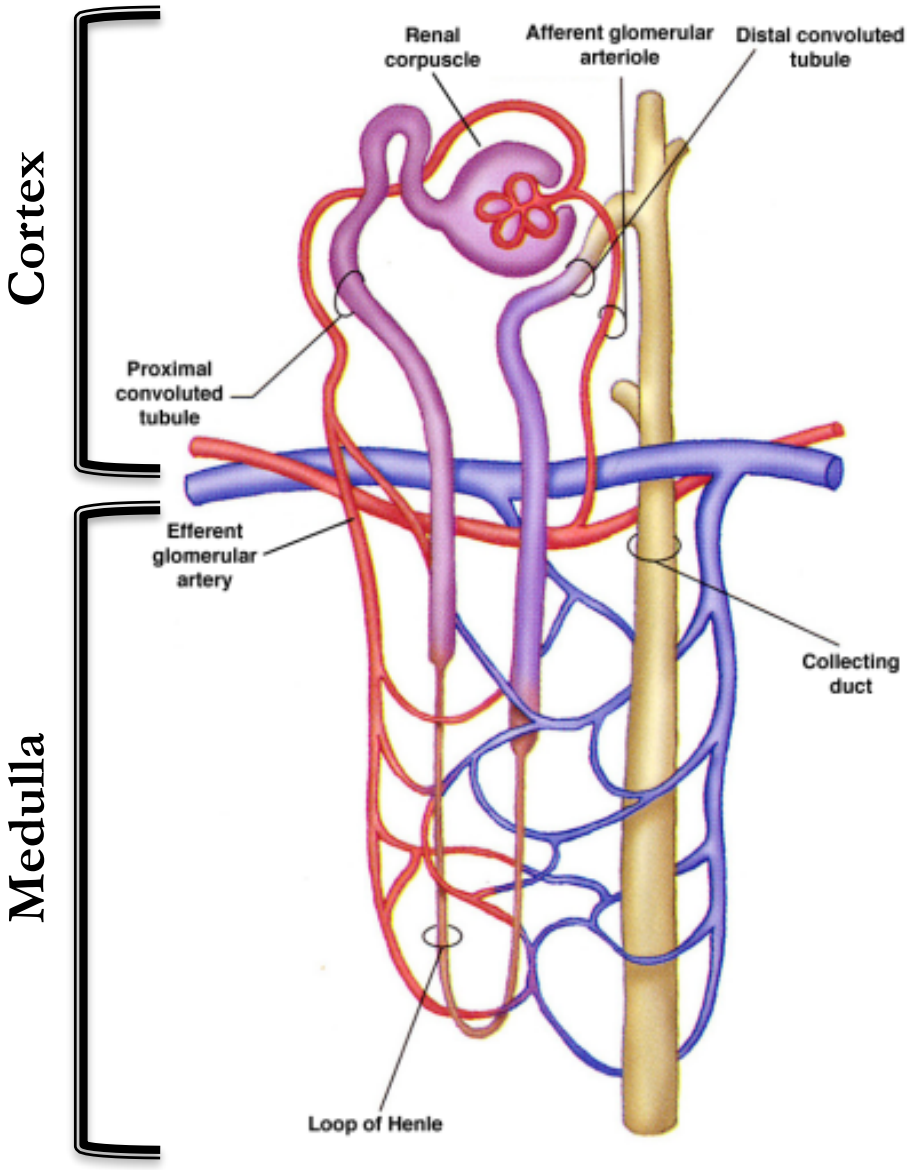

B)

Reprinted from http://medcell.med.yale.edu/systems_cell_biology/urinary/images/nephron_cartoon.png

Figure 1, continued.

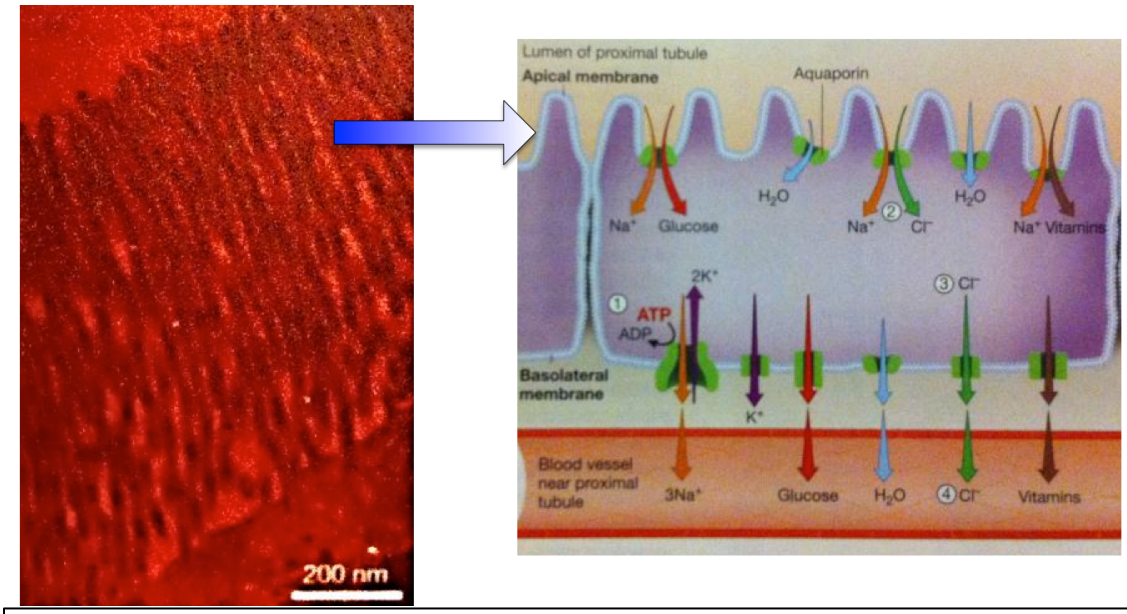

Figure 2. The Epithelial Apical and Basolateral Membranes. Shown above is a photo and figure of the epithelial cells lining the lumen of the distal convoluted tubule. It is here where the epithelial cells have a series of microvilli facing the lumen. These microvilli possess the transporters that regulate concentrations of various molecules. ENaC is not shown, but is typically found in the apical plasma membrane of polarized epithelial cells involved in Na^+ reabsorption. Sodium enters the cell down its electrochemical gradient through open ENaC channels, and is then pumped out across the basolateral membrane by the Na^+ K^+ ATPase.

Reprinted from Freeman, Scott. Biological Science. 3rd ed. 1301 Sansome St., San Francisco, CA 94111: Pearson Education, Inc., 2008. Print.

features including a large extracellular region, two transmembrane-spanning regions for each subunit, and two cytoplasmic N- and C- termini (**Figure 3**) [8, 22, 43]. It can be seen that each of ENaC's subunits share the described common structure, and each subunit can be broken down to relative sections representative of a hand, each comprising of a particular set of secondary structures (**Figures 3 and 4**). The "thumb" region is comprised of two α-helices, the "finger" region of 3 small α-helices, the "knuckle" region of 2 small α-helices, the "palm" region of several β-sheets, and a localized center region that is comprised of rotated β-sheets named the "β-ball". The extracellular portion of ENaC is needed for proper function. However, its exact role in moving ions through the membrane remains unknown. The transmembrane regions, labeled TM1 and TM2 in

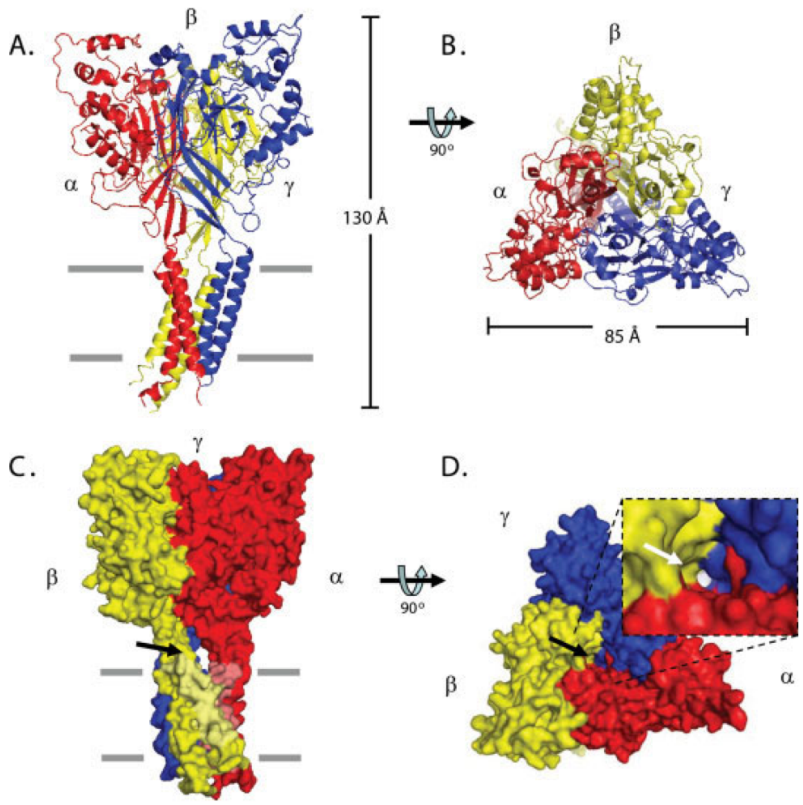

Figure 3. ENaC's Predicted Structure. Shown to the left is the predicted structure of hENaC. This predicted structure was obtained through comparison of the homotrimeric Chicken Acid Sensing Ion Channel (PDB: 2QTS) structural coordinates. The α-subunit is shown in red, the β-subunit is shown in yellow, and the γ-subunit is shown in blue. As can be seen in the upper row, the ion channel is predicted to have a height measuring 130 Å and a diameter of 85 Å. (A) Side view of ENaC ribbon structure across the lipid bilayer of the plasma membrane. (B) The side view has been rotated 90º to show a top view of the extracellular region. (C) Alternative view of A in that the molecular surfaces have been filled in. The interaction between Trans-Membrane 1 (light yellow) and Trans-Membrane 2 (light red) of adjacent monomers has been highlighted to show that cavities are formed in between the helical regions. (D) As in the view rotated in B, this view shows the top-down perspective of the molecule. Shown in the enlarged image is the channel that transverses the cell's membrane from the exterior down to the interior.

Figure 5, are also depicted, in addition to the intracellular N- and C-termini. The stoichiometric relationship between each subunit, however, has been subject to controversy [21, 27, 33, 38]. Recent studies, however, have shown that ENaC is comprised of 1 α, 1 β, and 1 γ subunit [36].

ENaC's individual α, β, and γ domains are each encoded for by separate genes

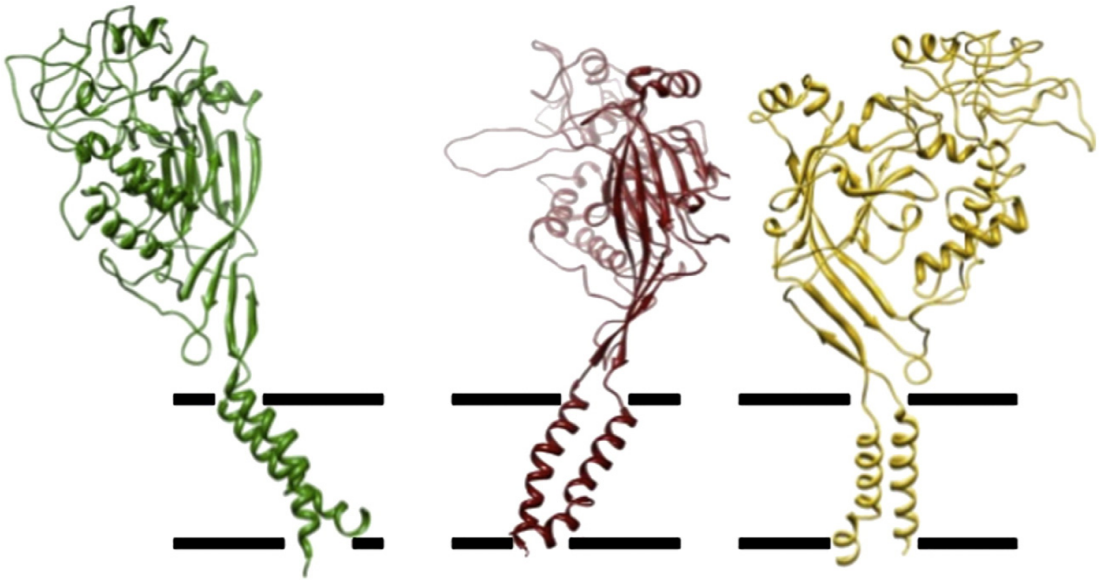

Figure 4. The Structural Similarities Between Subunits. Shown above are Schild's models for each of the ENaC subunits [35]. These homological models were constructed using the crystal structure of the Chicken Acid Sensing Ion Channel. Shown in green (left) is the α subunit. Shown in red (center) is the β subunit. Shown in yellow (right) is the γ subunit. As can be seen in the figure, each subunit has structural similarities that resemble each other subunit. There is a large, extracellular domain that consists of over half the protein and there are two transmembrane alpha helices that lead to each n- and c-terminus. According to Schild, the crystal structure used to model these subunits did not allow for the resolution of the n- and c-terminal tails and are therefore omitted.

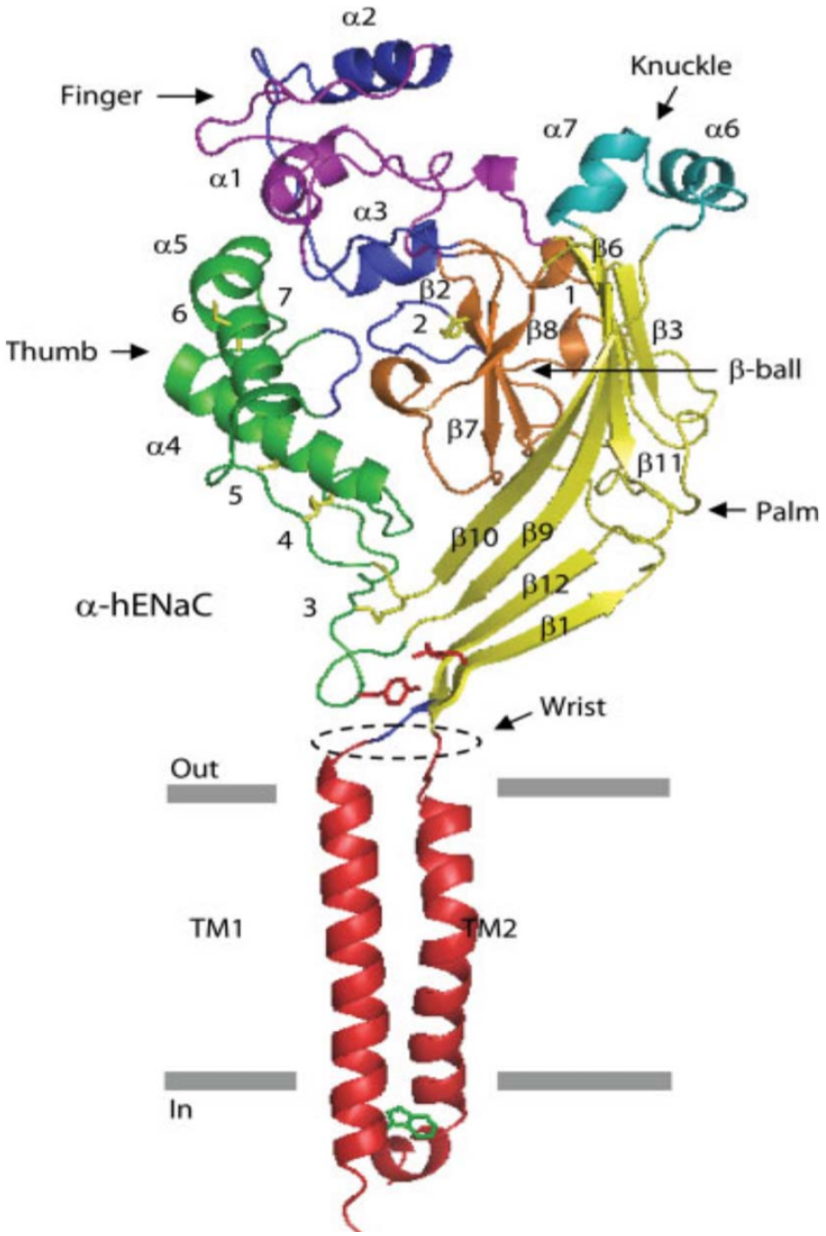

Figure 5. The Predicted Structure Of Alpha ENaC. Shown to the left is the predicted structure of α-ENaC. The "Thumb" (shown in green), "Finger" (shown in dark blue and purple), "Palm" (shown in yellow), and "Knuckle" (shown in light blue) regions nested above the "Wrist" comprise the extracellular portion of the protein. The transmembrane regions, labeled TM1 and TM2 are depicted in red, along with the intracellular N- and C-termini.

(SCNN1A, SCNN1B, and SCNN1G, respectively) that share near 35% identity in their primary sequences [15, 19, 32, 35, 36]. Although heterotrimeric ENaC is assembled by one subunit from each gene, a functional version of ENaC may be formed by three α subunits. This form, in nature, tends to be rare, and the formation of homomeric ENaC is less favored than that of the otherwise heteromeric version due to its lower activity [10, 40]. It has been established that the N-terminus of α ENaC is required for a functional pore, and ENaC comprised solely of β and γ subunits is not functional [8, 37]. This has led to the hypothesis that the α subunit plays an important part in forming the interior of the pore through which sodium is transported. Evidence has previously suggested that ENaC may be formed by two α-subunits combined with one β-subunit and one γ-subunit, and it has also been suggested that ENaC's stoichiometry resides at three of each of the three subunits, making for a protein with nine total subunits [21, 38, 40, 41]. Other evidence suggests there is the possibility of a fourth δ and fifth ε subunit [9, 12]. However, their appearances have been also been limited. The δ subunit, which appears to be human- and chimp-specific, can only be found in the brain, testes, ovaries, and pancreas. The ε subunit has only been found in *Xenopus* renal cells. Altogether, little is known about the secondary structures that form the channel's pore. Through mutations of the second transmembrane spanning region (TM2), it has been predicted that TM2 contributes the most towards the formation of the channel that allows passage of sodium [18, 38].

In a clinical setting, diseases in the lungs, kidneys, and colon that result from an imbalance between sodium and water have been attributed to malfunctions in ENaC. Sodium reabsorption has a direct effect on the extracellular fluid volume and is directly

related to the regulation of blood pressure within the body. The distal convoluted tubules, connecting tubules, and collecting ducts of the kidney, of which a significant amount of ENaC is centralized in, is the location of amiloride-sensitive Na^+ reabsorption. ENaC is a permanently active channel that exhibits slow kinetics, and one of the most prominent examples of disregulation due to ENaC is exhibited by what's known as Liddle's Syndrome, an autosomal dominant disease that directly leads to the early onset of salt-sensitive hypertension, low blood rennin levels, and hypokalemia [1, 4, 5, 36, 47]. This condition is caused by mutations in the β and γ subunits that result in an overactive ENaC, which in turn causes elevated amounts of Na^+ to be reabsorbed. Specifically, mutations that cause the last 45 to 75 amino acids to be truncated off the β subunit cause gain-of-function states on the ENaC pore. Truncation mutations on the α subunit don't have as large of an effect. Through studies performed on *Xenopus* oocytes, it has been shown that a proline-rich region within the c-terminus of the β and γ subunits, deemed the "PY Motif" for its PPPXYXXL sequence, is the target for channel-activation mutations [8, 11, 12, 22, 27, 28, 33, 35, 36, 39, 43]. With a C to T sequence change within the β subunit, a premature stop codon is introduced at Arg-564, truncating the cytoplasmic tail of the protein whilst leaving its transmembrane region intact [35]. This analysis is reinforced by the fact that this PY motif is conserved across all three ENaC subunits. It has been further shown that this PY motif also serves as a binding site for Nedd4-2, an ubiquitin-protein ligase that's also known as "neural precursor cell expressed developmentally down-regulated protein 4" [27, 39]. Via its WW domains, Nedd4-2 binds and ubiquitinates the c-terminus intracellular tail of ENaC, signaling it for internalization and degradation. It's easy to see that a truncated C-terminus would lessen

ENaC's ability to be ubiquitinated and internalized, thus resulting in an increased number of channels on the cell surface, leading to higher activity (i.e. Liddle's syndrome).

On the other hand, Pseudohypoaldosteronism Type I (PHA-1) has been characterized as a disease that results from an underactive ENaC protein, causing hypotension in addition to other potential symptoms, which can include hyperkalemia, metabolic acidosis, and the lack of responsiveness to mineralocorticoid hormones [9, 19, 33, 43]. PHA-1 is a salt-wasting nephropathic condition caused by loss-of-function changes to ENaC, reducing ENaC's ability to transport sodium. In short, having too much cell-surface expressed ENaC causes Liddle's syndrome; PHA-1 is caused by not having enough ENaC on an epithelial cell's surface.

ENaC regulation is under the control of aldosterone, a mineralocorticoid, and vasopressin, a peptide hormone, both of which indirectly affect the activity of Nedd4-2 (**Figure 6**) [4, 12 – 15, 24, 28, 34, 36, 38, 39]. Nedd4-2 is negatively regulated, or inhibited, through serum and glucocorticoid-inducible kinase (SGK), a Serine/Threonine kinase. Phosphorylation of three different sites on Nedd4-2 causes it to suppress its ability to bind and ubiquitinate ENaC. When aldosterone binds to its cytoplasmic mineralocorticoid receptor (MR), MR dimerizes and enters the cell's nucleus, inducing transcription for several proteins, one of which is SGK. SGK, in turn, phosphorylates Nedd4-2, leading to an increase in cell-surface expressed ENaC, which leads to an increase in sodium transport [6, 15]. In a similar manner, vasopressin also increases cell-surface ENaC expression. When vasopressin binds its basolateral receptors (V2), cytoplasmic production of cAMP is increased. Protein Kinase A (PKA), a cAMP-dependent kinase, also phosphorylates Nedd4, causing the same activation result as

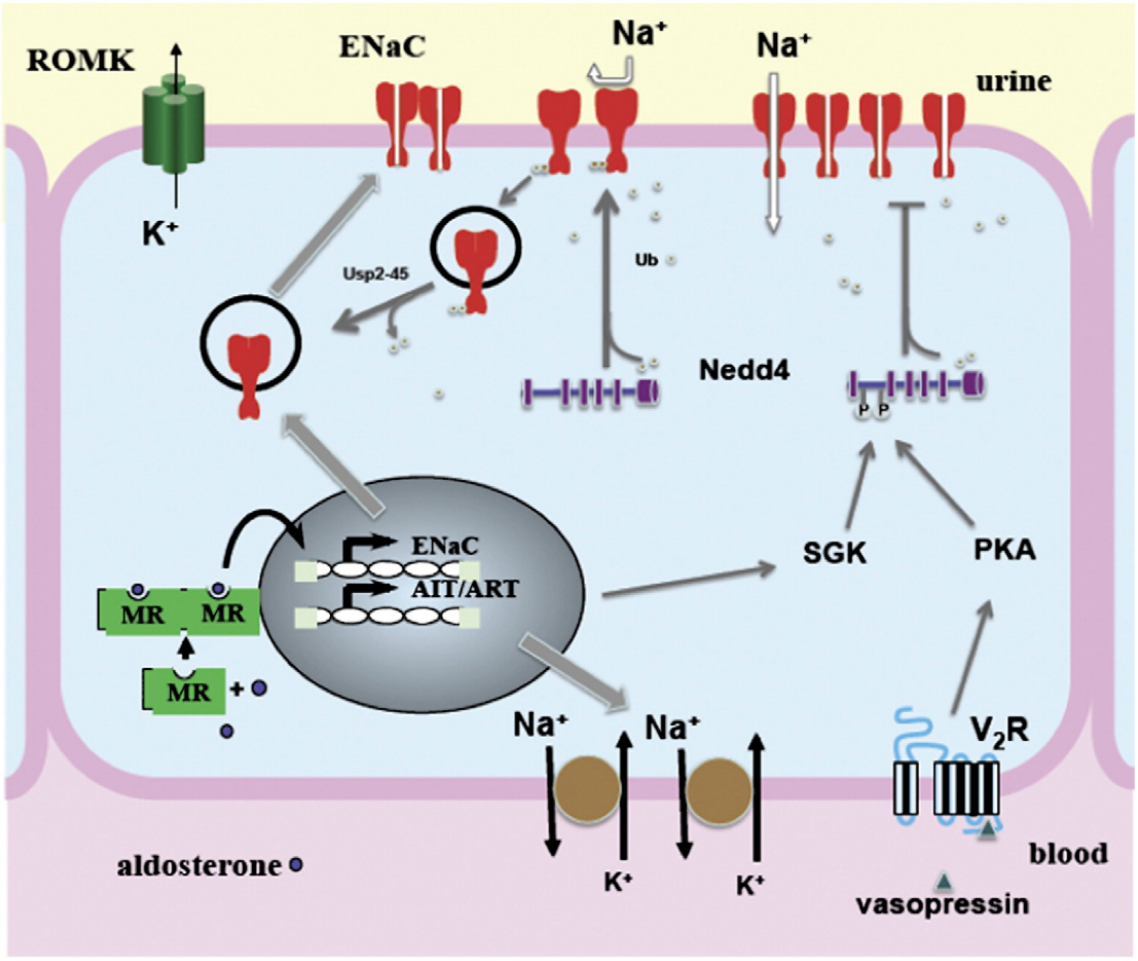

Figure 6. The Effects Of Aldosterone And Vasopressin. Shown above is Schild's [35] explanation on how aldosterone and vasopressin exhibit control over ENaC's cell surface expression. Aldosterone binds to its receptor (labeled MR for mineralocorticoid receptor), causing it to dimerize and stimulate ENaC transcription, as well as several Aldosterone-induced transcripts (AIT), such as SGK1, and Aldosterone-repressed transcripts (ART). Vasopressin binds to its membrane V2 receptors (V_2R), causing a downstream cascade that eventually activates protein kinase A (PKA). Both SGK and PKA inactivate "neural precursor cell expressed developmentally down-regulated protein 4" (Nedd4), a protein that causes the ubiquitination of ENaC, signaling it for degradation. Usp2-45, in turn, deubiquitylates ubiquitinated ENaC, resending internalized ENaC to the cell surface.

aldosterone. Additionally, aldosterone induces the expression of Usp2-45, a deubiquitylation enzyme that deubiquitylates internalized ENaC, effectively recycling ENaC proteins that were otherwise destined for degradation [34].

Sodium reabsorption through ENaC can be regulated in mainly two different ways: (1) changing the "open state" (or open probability termed P_0) of the channel or (2) directly modifying the number of channels present on the apical membrane of the cell [11, 28]. In the first method, quick changes in the levels of sodium can be induced by the proteolytic cleavage of the α and γ domains of ENaC. The cell is not limited to or restricted to the use of only one method and is capable of incorporating both methods simultaneously, giving it a high degree of control over the interior concentrations of sodium.

In view of the relationships between ENaC and its associated diseases, studying ENaC has come to hold a high priority in the medical field. Using knockout mice as animal models, diseases due to ENaC malfunction have been successfully reproduced and have served as a direct basis for the relationships between ENaC disregulation and the diseases that ENaC disregulation causes [5]. However, it has been shown that actual imbalances within mouse models have been due to improper diets. For example, it was demonstrated that when mice that were genetically engineered to reproduce Liddle's syndrome were fed appropriately, no hypertensive stasis was observed [16]. It was only when the mice were subject to high-salt diets that regulation of sodium could no longer be maintained, and the subsequent exhibition of hypertensive episodes were observed.

In light of ENaC's role in regulating blood pressure, it has become a central target of research. Through crystal structure investigation of the Chicken Acid Sensing Ion Channel and analysis of known ENaC mutation screening, amino acids that may be critical for interaction between ENaC subunits were identified (**Table 1**) [50]. Surface Plasmon Resonance (SPR) studies, when directed through this crystal structure analysis,

Structure		cASIC1	
Subunit 1	**Subunit 2**	**Subunit 1**	**Subunit 2**
Palm	Thumb	Arg 176	3 Carbonyl Oxygen (Asn 357)
Palm	Thumb	Lys 212	Buried Chloride
Palm-Loop	Thumb	Glu 178	Lys 355
Palm-Loop	Thumb	Asn 217	Arg 310
Knuckle	Finger	Trp 388 Lys 392	Glu 236
Knuckle	Finger	Gln 271	Glu 243
Wrist-Palm	Wrist-Thumb	Asp 79	His 74 Gln 421
Wrist-Palm	Wrist-Thumb	Glu 80	Tyr 283

Table 1. Identified Amino Acids. Shown on the left is a table representing amino acids (and their associated region on ENaC) that are predicted to be critical for interaction between adjacent ENaC subunits. For example, consider the third and fourth rows of the table. The Palm-Loop region's Glu-178 is predicted to interact with the Thumb region's Lys-355. Likewise, the Palm-Loop region's Asn-217 is predicted to interact with the Thumb region's Arg-310. In the case of the Wrist-Palm and Wrist-Thumb interaction that shows two amino acids in subunit 2, the cASIC amino acid residue has no direct correlation with a hENaC amino acid. Therefore, the corresponding amino acid has been predicted to be one of those two amino acids. The corresponding amino acid interactions of the homological model are presented below for hENaC. The amino acids highlighted in yellow are the amino acids that were targeted for this study. Amino acids labeled with a "?" have no direct cASIC amino acid, and so the nearest amino acid residue has been identified.

hENaC									
α	α	β	γ	β	α	γ	γ	α	β
Subunit 1	**Subunit 2**			**Subunit 1**	**Subunit 2**		**Subunit 1**	**Subunit 2**	
Asn 285	His 468	Glu 438	Glu 446	Gly 252	His 468	Glu 446	Asp 263	His 468	Glu 438
Met 321	Cl-	Cl-	Cl-	Asn 288	Cl-	Cl-	Met 299	Cl-	Cl-
Val 287	Ser 466	Gln 436	Gln 444	Glu 254	Ser 466	Gln 444	Val 265	Ser 466	Gln 436
Asn 326	Ile 417	Leu 387	Leu 395	Phe 293	Ile 417	Leu 395	Tyr 294	Ile 417	Leu 387
Trp 502 Met 506	Thr 345	Ser 312	Ser 323	Trp 471 Val 475	Thr 345	Ser 323	Trp 480 Val 484	Thr 345	Ser 312
Glu 274	Thr 347?	Ala 314?	Thr 325?	Glu 341	Thr 347?	Thr 325?	Val 352	Thr 347?	Ala 314?
Ile 118	Ala 113 Glu 532	Glu 78 Glu 503	Thr 80 Glu 512	Leu 83	Ala 113 Glu 532	Thr 80 Glu 512	Ile 85	Ala 113 Glu 532	Glu 78 Glu 503
Asn 119	Arg 386	Arg 353	Lys 364	Ser 84	Arg 386	Lys 364	Lys 86	Arg 386	Arg 353

have given insight as to whether the amino acids determined to be critical actually contribute to intersubunit interactions. Because SPR studies involve real-time analysis of interactions between molecules, synthesized polypeptides containing the critical amino acid residue's surrounding sequence can be used as analytes for quantifying interactions between those amino acid residues predicted to be critical. For example, a polypeptide containing the tryptophan and methionine residues at positions 502 and 506, respectively, of the alpha subunit can be synthesized from a PCR-amplified DNA segment from the alpha subunit's gene. For the purposes of this study, that PCR-amplified segment can then be ligated onto a vector (specifically, the pGEX-4T-2 vector) that contains a sequence for Glutathione S-Transferase (GST). This GST-fusion protein can then be immobilized via the GST portion of the protein, leaving the ligated peptide exposed for analysis. The "partnering" peptide can then be introduced into the immobilized GST-fusion's environment, and it is at this point where SPR studies acquire the targeted real-time, quantitative data.

SPR is a spectroscopic, quantitative technique that allows for the 'real-time' analysis of binding kinetics between protein-protein interactions [2]. Sheehan [48] describes SPR as a technique that relies on changes in the refractive index near metallic surfaces. When plane-polarized light strikes a metallic surface that rests upon another dielectric surface, a longitudinal charge density wave—that is, a surface plasmon—is propagated along the area between them. Metals are suited for this application due to their free oscillating electrons called plasmons. The beam of light (at a particular wavelength, l) that strikes the reflective surface and is totally internally reflected penetrates into the less optically dense medium to a distance that is smaller than l,

producing what is known as the evanescent wave. When the wave vector of the evanescent field equates that of the surface plasmon's wave vector, the waves couple, or "resonate". As a result of this resonance, or coupling, energy is lost from the incident light, causing a reduction in the intensity of the reflected light. The detector, which collects the beam of light upon reflecting the metallic surface, then registers this loss of energy as a response.

From the application perspective intended for this project, a GST fusion protein was first immobilized onto a gold sensor chip (one of the 'surfaces' previously mentioned). This fusion protein, whether the protein itself is a peptide or full protein, acts as a substrate for a secondary protein (the analyte) that is passed over the sensor chip [3]. The machinery used to study this interaction, given the name "BIAcore X", then registers any potential interactions as a response unit within the sensorgram (**Figures 7a**, **7b**, and **8**). These registered interactions include association and dissociation events, from which kinetic data (i.e. on/off rates) can then be derived. This technique can be most beneficial when native protein interactions are compared to mutated proteins, potentially revealing amino acids that are, indeed, vital for interaction.

The peptide pair targeted for this project comes from an $\alpha-\beta$ pair (W502/M506 and S312, respectively; **Table 1**). Due to cost restrictions accompanying commercially obtained peptides, along with the need for assurance of secondary structural integrity of the amino acids under study, peptides were synthesized with an expression system devised in a previous study (described below). In short, a GST-peptide fusion protein was synthesized and expressed in an *E. coli* system. Once purified and isolated, one of the pair of expressed proteins had their GST tag cleaved off via a one-step thrombin

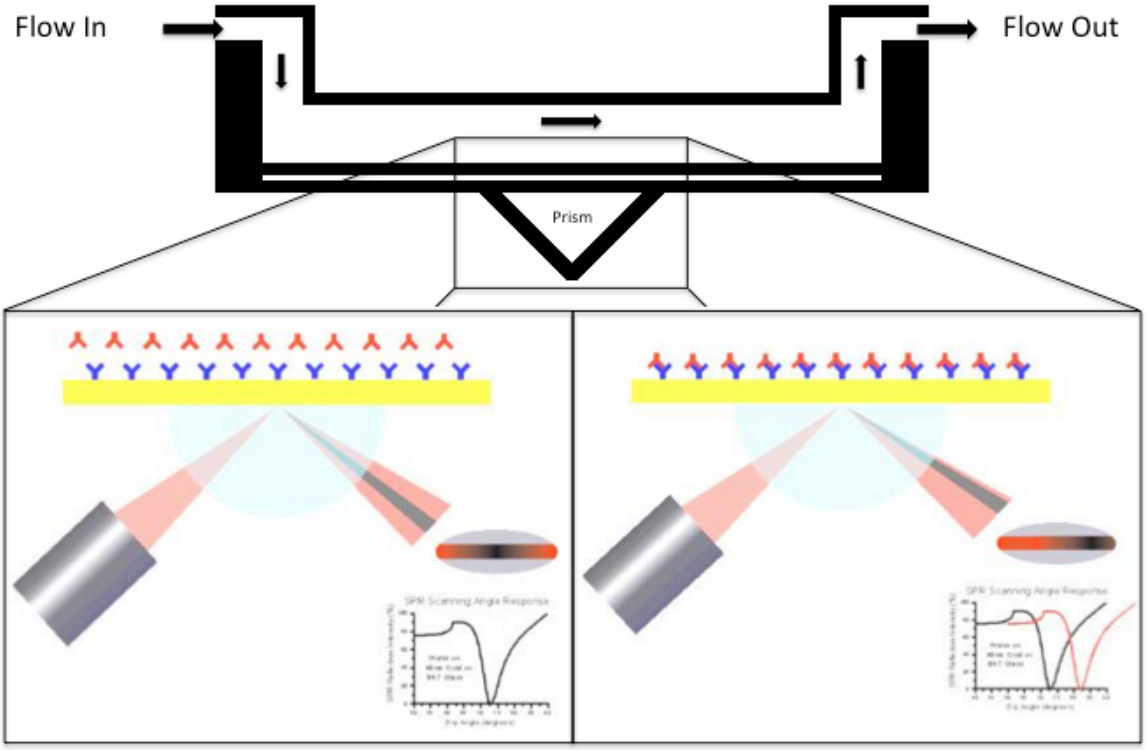

Figure 7a. Surface Plasmon Resonance: The Inner Workings. Shown above is a visual representation of the inner workings of Surface Plasmon Resonance, a spectroscopic technique used to monitor protein-protein interactions in real time. From collected data, binding kinetics and on/off rates can be calculated and derived. This technique can be most beneficial when native protein interactions are compared to mutated proteins, potentially revealing amino acids that are vital for interaction. The machinery used to perform SPR has a flow tube that's used to introduce proteins to a central chamber that contains a gold sensor chip resting directly above a glass surface. In the image, two different proteins (labeled red and blue) are being measured for their potential interaction. In the sample datagram, it can be seen that when the proteins interact, there is a change in the corresponding "dip angle," which is the angle at which energy from the light's evanescent wave is being absorbed by the bound protein(s). This change can then be used as a basis for the sensorgram presented in **Figure 7b**, through which binding kinetics are derived.

treatment for flow-through over a protein-immobilized gold sensor chip. Interactions were then analyzed and binding kinetics were derived from the analysis of the collected data.

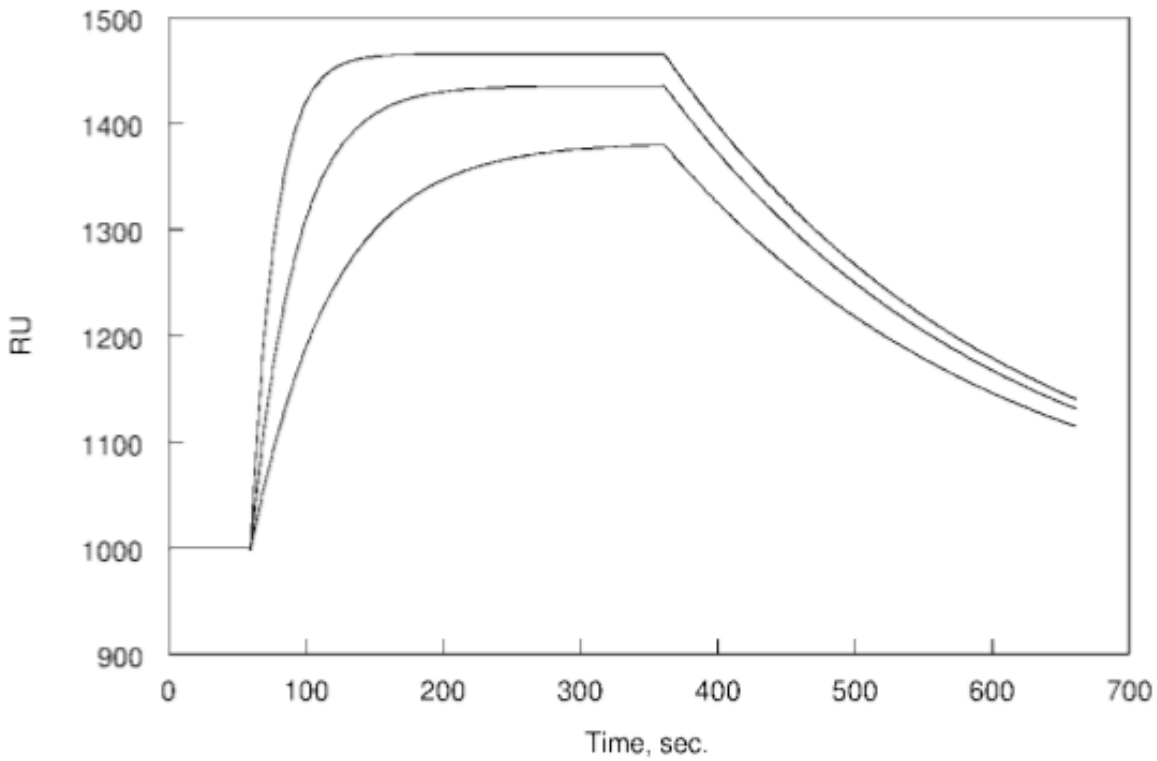

Figure 7b. Surface Plasmon Resonance: An Example Of An SPR Sensorgram. Shown above is a sample of the representative data obtained when performing SPR. On the y-axis, units are arbitrarily chosen as Response Units (RU) (1 RU is measured as 1 picogram/millimeter^2, but exact measurement also depends on other factors [44]). On the x-axis, units for time are depicted in seconds. After immobilizing (for example) protein A on the gold sensor chip (**Figure 8**), protein B is introduced into the flow channel. If protein A is capable of interacting with protein B, the datagram will increase in RUs as shown near time = 75 seconds. As potential interaction sites are used up on the sensor surface, there is a leveling-off of RUs, indicating that there are no more interaction sites available for protein B to interact with protein A. When protein B is removed from the flow channel, bound protein B begins to dissociate, giving the response seen near time = 400 seconds. Binding kinetics are then derived from this data, allowing for the direct quantifiable comparison for any other potential interaction partners (i.e. protein C).

Sample data taken from: Englebienne, P., Hoonacker, A.V., and Verhas, M. (2003) Surface plasmon resonance: principles, methods and applications in biomedical sciences. *Spectroscopy* **17**:255-273

A)

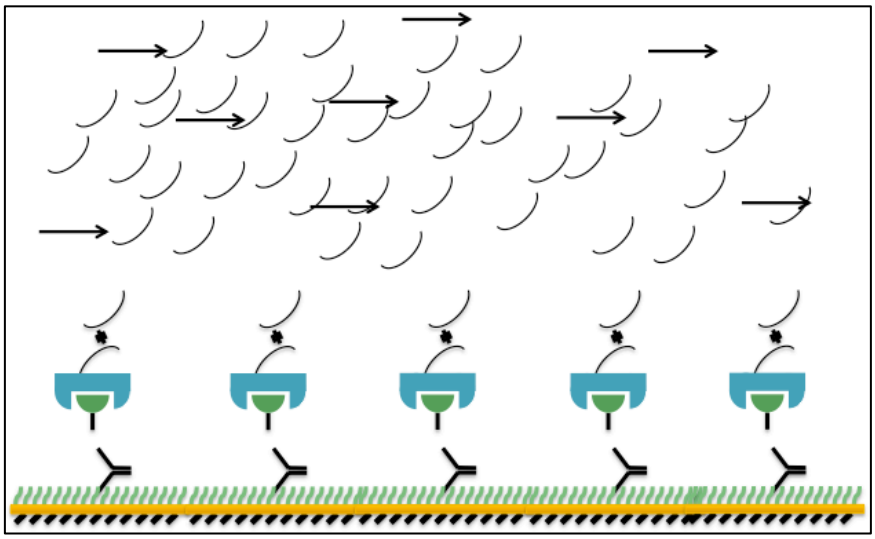

B)

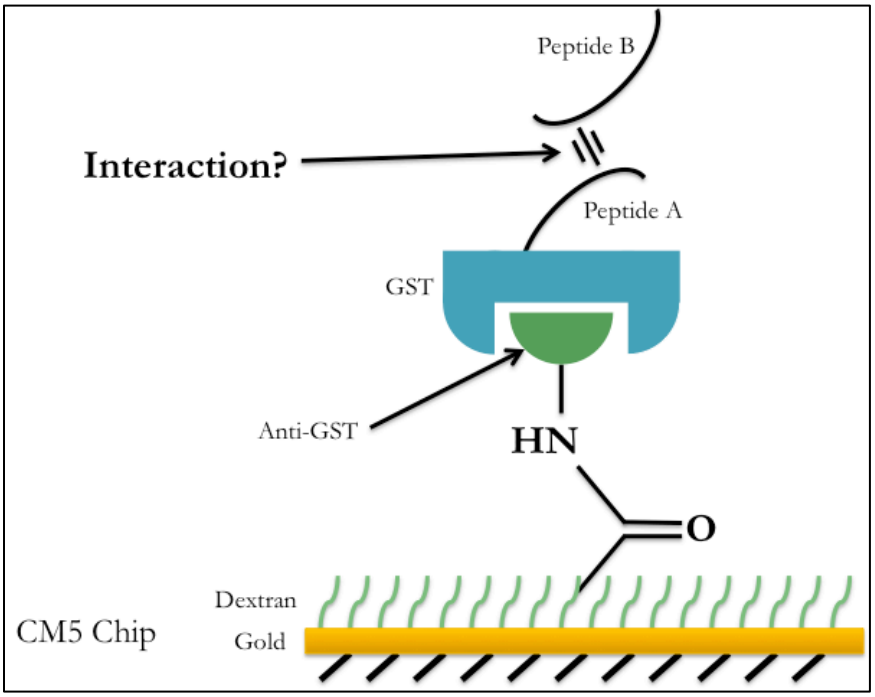

Figure 8. **The Interaction Between Immobilized Protein And Analyte.** Shown above is a representation of how proteins are immobilized onto a CM5 Sensor Chip within the BIAcore X, the apparatus used to perform Surface Plasmon Resonance studies. (A) A bird's-eye view cartoon representation of what's happening within the flow channel of the BIAcore X's sensor chip. (B) This is a cartoon representation of how peptides are immobilized onto a CM5 Sensor Chip. The gold chip has a layer of Dextran resting atop the chip's surface, to which an anti-GST (glutathione S-transferase) is covalently attached. GST fusion proteins ("Peptide A" in the figure) that contain the target amino acid (see Introduction) are expressed and anchored to the anti-GST. Peptide B, having its GST tag cleaved previously (see Materials and Methods) is introduced into the flow channel. The BIAcore X then registers any interactions into its datagram (**Figure 7b**).

CHAPTER II

MATERIALS AND METHODS

The following expression system was devised as a means of expressing GST fusion proteins that can then be used for surface plasmon resonance studies. In order to successfully ligate synthesized peptides onto a GST protein, there were two preparative methods that were performed in conjunction with each other (one to prepare the GST vector (pGEX-4T-2) and one to prepare the gene segments corresponding to peptides via a PCR reaction from ENaC templates).

Plasmid pGEX-4T-2 Preparation Protocol

Transformation of the pGEX-4T-2 plasmid into *E. coli* Top10 cells for high-efficiency cloning and plasmid propagation

The pGEX-4T-2 plasmid was transformed into *E. coli* Top10 cells using a standard heat shock protocol.

Competent *E. coli* Top10 cells, as well as plasmid DNA to be transformed, were removed from -80 ºC storage and placed on ice to thaw out. Once thawed, 1.0 µL of plasmid (which should provide for more than 1.0 µg of DNA) was mixed with 50.0 µL of *E. coli* and was incubated on ice for 20 minutes. The *E. coli*/plasmid solution was then heat-shocked at 42 ºC for 1 minute and returned to the ice for an additional 2 minutes. One milliliter of LB broth (1 liter contents: 10 g Tryptone, 5 g Yeast Extract, and 10 g NaCl) was added and the solution incubated at 37 ºC shaking at 225-rpm for 1 hour. After incubation, 20 to 30 µL of the transformed solution was spread onto an

LB/ampicillin (0.1 mg / mL) agar plate (successfully transformed pGEX plasmids into *E. coli* are artificially selected for by the expression of the ampicillin resistance gene on the pGEX vector, thus only allowing plasmid-containing *E. coli* cells to form colonies). The cells were incubated overnight at 37 ºC. Remaining transformation solution was stored at 4 ºC.

Plasmid Isolation

An individual colony from an LB agar plate was placed into a solution of 5.0 mL LB with 0.1 mg/mL ampicillin. The inoculated culture was then incubated overnight at 37 ºC shaking at 225 rpm.

The plasmid DNA was isolated according to the QIAGEN QIAprep® Spin Miniprep Kit manufacturer's protocol. One and half milliliters of overnight culture was centrifuged at 6800 × g for 3 minutes at room temperature, and the supernate was discarded. This process was then repeated 2 more times in order to obtain a 4.5 mL *E. coli* pellet (supernate discarded). The cell pellet was resuspended in 250 µL "Buffer P1". Then, 250.0 µL of "Buffer P2" was added to the cell suspension and thoroughly mixed by immersion, followed by the addition of 350 µL "Buffer N3". This solution was then centrifuged for 10 minutes at 17,900 × g. The supernate was decanted into a QIAprep spin column and centrifuged at 17,900 × g for 1 minute, and the flow-through was discarded. The spin column was washed with 0.5 mL "Buffer PB", centrifuged for 1 minute, and this flow-through was also discarded. The column was then washed using 0.75 mL of "Buffer PE" and centrifuged for 1 minute at 17,900 × g. The flow-through was discarded, and the spin column was recentrifuged for an additional minute to remove

residual wash buffer. The plasmid DNA was eluted from the column with 50.0 µL of 50 ºC pre-warmed water by centrifuging for 1 minute at 17,900 × g.

Quantitation of Plasmid DNA

The isolated plasmid was quantitated using a Thermo Fisher Scientific NanoDrop 2000c Spectrophotometer measuring absorbances at 260 and 280 nm.

Digestion of pGEX-4T-2 for Ligation

The pGEX-4T-2 plasmid contains a promoter for the expression of Glutathione S-Transferase (GST). Unique restriction enzyme cut sites, BamHI and NotI, are seated at the end of the GST gene, where the expression of the subsequent DNA allows for the expressed protein to have a GST tag.

Digestion was carried by combing the following: 40.0 µL of isolated plasmid (125.0 ng / µL), New England BioLabs Buffer 2 (1X Buffer Components: 50.0 mM NaCl, 10.0 mM Tris-HCl, 10.0 mM $MgCl_2$, 1.0 mM Dithiothreitol (DTT); pH 7.9 at 25 °C), 10 units of BamHI and NotI each, and sterile water in a 50 µL reaction. The digestion reaction was incubated at 37 ºC for 120 minutes. The restriction enzymes were then heat inactivated at 65 ºC for 15 minutes.

Removal of Terminal Phosphate by Antarctic Phosphatase ("CIP'ed")

Removal of the 5' phosphate on the pGEX-4T-2 would prevent the random re-circularization of the digested plasmid during the ligase reaction. The digestion reaction was treated with the addition of 1x Antarctic Phosphatase Reaction Buffer (1X Buffer

Components: 50.0 mM Bis-Tris-Propane-HCl, 1.0 mM $MgCl_2$, 0.1 mM $ZnCl_2$, pH 6.0 at 25°C), 5 units of Antarctic Phosphatase, and sterilized water to a 60.0 µL total reaction. The reaction was incubated at 37 ºC for 15 minutes, and the phosphatase was then heat inactivated at 65 ºC for 5 minutes.

Gel Extraction of pGEX-4T-2

A 1.5% (w/v) Tris base, Acetic Acid and EDTA (TAE) agarose gel was run for 80 minutes at 120 V with DNA samples. The portion of the gel containing the GST segment of the plasmid was then cut out using a scalpel. These small cutouts were then treated with a Wizard® SV Gel and PCR Clean-Up System (Promega), which removed all components but the desired DNA.

The Wizard® SV Gel and PCR Clean-Up protocol consisted of excising the DNA from the agarose gel, where 10.0 µL of Membrane Binding Solution (4.5 M guanidine isothiocyanate and 0.5 M potassium acetate (pH 5.0)) were added for every 10 mg of gel slice. The gel slice was then incubated at 60 ºC until completely dissolved. Next, the solution was transferred into a minicolumn, where it was incubated at room temperature for 1 minute, followed by elution by centrifugation at 16,000 × g for 1 minute. The flowthrough was discarded, the minicolumn was refilled with 700 µL of Membrane Wash Solution (10.0 mM potassium acetate (pH 5.0), 80% ethanol, and 16.7 µM EDTA (pH 8.0)), and centrifuged at 16,000 × g for an additional minute. The flowthrough was discarded, 500 µL of wash solution was added, and the minicolumn was centrifuged for 5 minutes. The collection tube was emptied and the minicolumn was recentrifuged for 1 minute, removing any remaining ethanol. Fifty microliters of nuclease-free water was

then added, incubated for 1 minute, and centrifuged at 16,000 × g for 1 minute, eluting the DNA.

Human Alpha, Beta, And Gamma ENaC Gene Segment Preparation Protocol

This part of the protocol was performed in conjunction with the steps mentioned above in "Plasmid pGEX-4T-2 Preparation Protocol".

Transformation of the pSWICK plasmid into *E. coli* Top10 cells for high-efficiency cloning and plasmid propagation

"pSWICK" plasmids that contained the genes for human α, β, and γ ENaC were provided by J.D. Stockand's research lab at University of Texas Health Science Center San Antonio and were transformed into *E. coli* Top10 cells following the steps mentioned above for the pGEX-4T-2 plasmid.

Plasmid Isolation via the QIAGEN QIAprep® Spin Miniprep Kit

E. coli containing plasmids were grown overnight as mentioned above for the pGEX-4T-2 plasmid, and pSWICK plasmid was isolated from overnight *E. coli* cultures as mentioned above for the pGEX-4T-2 plasmid. The isolated plasmid was quantitated using a Thermo Fisher Scientific NanoDrop 2000c Spectrophotometer measuring at wavelengths of 260 and 280 nm.

Amplification of gene segments from hENaC using Polymerase Chain Reaction

The Polymerase Chain Reaction (PCR) technique was used to amplify the targeted gene segments from the corresponding pSWICK plasmids (i.e. the peptide

segment containing the predicted a tryptophan 502 and methionine 506 residue was amplified from the pSWICK plasmid containing the α human ENaC gene). Forward and reverse primers were designed to add restriction sites surrounding the targeted sequence (**Table 2**). In this manner, the pGEX-4T-2 plasmid containing the glutathione S-transferase tag could also be digested with the same restriction enzymes. This would allow for the digested gene segment ends and plasmid ends to have complementary sequences, thus, allowing for the ligation of the pGEX plasmid to the amplified ENaC gene segments. All forward primers contained a restriction site for the use of the BamHI restriction enzyme; BamHI digests solely at "GGATCC" sequences. Likewise, all reverse primers contained a restriction site for the use of the NotI restriction enzyme; NotI digests solely at "GCGGCCGC" sequences.

The 50 µL PCR reaction was comprised of the following: 100 ng of DNA template, ThermoPol Reaction Buffer (1X buffer components: 20.0 mM Tris-HCl, 10.0 mM $(NH_4)_2SO_4$, 10.0 mM KCl, 2.0 mM $MgSO_4$, 0.1% Triton® X-100, pH 8.8 at 25°C), 10.0 mM dNTPs, 1.0 µM forward primer, 1.0 µM reverse primer, and 2 units of Vent (a proofreading polymerase). An Applied Biosystems GeneAmp® PCR System 2700 was used for the reaction and was set to 25 cycles of 95 ºC for 1 minute, 55 ºC for 30 seconds, and 72 ºC for 30 seconds.

Digestion of PCR Product

Similar to the digestion reaction required for the pGEX-4T-2 plasmid (see above), the digestion reaction for the PCR product incorporated the use of BamHI and NotI. The 50 µL reaction mixture consisted of 40.0 µL of PCR product, NEB Buffer 2, 10 units of

Table 2. Elongated Peptides Containing Targeted Amino Acids. Shown above is a table representative of the peptide segments used in this study (with the exclusion of b Ser 84), along with the primers used in PCR to elongate the segments from ENaC plasmid templates. The targeted peptide segments are aligned with their respective primers, while also showing the amino acid sequence that is representative of the peptide segment. Highlighted in yellow are the amino acid residues believed to be critical for ENaC's inter-subunit interactions. GC content and melting temperatures are indicated above the respective primer sequences. Primer sequences shown in red and blue lettering are indicative of restriction enzyme BamHI and NotI cut sites, respectively.

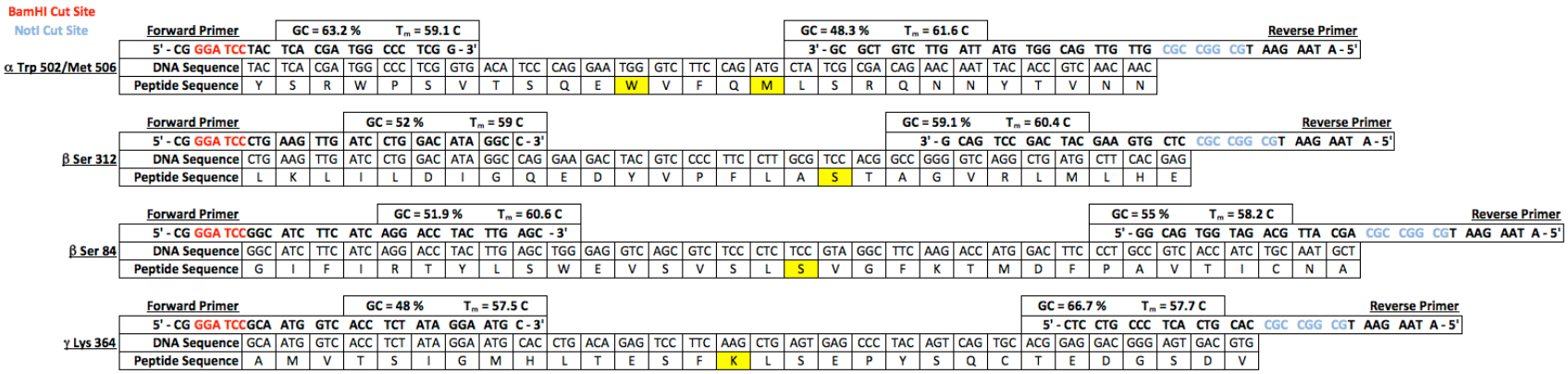

BamHI and NotI each, and sterile water. The reaction mixture was incubated at 37 ºC for 120 minutes, and the restriction enzymes were subsequently heat-inactivated by incubation at 65 ºC for 15 minutes.

Cleaning the PCR product

In order to isolate PCR product from the rest of the previous reactions' components, a Wizard® SV Gel and PCR Clean-Up System (Promega was used on the digested PCR product according to manufacturer's instruction.

The Wizard® Clean-Up protocol was carried out in the same manner as mentioned in the previous Gel Extraction of pGEX-4T-2. The initial step, however, involved doubling the volume of the PCR reaction with Membrane Binding Solution (4.5 M guanidine isothiocyanate and 0.5 M potassium acetate (pH 5.0)), after which the subsequent transfer to a minicolumn and incubation at room temperature for 1 minute takes place. The rest of the cleaning protocol is carried out in the same manner.

Combining The Plasmid and PCR Product for Recircularization

The digested pGEX-4T-2 plasmid and ENaC segments were combined to produce a newly formed plasmid that contained the appropriate sequence for a GST protein followed by the ENaC segment that was to be studied.

Ligation with T4 DNA Ligase

The digested and cleaned PCR product (after restriction enzyme heat inactivation) was combined with the digested, dephosphorylated, gel-separated and cleaned of pGEX

vector. Additionally, T4 DNA Ligase Buffer (1X Buffer Components: 50 mM Tris-HCl, 10 mM $MgCl_2$, 1 mM ATP, 10 mM DTT, pH 7.5 at 25°C) and 400 units of T4 DNA Ligase were included in the reaction. This 20 µL reaction solution was incubated at 16 ºC over 72 hours.

Transformation of Ligated Plasmid

Ligation reactions were transformed into *E. coli* Top10 cells following the steps mentioned above for transformation of the pGEX-4T-2 plasmid. Twenty to thirty microliters of transformed Top10 *E. coli* was plated and allowed to grow overnight. If the plasmid was successfully recircularized, colonies grew. However, there was the chance that the plasmid may have been recircularized without insert. Verification for a successful ligation was checked by plasmid sequencing.

Overnight Culture and Isolation of Ligated Plasmid

Colonies that grew after successful transformation of newly synthesized plasmid were picked and grown overnight as mentioned above for the pGEX-4T-2 plasmid. Subsequently, the plasmid was isolated from the culture as mentioned above via the QIAGEN Plasmid Isolation Kit.

Sequencing Verification of Plasmid Ligation

In order to verify successful ligation, isolated plasmids were sequenced at QuintaraBio, a company that provides sequencing services based in Albany, California. The sequence data were aligned with the sequence of both the pGEX-4T-2 plasmid and

the targeted peptide's DNA sequence using Clustal Omega (http://www.ebi.ac.uk/Tools/msa/clustalo/).

Transformation of Verified Plasmid into *E. coli* BL21 cells

The verified plasmid was then transformed into *E. coli* BL21 cells—that was, cells that are designed to express recombinant proteins in high quantities. The RNaseE gene (rne131) has been mutated, thus reducing intracellular levels of RNases and increasing mRNA stability (http://www.lifetechnologies.com). Note that the transformation protocol for *E. coli* BL21 differs from the transformation protocol designed for Top10 *E. coli* cells.

Frozen BL21 cells were removed from -80 ºC storage and placed on ice to thaw out for 10 minutes. The sequenced-verified plasmids were also placed on ice. Once thawed, 100.0 µL of BL21 cells and 100.0 µL of cold KCM buffer (100 mM KCl, 30 mM $CaCl_2$, 50 mM $MgCl_2$) were combined. Five microliters of plasmid were added to the solution, and the tube was placed on ice for 20 minutes. Nine-hundred microliters of SOC broth (0.1 M $MgCl_2$, 0.1 M $MgSO_4$, and 0.4% Glucose in 100 mL of SOB (2.0% Tryptone (m/v), 0.5% Yeast Extract (m/v), 0.05% NaCl (m/v) in sterile water)) was added to the mix, and the solution was incubated at 37 ºC for 1 hour in a 225 rpm shaker. One-hundred and fifty microliters of solution were then spread onto LB/ampicillin agar plates. The plates were inverted and incubated at 37 ºC overnight.

Overnight Culture in LB/AMP

Successfully transformed plasmids were grown overnight as mentioned above for

the pGEX-4T-2 plasmid.

Expression of Plasmid and Cell Lysis

BL21 cells were expressed in a media known as 2X-YTG (4 g Tryptone, 5 g Glucose, 2.5 g Yeast Extract, 1.25 g NaCl, and 100 μg/mL ampicillin in 500 mL of sterile water). One-and-a-half milliliters of overnight culture was added to 500 mL of expression media and incubated in a 37 ºC 225 rpm shaker for 3 hours. After the 3-hour incubation, 0.1 mM isopropyl β-D-1-thiogalactopyranoside (IPTG) as added in order to express protein, upon which the media was incubated for 3 more additional hours. The cells were pelleted by centrifugation in order to collect and lyse the cells. Two hundred and fifty milliliters of the culture was centrifuged at 9800 × g for 15 minutes. The supernatant was then removed, and the remaining 250 milliliters of culture were centrifuged (supernatant also removed). The cells were resuspended in 25.0 mL of Phosphate Buffered Saline (PBS: 137.0 mM NaCl, 2.7 mM KCl, 10.0 mM $Na_2HPO_4 \cdot 2H_20$, 2.0 mM KH_2PO_4, pH 7.4). In order to lyse the cells open, the cells were frozen at -80 ºC, thawed, then frozen and thawed twice more. DNase was added to the resultant slurry of cell extract at a final concentration of 2.0 μg/mL, as well as 20.0 μM $MgCl_2$ (final concentration). The DNase reaction was incubated at 37 ºC for 30 minutes, and the solution was then centrifuged at 15,300 × g for 25 minutes. The resulting supernatant carrying the protein-expressed cell extract was then decanted out.

Purification of GST Protein from Cell Extract

Purification was achieved through the use of glutathione agarose resin for affinity

purification of GST fusion proteins in gravitational column chromatography. To begin purification, 1.5 mL of immobilized glutathione (ThermoScientific; supported in 4% beaded agarose with a capacity of 8 mg GST per milliliter of gel) was added to the cell extract. The solution was rocked for 1 hour at 4º C and subsequently rested to allow the resin to settle. The supernate was removed, and 10.0 mL of fresh PBS was added to wash the remaining slurry. The resin was once again allowed to settle and had its supernatant removed. The wash was repeated once more, and once the supernatant was removed, the resin was transferred to a 5.0 mL polypropylene column. To elute the protein from the resin, 1.0 mL of elution buffer (10.0 mM reduced glutathione in 50 mM Tris-HCl pH 8.0) was added to the column and mixed. The column slurry was allowed to settle for 10 minutes. Once settled, the column would be allowed to flow through, and fractions were collected in 0.5 mL fractions.

SDS-PAGE and Western Blot

Expressed proteins were visualized by SDS-PAGE analysis. The 12% resolving gel consisted of the following: 4.0 mL 30% acrylamide, 2.5 mL 1.5 M Tris-HCl pH 8.8 buffer, 100.0 µL 10% SDS, 3.35 mL ddH_2O, 50.0 µL ammonium persulfate (APS), and 5.0 µL tetramethylethylenediamine (TEMED) (APS and TEMED components were added last, respectively). The resolving gel was allowed to solidify for 40 minutes, onto which the stacking gel would be added. The 4% stacking gel consisted of the following: 1.32 mL 30% acrylamide, 2.52 mL 0.5 M Tris-HCl pH 6.6 buffer, 100 µL 10% SDS, 6.0 mL ddH_2O, 50 µL APS, and 10.0 µL TEMED. Once components were combined, the stacking gel was allowed to solidify for 40 minutes. Fifteen microliter samples were

combined with 5.0 µL 4X SDS sample buffer (1X buffer components: 40% (v/v) glycerol, 240 mM Tris-HCl pH 6.8, 8% SDS, 0.04% bromophenol blue, 5% beta-mercaptoethanol (BME)) and heated at 100 ºC for 5 minutes prior to analysis. Gels were run at 120 V for 80 minutes.

After running the gel, it was transferred to a tray, washed with 25 mL ddH_2O 3 times at 5 minute intervals, and then stained with SimplyBlue™ SafeStain (Life Technologies) for 1 hour. The gel was destained overnight in pure water, and then imaged.

Gels that were run for Western Blot were not stained with SimplyBlue™. Instead, the gel was rinsed for 5 minutes in ddH_2O and then assembled into a transfer rig. The transfer was run at 100 V for 1 hour in transfer buffer (1X buffer components: 25 mM Tris, 192 mM glycine, 20% (v/v) methanol (pH 8.3)). Once transferred, the nitrocellulose paper containing the transferred protein was placed in 5.0 mL blocking solution (5.0 mL Tris Buffered Saline (TBS; 1X buffer components: 0.25 mM Tris, 0.15 M NaCl, pH 7.2), 5 µL Tween-20, and 0.25 g dry milk) for 30 minutes. One microliter of Anti-Glutathione-S-Transferase Rabbit primary antibody (Sigma-Aldrich) was added (to give a 1:5000 solution to antibody ratio) and incubated at 4 ºC overnight. The membrane was then washed for 5 minutes in 20.0 mL TBS-Tween (TBST; 0.1% (v/v) Tween20 in 1X TBS) three times, onto which 1.0 g dry milk was added to the last wash. It was incubated for 1 minute. Anti-rabbit alkaline phosphate conjugated secondary antibody was added at a 1:20000 ratio (1 µL antibody in 20 mL solution), and the solution was rocked for 1 hour at room temperature. The blot was then rinsed in TBST three times for 5 minutes each time, and then washed in TBS for 5 minutes. Alkaline

phosphate activity was then carried out using Thermo-Scientific 1-Step NBT/BCIP (nitro-blue tetrazolium and 5-bromo-4-chloro-3'-indolyphosphate, respectively) substrate solution; 66.0 µL of NBT and 33.0 µL of BCIP were added to 10.0 mL alkaline phosphate buffer (100 mM diethanolamine, 100 mM NaCl, 5 mM $MgCl_2$, pH 9.5). The blot was developed for 30 minutes and then stopped by washing the membrane in ddH_2O for 5 minutes twice.

Cleavage of GST from GST-fusion proteins

Cleavage of GST from the expressed GST-fusion proteins was achieved by treatment with thrombin (GE Healthcare). GST-fusion proteins were first bound to glutathione agarose by rocking at room temperature for 1 hour. The agarose was washed with PBS buffer three times, and the resulting solution was incubated on a rocker for 16 hours at room temperature with 50 units of thrombin working mixture (50 µL of 1 unit/µL stock thrombin solution and 950 µL PBS). Peptides were then eluted with PBS in fractions, leaving a mix of thrombin and peptides in solution. Thrombin was removed from solution using p-Aminobenzamidine agarose (Sigma). One milliliter of p-Aminobenzamidine agarose was added to a column and was washed with Tris buffer (50 mM Tris-HCl, 0.4 M NaCl, pH 8.15) three times. The peptide/thrombin solutions were combined into the column, and the column was rocked overnight at 4º C. Elution of the peptides was then carried out with Tris buffer in 0.5 mL fractions.

BCA Assay

Protein concentrations were determined via a BCA Assay (BCA Protein Assay

Kit – ThermoScientific) using a 96 well plate and a BioRad iMark™ Microplate Reader. BSA standards were 50.0 µL of 2000, 1500, 1000, 750, 500, 250, 125, and 25 µg/mL. A 50:1 solution of BCA reagent A and reagent B, respectively, made a working solution of BCA and 200 µL of the working solution was added to each well containing 50 µL of standard and sample . The well plate was then shaken for 30 seconds and incubated at 37º C for 15 minutes. Following incubation, absorbances were measured at 590 nm. Samples were measured in duplicate and averaged.

SPR Analysis

Immobilization of Anti-GST

The BIAcore X's sensor chip was derivatized according to the protocol outlined in the GST Capture Kit (GE Healthcare Life Sciences – Instruction 22-0522-19 AG). Anti-GST antibody was first diluted to 30 µg/mL in immobilization buffer (5 µL anti-GST antibody with 95 µL immobilization buffer). Activation, immobilization, and subsequent deactivation of the sensor chip was carried out at 25 ºC at a flow rate of 5 µL/min in HBS-EP running buffer (10 mM HEPES, pH 7.4, 0.15 M NaCl, 3 mM EDTA, 0.005% Surfactant P20). To both flow cells (Fc) 1 and 2, a 7-minute injection of a 1:1 solution of 1-Ethyl-3-(3-dimethylaminopropyl)-carbodiimide and N-hydroxysuccinimide (EDC/NHS) was followed by a 5-minute injection of the diluted anti-GST antibody. The flow cells were then deactivated with a 7-minute injection of ethanolamine. A 3-minute injection of recombinant GST was then added to the flow cells. Capturing recombinant GST serves two purposes: (1) it serves as a reference for analysis of peptides through Fc2, and (2) it blocks high-affinity GST sites on the antibody. Due to the fact that the

polyclonal anti-GST antibody contains sites that would normally be difficult to regenerate, blocking of high-affinity sites is necessary. Fc2 is then regenerated with a 2-minute injection of regeneration solution (10 mM glycine-HCl, pH 2.1), leaving Fc1 as a reference cell and allowing Fc2 to be the peptide analysis flow-through channel.

Binding Assays

Subsequent GST-fusion protein capture and peptide analysis was first carried out in 50 mM Tris, pH 8.5 buffer. Sensor chip regeneration was carried out in 2-minute injections of regeneration solution, and GST-fusion protein capture was performed in 15 μL injections of GST-fusion protein samples in Tris-HCl buffer, pH 8.15. Peptide analyte α-Trp502/Met506 was initially assayed against immobilized GST-(α Trp502/Met506), GST-(β Ser 312), and GST-(γ Lys364) at serial dilution concentrations of 97.0, 48.5, 24.2, 12.1, and 6.1 μg/mL; subsequent α-Trp502/Met506 peptide concentrations were 30.0, 15.0, 7.5, 3.8, and 1.9 μg / mL. Peptide analyte β Ser312 was initially assayed against the same immobilized proteins at concentrations of 48.0, 24.0 12.0, 6.0, and 3.0 μg / mL; subsequent β Ser312 peptide concentrations were 51.0, 25.5, 12.8, 6.4, and 3.2 μg / ml. Note that even though β Ser 84 was a peptide aimed for study in this project, it was not utilized for the assays. Analytes α-Trp502/Met506 and β–Ser 312 were assayed against immobilized GST-(γ Lys364) as a means of furthering the data collected in this study. Because the GST-(γ Lys364) analyte was predicted to interact with β Ser 84, β Ser 312 was used as a means of validating its possible electrostatic interactions with GST-(γ Lys364). It was predicted that analyte α–Trp502/Met506 would exhibit weaker binding kinetics because of the aimed-for

amino acid electrostatic properties.

A second binding assay was performed in a manner similar to the first. However, in this second analysis, immobilization injections of GST-fusion proteins were twice repeated. In other words, after regenerating the CM5 chip for re-immobilization of a GST-fusion protein, the GST-fusion protein was injected a total of three times (i.e. 15 μL of GST-(α Trp502/Met506), followed by a second 15 μL injection, followed by a third). This triple-injection was performed as a means of capturing more GST-fusion protein on the sensor chip surface with the hopes of providing more pronounced interactions within the sensorgram data.

A third binding assay was performed by adding 0.4 M NaCl to peptide samples. Previous SPR studies used buffers that contained this high concentration of salt [50]. However, initial SPR studies within this project did not contain salt in buffers nor samples.

CHAPTER III

RESULTS AND DISCUSSION

The goal of this project was to further understand what intersubunit contacts are necessary for ENaC's structure. Initial investigations of subunits regions that may stabilize ENaC structure were directed by analysis of the homological model of ENaC, the chicken acid sensing ion channel. Candidate peptide regions were chosen on the basis of 3 criteria: (1) their relative proximity to the opposing subunit, (2) their relative directionality of side-chain groups in the secondary structure, and (3) potential electrostatic interactions with the opposing side chain [50]. Peptides containing amino acids from the α and β subunits were expressed as GST-fusion proteins, and these proteins were then analyzed for binding kinetics via SPR.

Plasmid Verification and PCR

To begin the project, pSWICK plasmids containing α, β, and γ ENaC genes were verified via agarose electrophoresis (**Figure 9**). All three plasmids were confirmed by the presence of DNA fragments near the appropriate kilobase marker. Following this verification was the amplification of DNA segments for the targeted amino acid regions of the ENaC subunits via PCR. Each PCR segment (each near 100 bases in length) appeared just slightly above the 100 bp ladder marker (**Figure 10**). As a means of verification for using the correct plasmids, controls were performed by amplification of ENaC segments used in previous research [50]; appropriate PCR products were formed according to the primers and plasmids used—that was, an 81-bp DNA fragment appeared

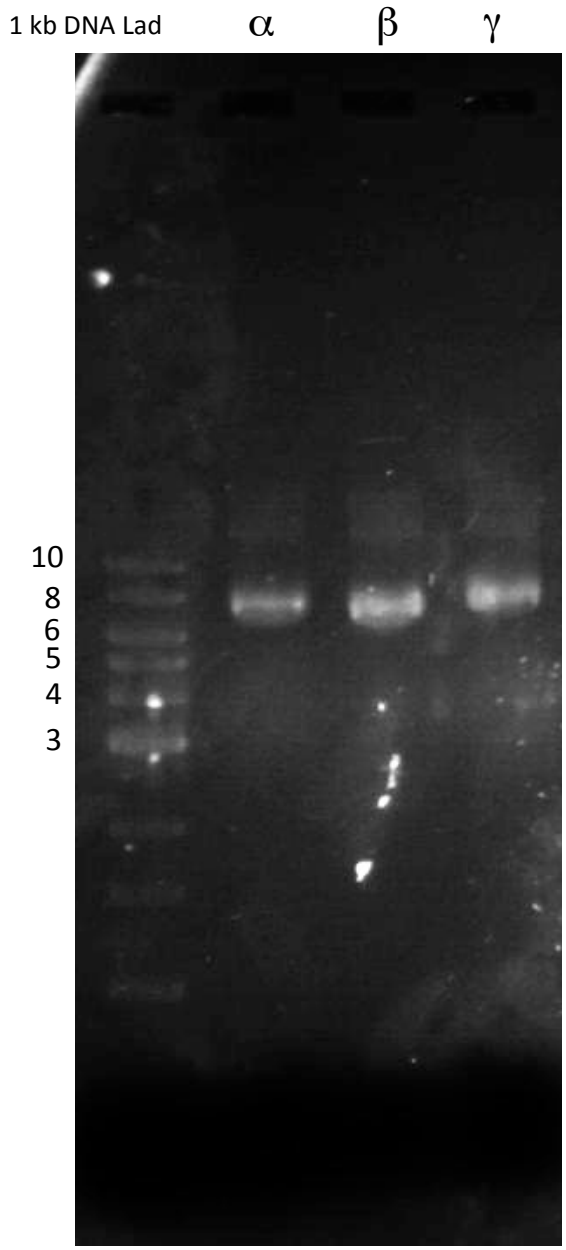

Figure 9. Agarose Gel Electrophoresis To Check For Presence Of Correct Plasmid. Shown on the left is a 1% agarose gel run at 110 volts for 70 minutes. The DNA fragments are indicative of the presence of pSwick plasmids that each contain their respective ENaC alpha, beta, and gamma plasmids.

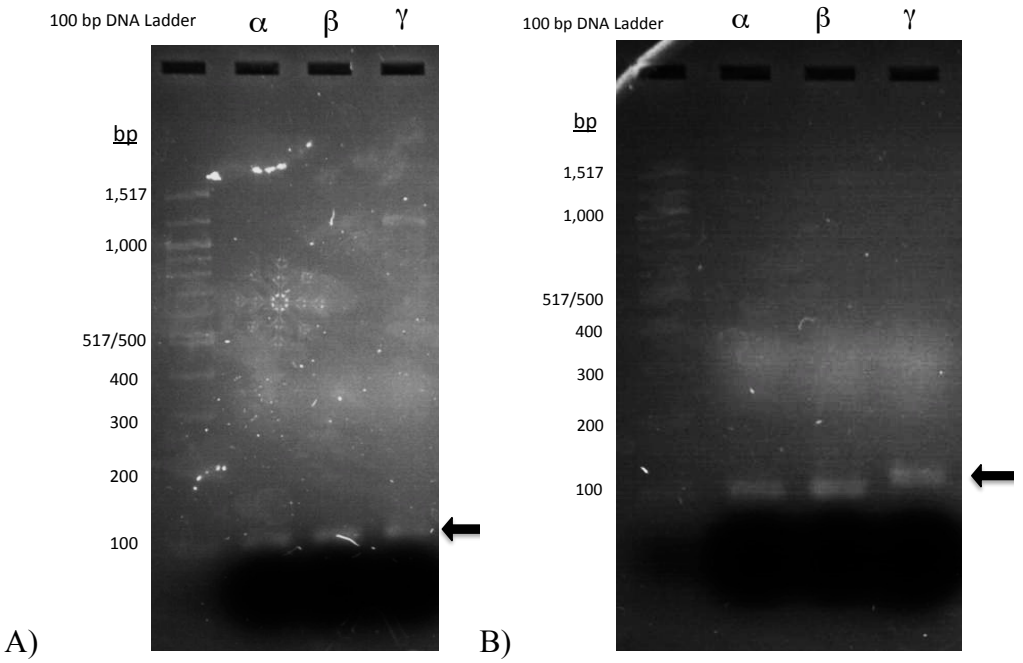

Figure 10. Agarose Gel Electrophoresis To Check For PCR Product. PCR was used to amplify segments of DNA containing the targeted amino acids. A) DNA fragments appear at the appropriate location for each plasmid's PCR-amplified segment, showing that a near-100 base strand was present. B) As further verification that the elongated segments were the targeted segments, template DNA (α N285, β E438, γ Q444) from previous research was used as a control [50].

slightly above the 100 bp ladder mark for the α control, an 84-DNA fragment appeared slightly above the 100 bp mark and α DNA fragment for the β control, and a 96-bp DNA fragment appeared above both the α and β DNA fragments (**Figure 10**). The PCR products were then cleaned with the Wizard® SV Gel and PCR Clean-Up System, digested with BamHI and NotI, and stored at -20 º C until ligation.

GST plasmid (pGEX-4T-2) Preparation - Digestion and Dephosphorylation

The pGEX-4T-2 plasmid containing GST was digested with restriction enzymes BamHI and NotI, initially removing an unrelated gene, hQC, from the rest of the plasmid (**Figure 11**). Removal of the 5'-terminal phosphate group was performed with antarctic phosphatase, after which an agarose gel was run. The appearance of two DNA fragments near the 5 kb and 0.5 kb marks indicated proper digestion occurred (**Figure 11**). Subsequent excision and cleanup of the pGEX-4T-2 portion from the gel was carried out according to the Wizard® SV Gel and PCR Clean-Up System protocol.

Ligation and Sequencing

The PCR product that was also previously digested with BamHI and NotI containing the targeted ENaC segment was then ligated with the digested pGEX-4T-2 using T4 DNA Ligase. The ligated plasmid was then transformed into Top10 *E. coli* cells, and these cells were grown overnight in an LB/ampicillin solution, followed by plasmid isolation via the QIAGEN plasmid isolation kit. Attempts at digesting ligated plasmids with restriction enzymes for ligation verification did not provide enough evidence to suggest the ligations were successful—that is, DNA fragments appeared

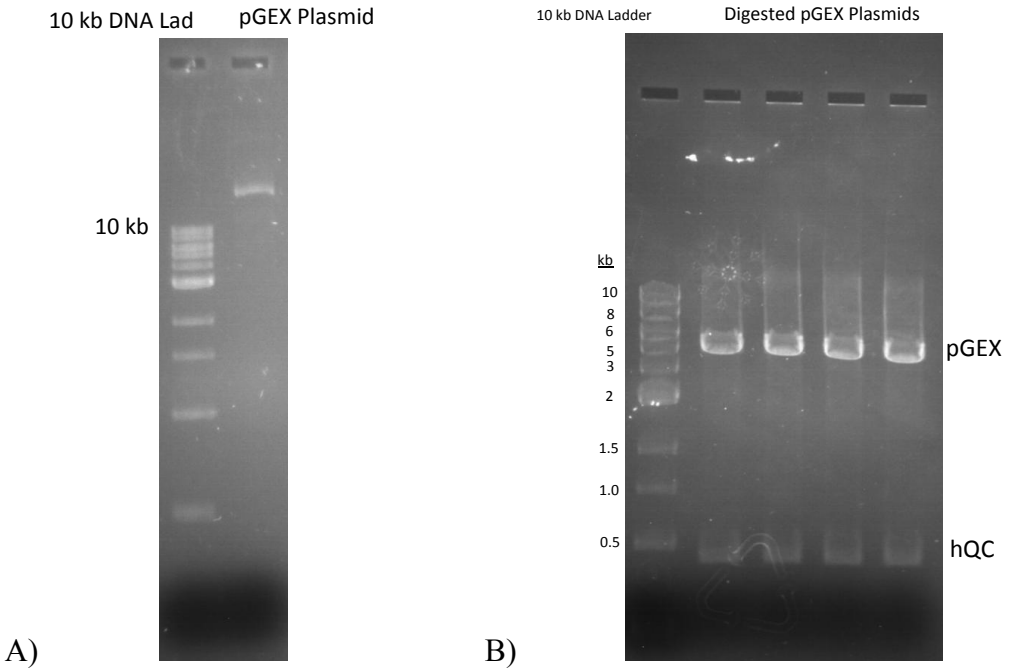

Figure 11. pGEX-4T-2 Plasmid Verification And Digestion With BamHI And NotI. Shown above are the gels run in order to verify (and subsequently excise) the GST plasmid being used for production of a GST-fusion protein. A) An agarose gel showing the presence of the pGEX-4T-2 plasmid embedded with hQC. B) An agarose gel showing the separation of hQC from the rest of the pGEX plasmid after digestion with BamHI and NotI.

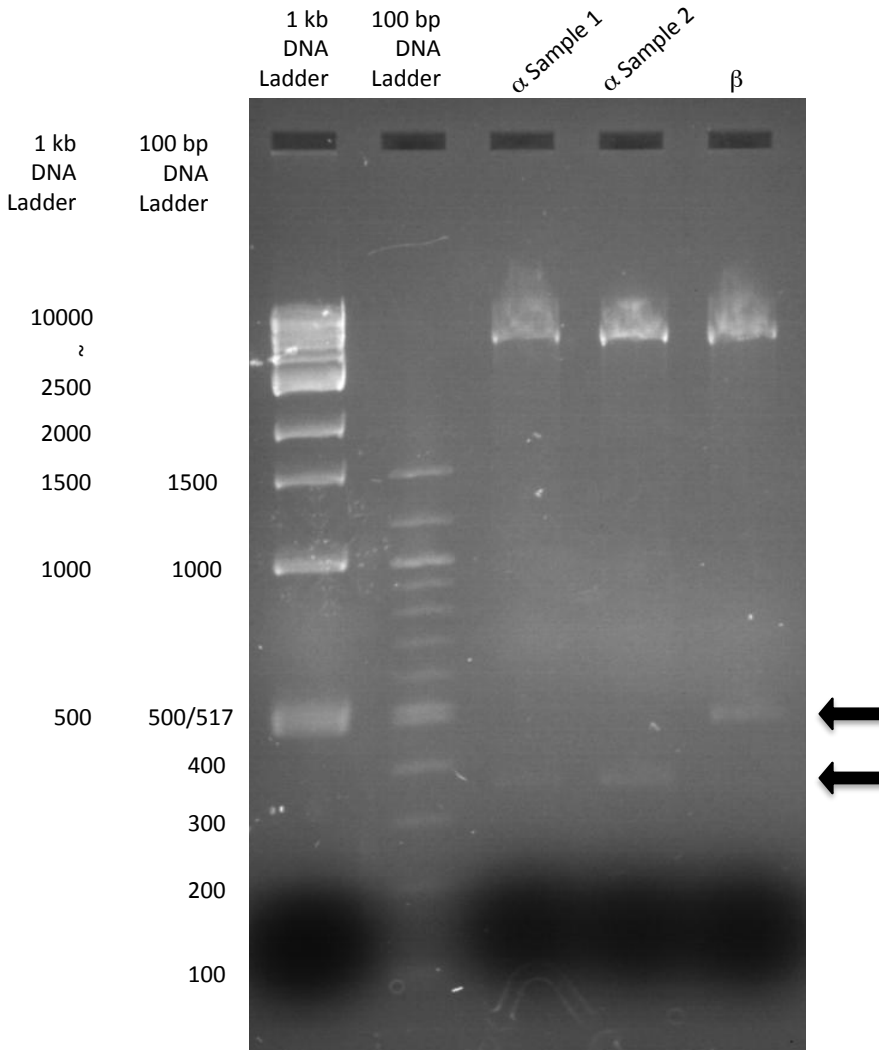

Figure 12. Post-Ligation And Cloning Verification With BamHI And ZraI. To verify whether the ligation reactions worked, restriction enzymes BamHI (cuts at bp #930) and ZraI (cuts at bp #1244) were used to cut transformed and isolated plasmid. One can note the appearance of DNA fragments near the 400 and 500 bp mark. The α ligated plasmid was predicted to show a signal near 384 bp. However, due to the fragment near the 500 mark for the β sample, this gel was deemed inconclusive (the β ligation should only have 3 base pairs more than α).

under the 400 bp and near the 500 bp marks, even though the ligation with β PCR products only differed from the α PCR products by 3 base pairs (**Figure 12**). After ligation, transformation, and isolation of each (pGEX-4T-2-αENaC-W502M506, pGEX-4T-2-βENaC-S312, pGEX-4T-2-γENaC-K364) plasmid, verification of successful ligation was observed through sequencing (**Figure 13**).

```
Seq         GCAGTCCGGCTCCTCACATCGGATCTGGTTCCGCGTGGATCCTACTCACGATGGCCCTCG
Alpha       ----------------------------------------TACTCACGATGGCCCTCG
                                                    ******************

Seq         GTGACATCCCAGGAATGGGTCTTCCAGATGCTATCGCGACAGAACAATTACACCGTCAAC
Alpha       GTGACATCCCAGGAATGGGTCTTCCAGATGCTATCGCGACAGAACAATTACACCGTCAAC
            ************************************************************

Seq         AACGCGGCCGCATCGTGACTGACTGACGATCTGCCTCGCGCGTTTCGGTGATGACGGTGA
Alpha       AAC---------------------------------------------------------
            ***
```

Figure 13. Verification Of Elongated Peptide Segment Ligation. Shown above is sequencing data received from Quintara Biosciences, a company based in California that provides sequencing services, aligned with the peptide sequence that should be present had ligation reactions of pGEX vector with PCR-amplified segments worked. Provided for by Clustal Omega, the sequence shown above displays the alignment of the DNA segment that was elongated with PCR, ligated, and sequenced via Quintara Biosciences with the sequence of the targeted "Alpha" peptide. Not entirely shown, but as can be noticed following the alignment, is the sequence that follows the pGEX plasmid, including the restriction sites for BamHI and NotI. This alignment verified that the ligation reactions were successful. Not shown, but equally as effective, were the reactions confirming correct insertion in plasmids for the β and γ subunits.

Transformation and Expression

Following the ligation reaction, the pGEX-4T-2-αENaC-W502M506, pGEX-4T-2-βENaC-S312, and pGEX-4T-2-γENaC-K364 plasmids were then transformed into BL21 *E. coli* cells in order to express proteins. For expression, transformed cells were grown overnight in an 5 mL LB/ampicillin solution, of which 1.25 mL of overnight solution would then be transferred to 2X-YTG expression media. Cells were incubated at

37 ºC for in a 225 rpm shaker for 3 hours. Protein expression was induced by adding 0.1 mM IPTG (final concentration) and by allowing the cells to incubate for 3 additional hours. The cells were then pelleted by centrifugation, resuspended in PBS, and lysed open via freeze/thaw cycles. DNase and $MgCl_2$ were added to final concentrations of 2 µg / mL and 20 µM, respectively. The cells were then incubated at 37 ºC for 30 minutes and recentrifuged. The supernate (cell extract) was then collected and used to purify the expressed GST-fusion proteins. Glutathione agarose was added to the cell extract to bind GST-fusion proteins, and these proteins were then removed from the glutathione agarose resin using reduced glutathione through column chromatography. SDS-PAGE analysis of cell extract and purified samples indicated that GST-fusion protein was partially "purified" (**Figure 14**). However, the appearance of two proteins post-purification of

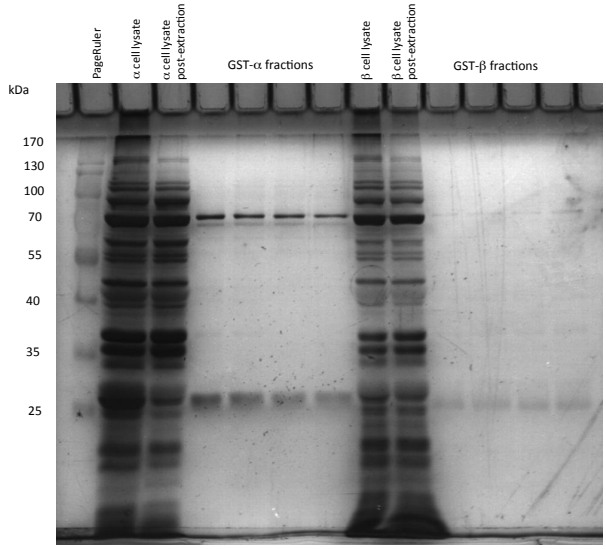

Figure 14. GST-Peptide Expression And Purification. Shown to the left is an SDS-PAGE gel of each step along the purification scheme of the GST-fusion proteins. Following the ladder, the gel contains a lane for the α cell lysate, another lane for the same cell lysate post-GST-purification, and 4 lanes of fractions that contained the purified a GST-fusion proteins. This pattern repeats for the next four lanes for the beta peptide. Naturally, one would expect to find only one protein near the 25 kDa ladder mark, but as can be seen, that was not the case. Western blot revealed that the upper protein marker was an aggregation of GST-fusion proteins (**Figure 20**).

GST-fusion proteins raised a question as to whether the proteins were GST trimers or were co-eluting through the column with DnaK, a protein which troubleshooting guides note that may co-elute with GST. Re-expression was performed on both α and β samples in order to eliminate possible human error, but upper protein markers still remained (**Figure 15**). Initial SDS-PAGE samples were not heated prior to running, but heating samples before running on an SDS-PAGE still presented upper protein markers (**Figure 16**). According to a Biontex GST Agarose Troubleshooting guide, treating cell lysates with 10 mM $MgSO_4$ and 5 mM ATP should have eliminated the presence of the upper protein markers had they been DnaK, a protein that tends to co-elute with GST proteins using agarose purification methods. When α cell lysates were treated with 10 mM $MgSO_4$ and 5 mM ATP, however, protein intensities increased. This suggested that the upper protein markers were not DnaK (**Figure 17**). Blue native PAGE gels were run, but remained inconclusive due to the appearance of smears on the gels (**Figure 18**). As a possible means of eliminating the upper markers, Centricon filters with a 100 kDa nominal molecular weight limit (NMWL) were used on "purified" samples, but upper protein markers remained following centrifugation (**Figure 19**). Western blot analysis revealed that the upper proteins were indeed GST (**Figure 20**). A second SDS-PAGE was then performed on the GST-fusion protein samples. This time, however, the sample buffer included dithiothreitol (DTT) instead of β-mercaptoethanol (BME) (**Figure 21**). This suggested that the trimerization of GST-fusion proteins was the possible result of a contaminated BME stock solution or was an artifact of running the samples with BME itself. DTT is helpful in regards to the fact that DTT is a permanent reducer, whereas BME is a reducer that performs its mechanism via an equilibrium reaction. Upon

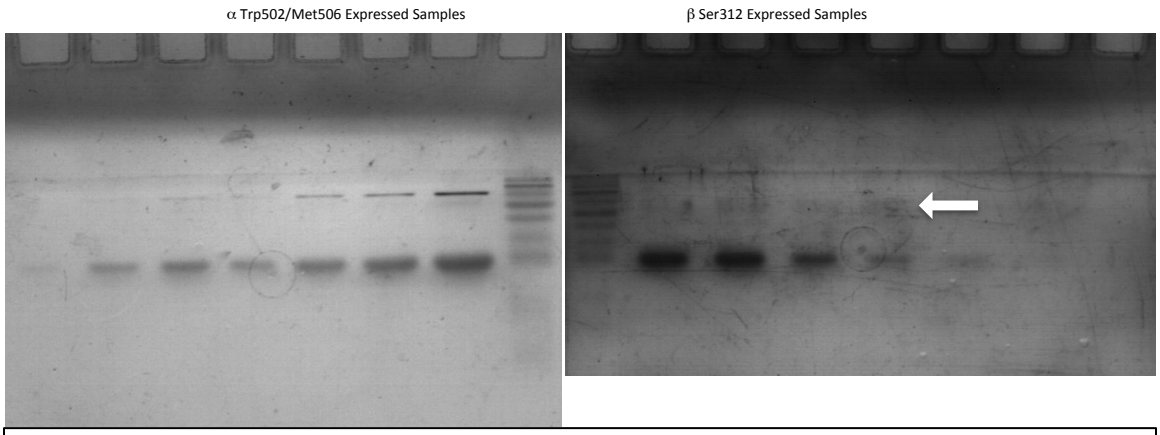

Figure 15. Both Alpha And Beta Expressed GST-Fusion Proteins Presented Upper Protein Markers. Shown above are re-expressions of GST-fusion proteins (left gel is alpha, right gel is beta). In order to eliminate possible human error, re-expressions were performed as a means of verification. However, upper proteins remained.

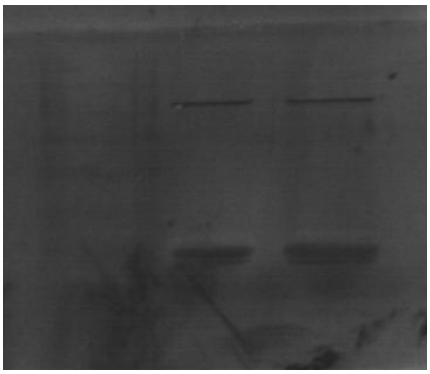

Figure 16. Heated SDS-PAGE Samples Still Showed Upper Protein Markers. Alpha expressed GST-fusion proteins that were properly heated prior to running SDS-PAGE still exhibited upper protein markers.

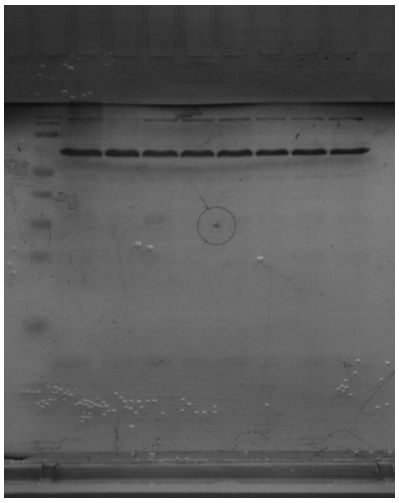

Figure 17. Treating With 10mM $MgSO_4$ And 5 mM ATP Did Not Eliminate Upper Protein Markers. According to a Biontex GST Agarose Troubleshooting guide, treating cell lysates with 10mM $MgSO_4$ and 5 mM ATP should have eliminated upper proteins had they been DnaK, a protein that tends to co-elute with GST proteins using agarose purification methods. When alpha cell lysates were treated with 10mM $MgSO_4$ and 5 mM ATP, it strengthened the upper proteins rather than eliminating them. This revealed that the upper proteins were not DnaK.

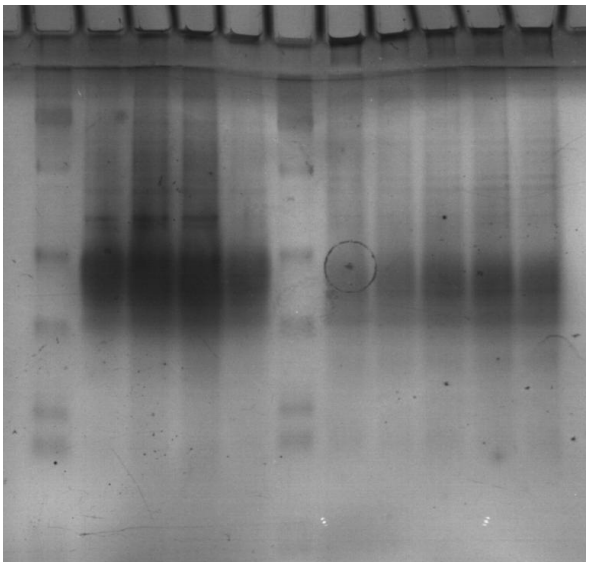

Figure 18. Blue Native Page Was Inconclusive Concerning Previously Observed Upper Protein Markers. A blue native PAGE with nondenaturing conditions was run in order to elucidate more information about the upper proteins present on previous SDS-PAGE gels. Results, however, were inconclusive.

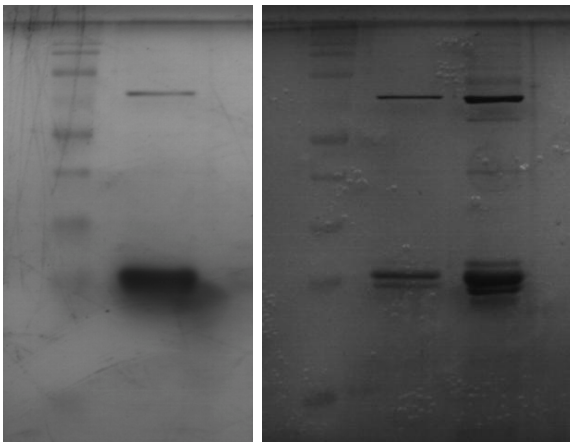

Figure 19. Centricon Filtration Did Not Eliminate Upper Protein Markers. Glutathione agarose "purified" samples were spun with a 100 kDa nominal molecular weight limit (NMWL) Centricon filter at 7500 × g for 20 minutes. After centrifugation, gels revealed that upper proteins were still present in solution, suggesting that upper protein markers were GST-fusion protein trimers.

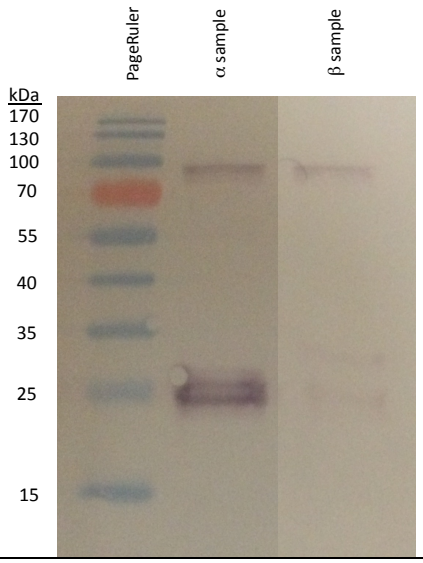

Figure 20. Western Blot For Analysis Of Upper Protein Markers Appearance Post-Purification. The appearance of two proteins post-purification of GST-fusion proteins raised a question as to whether the proteins were co-eluting through the column with DnaK, a protein which troubleshooting guides note that may co-elute with GST. Western blot analysis revealed that the upper protein markers were indeed GST.

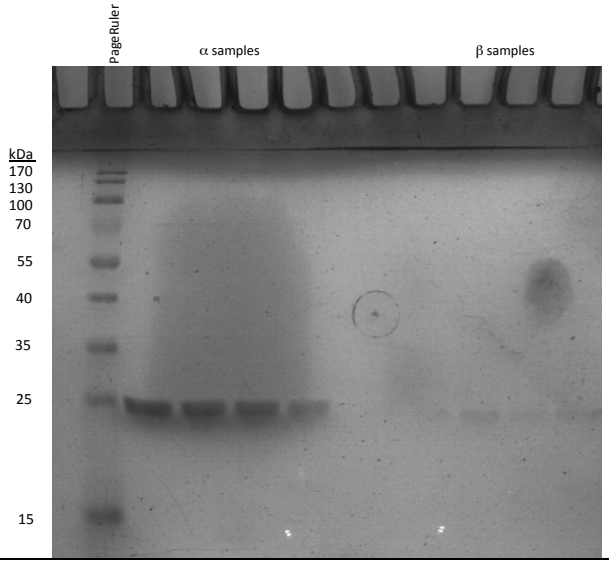

Figure 21. SDS-PAGE Using DTT As A Reducer. A second SDS-PAGE was performed on the GST-fusion protein samples. This time, however, the sample buffer used included dithiothreitol (DTT) instead of β-mercaptoethanol (BME). This suggested that the trimerization of GST-fusion proteins was the possible result of a contaminated BME stock solution or was an artifact of running the samples with BME itself. DTT is a permanent reducer, whereas BME is a reducer that performs its mechanism via an equilibrium reaction.

identification and rectification of this anomaly, peptides were then separated from their GST portion via a thrombin cleavage and verified via the presence of weak signal under the 10-kDa mark (**Figure 22**). These were the result of concentrating protein fractions following the thrombin removal of the GST-peptide cleavage reactions. Once peptides were visualized, proteins concentrations were found via BCA assay (see sensorgrams for specific concentrations of analyzed peptides). Interactions between (α-W502/M506 and β-S312) peptides and (α-W502/M506, β-S312, and γ-K364) GST-fusion proteins were measured via SPR analysis. The α-W502/M506 GST-fusion protein would be immobilized, and its interactions with the α-W502/M506 and β-S312 peptides would be measured. Then, the β-S312 GST-fusion protein replaced the α-W502/M506 GST-fusion protein and had its interactions measured against α-W502/M506 and β-S312 peptides. These same interactions were then measured against the γ-K364 GST-fusion peptide (**Table 3**).

Table 3. Interactions Analyzed Using BIAcore X. GST-fusion proteins containing the indicated amino from the left column were immobilized, and GST-fusion proteins from the right column had their GST-tag cleaved and removed from solution. The remaining peptide was then analyzed against the immobilized GST-fusion protein.

GST – Immobilized	Peptide
α W502/M506	α W502/M506
	β S312
β S312	α W502/M506
	β S312
γ K364	α W502/M506
	β S312

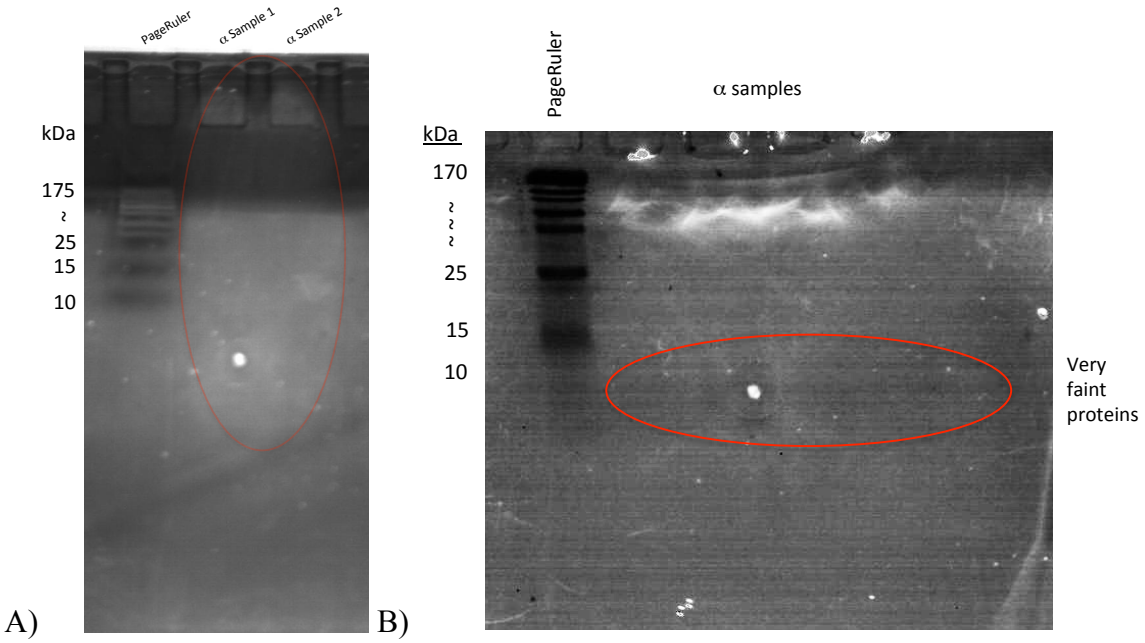

Figure 22. Verification Of GST Cleavage From Peptides. High percentage gels were run for the detection of cleaved peptides from GST. A) Initial eluted peptide samples contained 0.4 M NaCl in their elution buffer. However, when samples were run on a high-percentage gel to check for the presence of cleaved peptide, staining solution left a yellow smear along the lanes. B) An 18% SDS-PAGE revealing the GST-cleaved peptides post-thrombin cleavage and removal followed by a protein concentration. This particular set of peptide elutions did not contain NaCl in their elution buffer. Though difficult to see in the image, Coomassie Blue staining revealed the presence of peptides. It is believed that, due to the size of the protein (only being a 30-amino acid protein after having its GST portion removed), Coomassie staining was unable to effectively interact with proteins. Attempts at silver staining gels also proved ineffective, and the fact that proteins were extremely dilute also caused trouble for Coomassie Blue interaction.

SPR Preparation and Analysis

Preparation of a new CM5 sensor chip was carried out according to manufacturer protocol—that was, immobilization of anti-GST antibody exhibited the same response as

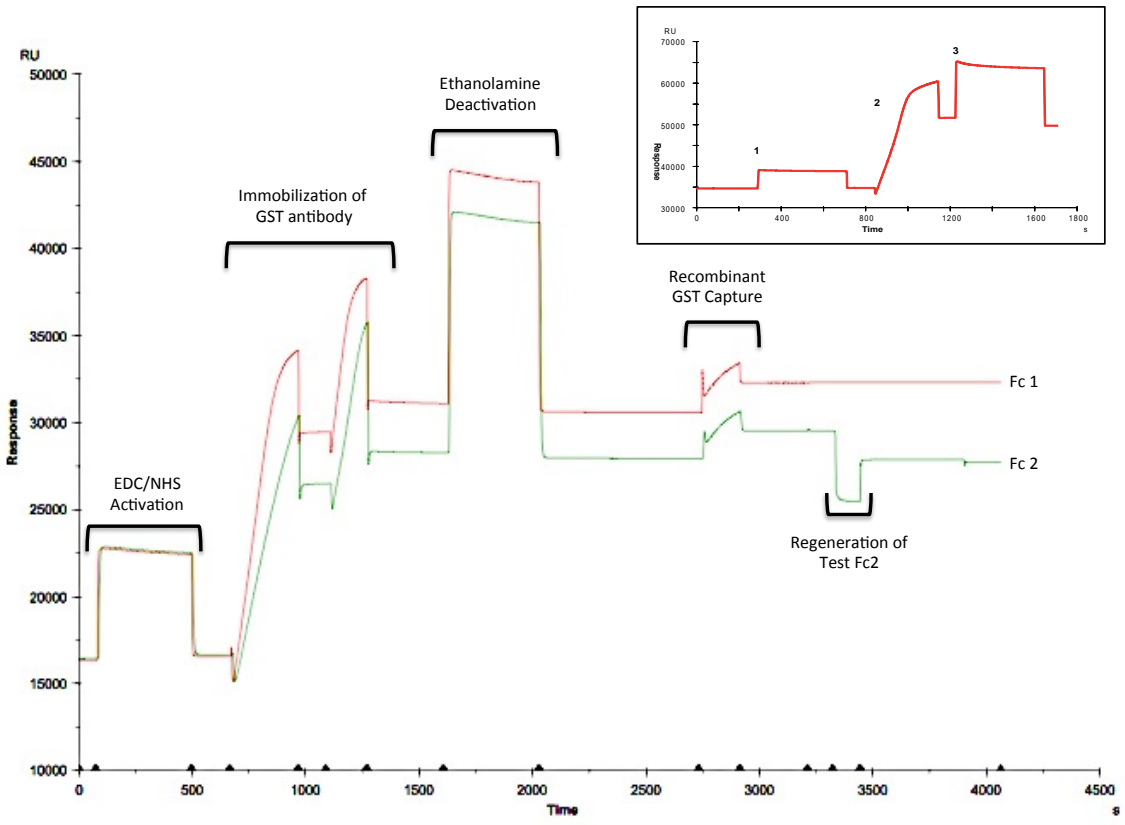

Figure 23. Capture Of Anti-GST Antibody. Shown above is the sensorgram generated by the BIAcore upon preparation of a new CM5 chip. To initiate studies for GST-fusion proteins, a GST antibody must first be immobilized onto the CM5 sensor chip as a means of immobilizing those GST fusion proteins (**Figure 9**). Anti-GST was captured on the CM5 chip per the protocol described in the GE Healthcare Life Sciences GST Capture Kit (Instruction 22-0522-19 AG). The additional figure shown above is an image taken from the GST Capture Kit Manual, which describes what should be seen when preparing a new sensor chip. Labeled "1" is the response that should be seen for sensor chip activation with 1:1 solution of 1-Ethyl-3-(3-dimethylaminopropyl)-carbodiimide and N-hydroxysuccinimide (EDC/NHS). EDC serves as crosslinking agent for coupling carboxyl groups to primary amines, and NHS serves to stabilize the activated chip. Labeled "2" is the response that should be seen when injecting GST antibody into the flow cell, and the response labeled "3" is what should be observed with deactivating the sensor chip with ethanolamine. Notably, the same responses were observed when preparing the sensor chip for this study. Additionally shown is the capture of recombinant GST and regeneration of flow cell (Fc) 2. Capturing recombinant GST serves two purposes: (1) it serves as a reference for analysis of peptides through Fc2, and (2) it blocks high-affinity GST sites on the antibody. Due to the fact that the polyclonal anti-GST antibody contains sites that would normally be difficult to regenerate, blocking of high-affinity sites is necessary. Regeneration of Fc2 is necessary for analyzing partnering peptides.

indicated in the GE GST Capture Kit manual (**Figure 23**). The generated sensorgram was representative of the sensorgram shown in previous research, indicating the same successful preparation of the sensor chip [50]. The proper responses were then observed when capturing recombinant GST in both flow cells. The regeneration of flow cell (Fc) 2 for analysis of GST fusion proteins and peptides followed recombinant GST capture.

The first series of assays involved capturing GST-fusion proteins with single injections into the flow cell being used for analysis. Initial attempts to immobilize diluted GST fusion proteins onto the sensor chip exhibited minimal response. When undiluted samples were injected, however, a notable change in response units was observed. This indicated that an appreciable amount of GST fusion protein was then immobilized onto the sensor chip surface (**Figure 24)**. Flow cell 2 was regenerated, and GST-(α W502/M506) was immobilized (**Figure 25**).

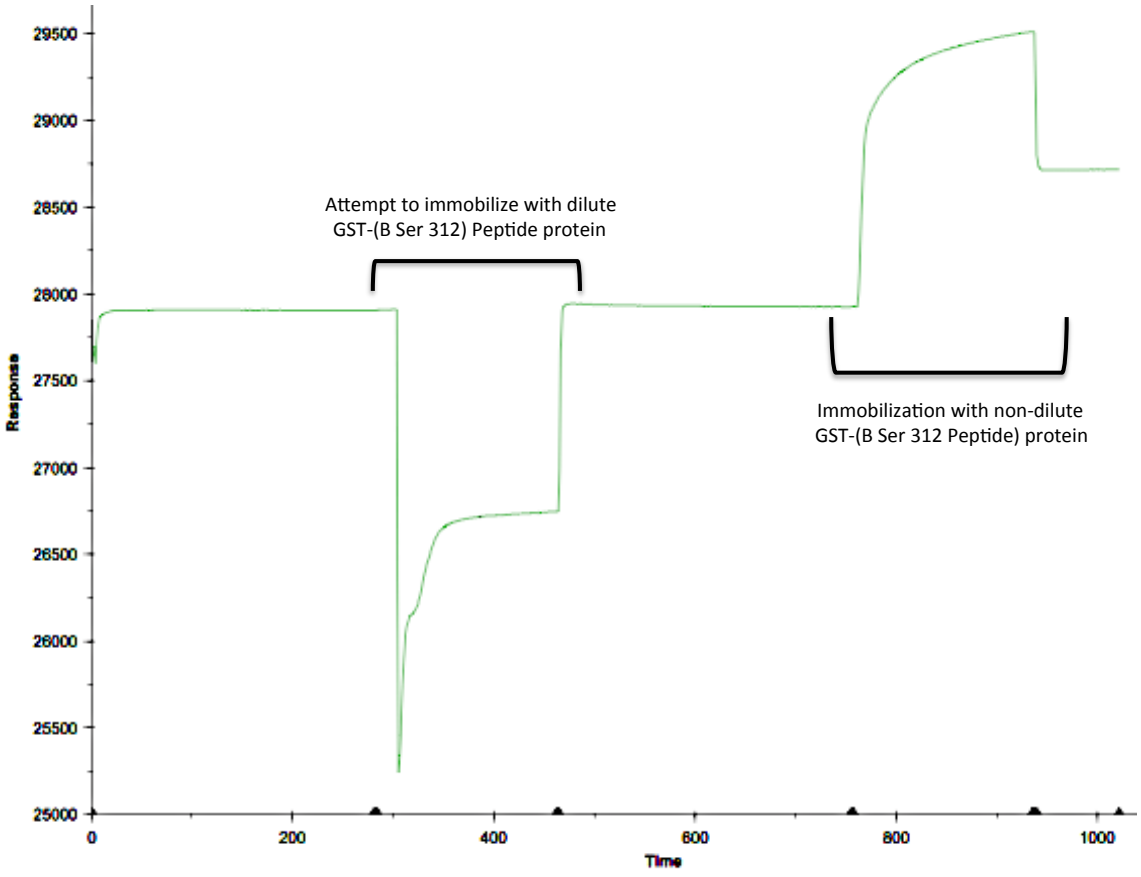

Figure 24. Immobilization Of GST-(B Ser 312) Fusion Protein. Shown above is the sensorgram generated by the BIAcore for the capture of GST-(β Ser 312) fusion protein. Attempts at immobilizing diluted GST-fusion protein generated minimal response (shown near t = 300 s). However, attempts at immobilizing undiluted GST protein exhibited a notable change in response units (shown near t = 800).

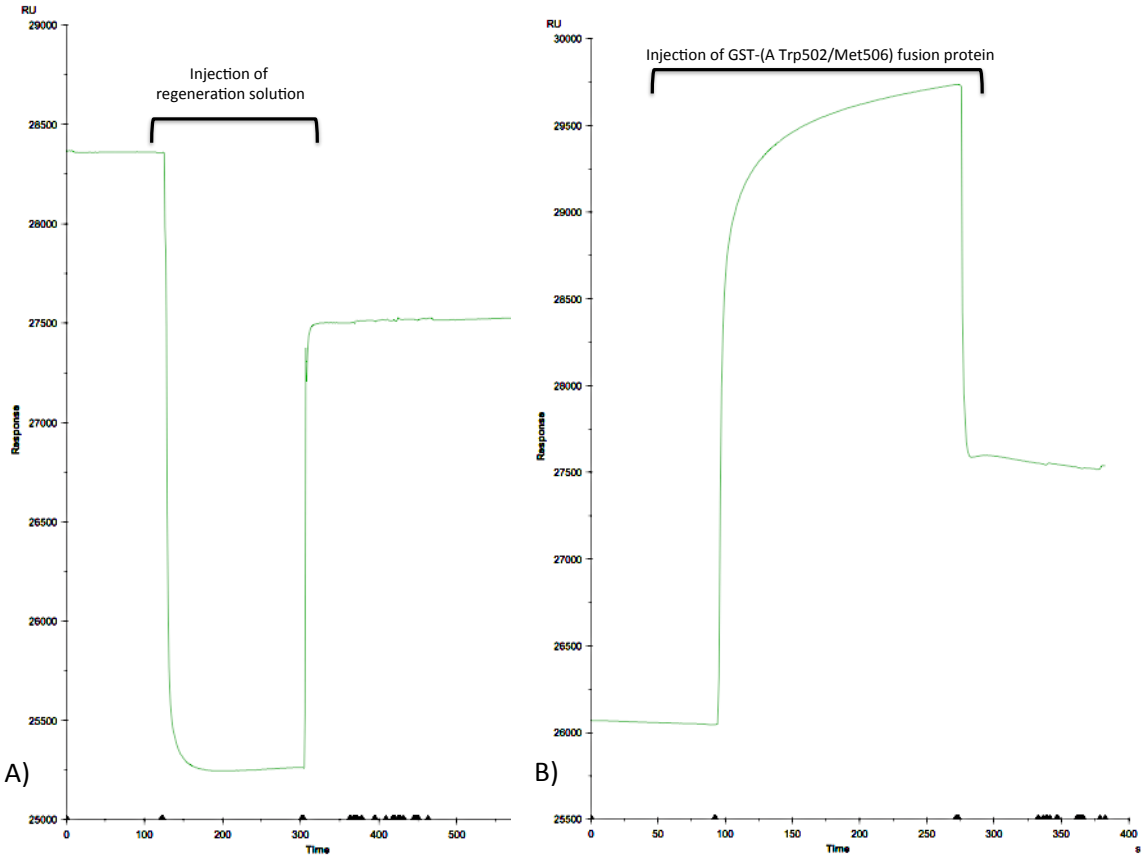

Figure 25. Regeneration Of Sensor Chip Followed By Immobilization. Shown above is the sensorgram generated by the BIAcore for the regeneration of the sensor chip, followed by the subsequent immobilization of the GST-(α Trp502/Met506) fusion protein. A) Similar to the response given in **Figure 23**, regeneration of the flow cell with regeneration solution (10 mM glycine-HCl, pH 2.1) caused decrease in the sensorgram. B) Attempt at immobilization of GST-(α Trp502/Met506) was shown to be successful by the increase in response by the sensorgram. This is the general form of sensorgram generated when the sensor chip is both regenerated (shown by a permanent decrease in response units) and immobilized with new GST-fusion proteins (indicated by a permanent increase in response units).

Peptide β S312 was injected into both flow cells, a correlation in response units and peptide concentration was observed, causing a greater change in response units for peptides that had higher concentrations (**Figure 26 a** and **b**). However, when peptides with lower concentrations were assayed, negative changes in response units were observed. This negative change was believed to be a response to the change in environment between the running buffer and injected samples. Both flow cells exhibited similar changes in response units, and when the reference cell (flow cell 1) response was subtracted from that of the flow cell used for analysis (flow cell 2), higher overall magnitudes of changes in response units were observed for those peptides that had higher concentrations. In other words, there was a greater negative response registered within the sensorgram for peptides with higher concentrations (**Figure 26c**). From this data, it was thought that the β S312 peptide had nonspecific interactions with both recombinant GST and immobilized GST-(α W502/M506). This interaction was deemed to be greater with recombinant GST due to the fact that the reference-subtracted sensorgram showed an overall negative change in response units.

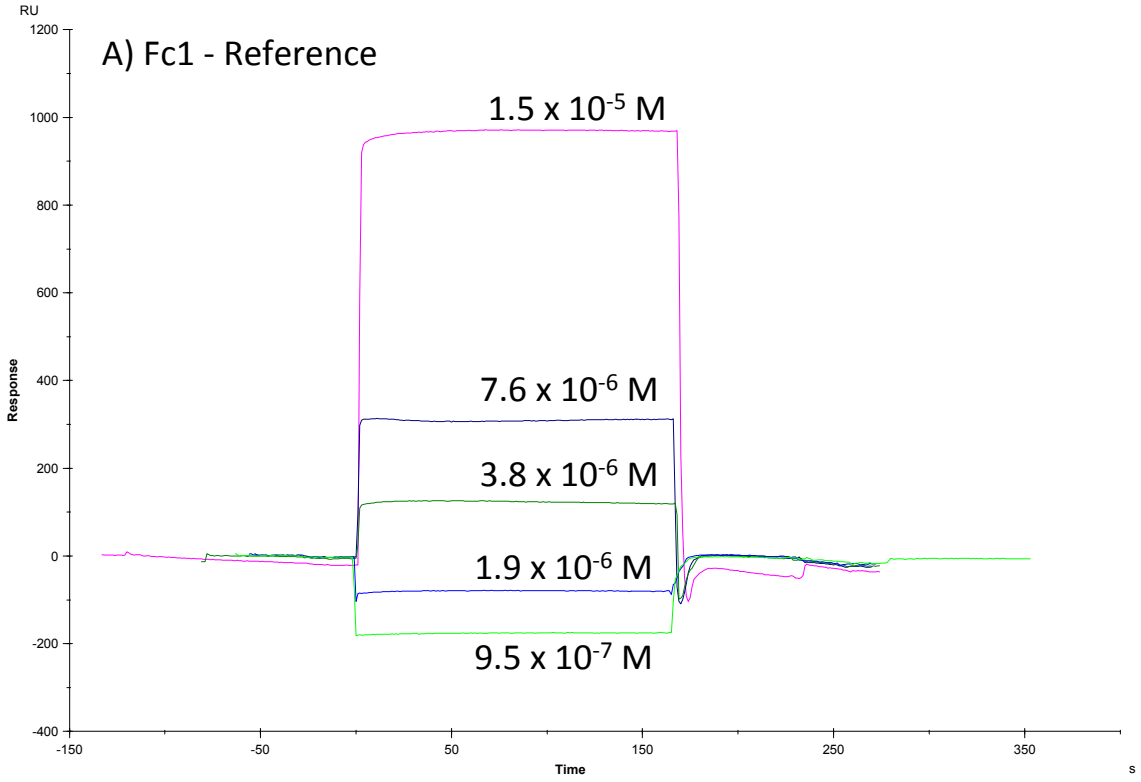

Figure 26. β Ser312 Assay Against Immobilized GST-(α Trp502Met506). A) The sensorgram generated by the injection of peptides into flow cell 1, the reference cell. B) The sensorgram generated by the injection of peptides into flow cell 2, the analyte cell. C) The sensorgram generated by reference-subtracting the reference sensorgram from the analyte sensorgram.

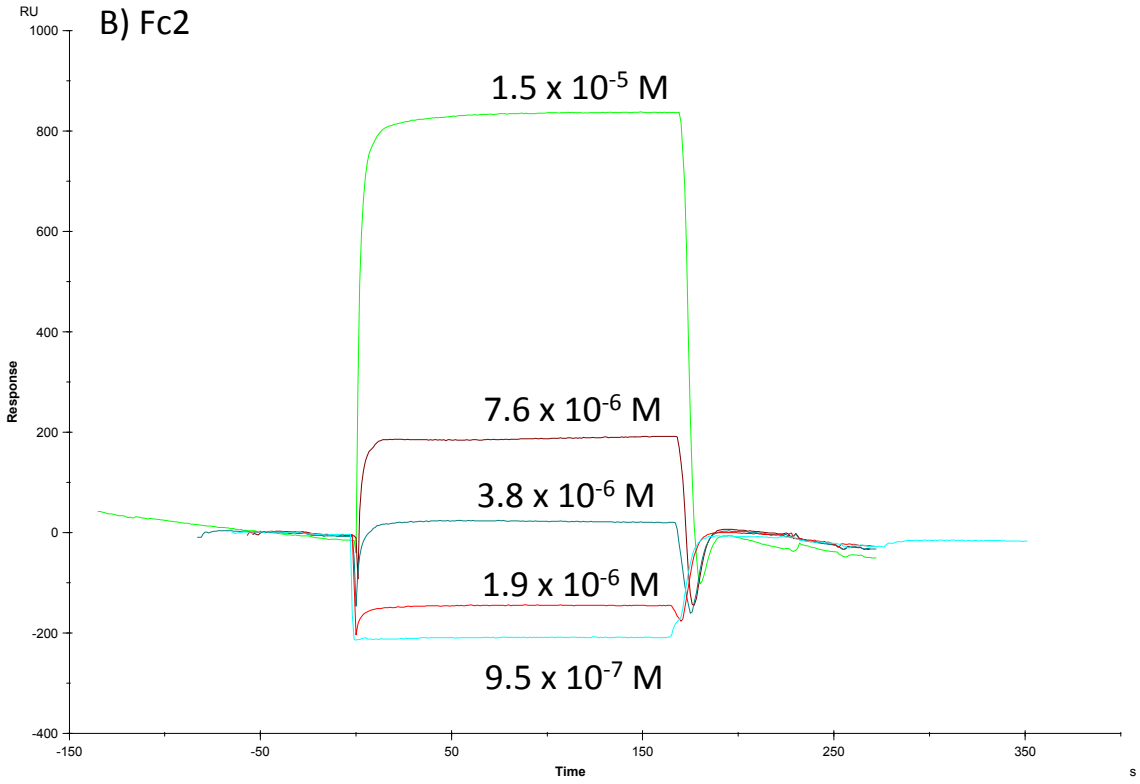

Figure 26, continued.

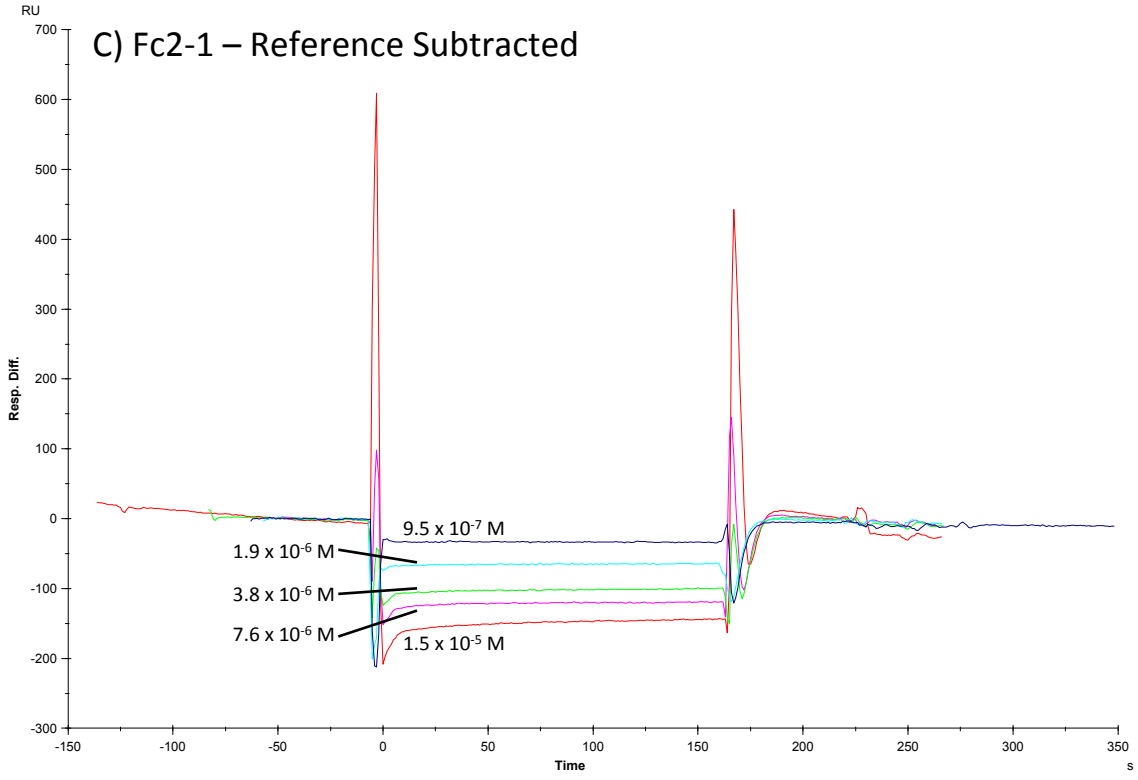

Figure 26, continued

As a negative control, peptide α W502/M506 was also assayed against immobilized GST-(α W502/M506) (**Figure 27**). This particular interaction was predicted to be weaker than that of the interaction between β S312 and immobilized GST-(α W502/M506), but the data collected reflected a similar response. Higher concentrated samples exhibited greater changes in response units, but the interaction between peptide α W502/M506 and recombinant GST was greater than that of its interaction with immobilized GST-(α W502/M506). Because of this, binding kinetics could not be interpreted. Interestingly, the same responses were observed when GST-(β S312) was immobilized and peptides α W502/M506 and β S312 were assayed (**Figures 28** and **29**). Furthermore, this response was also observed when these peptides were assayed against immobilized γ K364 (**Figures 30** and **31**).

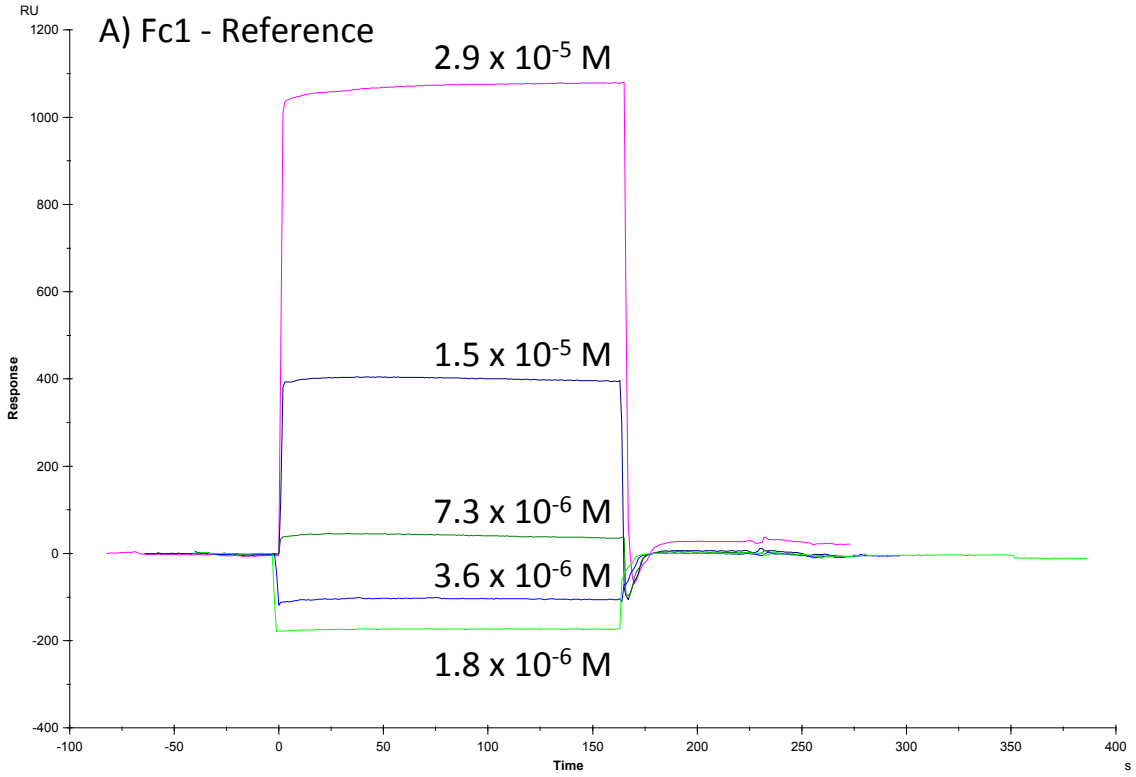

Figure 27. α Trp502Met506 Assay Against Immobilized GST-(α Trp502Met506). A) The sensorgram generated by the injection of peptides into flow cell 1, the reference cell. B) The sensorgram generated by the injection of peptides into flow cell 2, the analyte cell. C) The sensorgram generated by reference-subtracting the reference sensorgram from the analyte sensorgram.

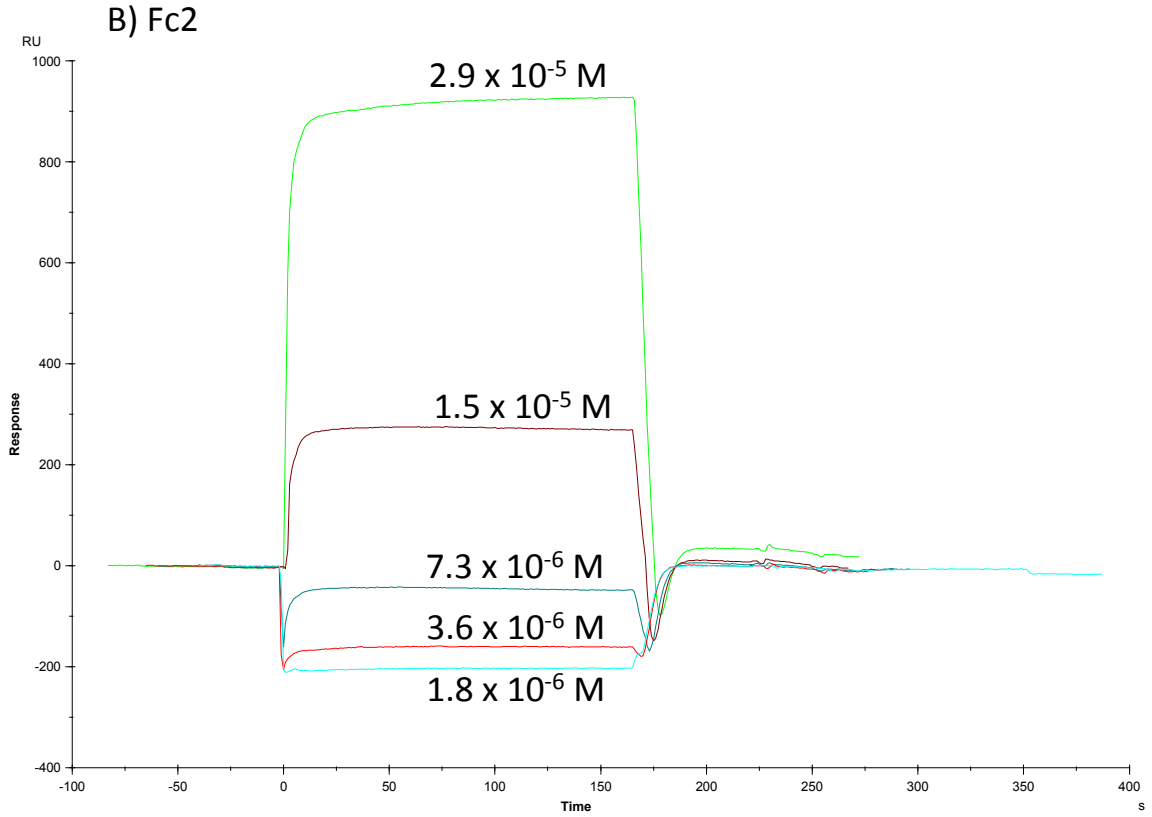

Figure 27, continued.

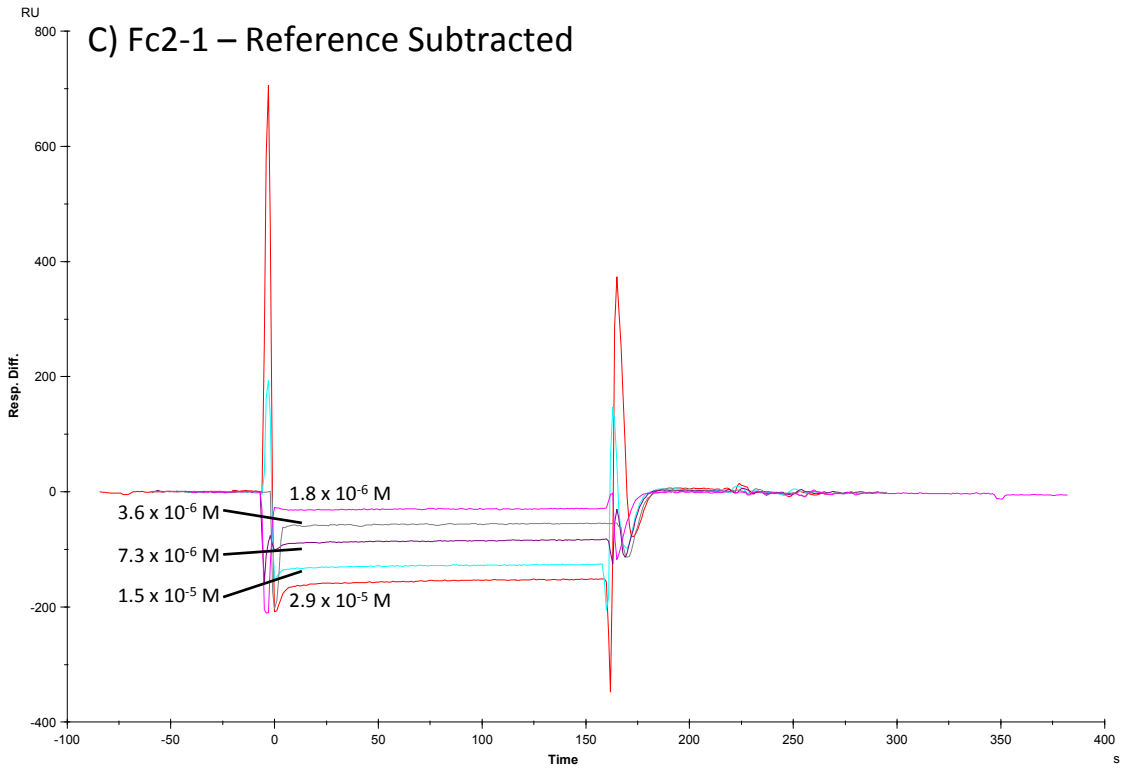

Figure 27, continued.

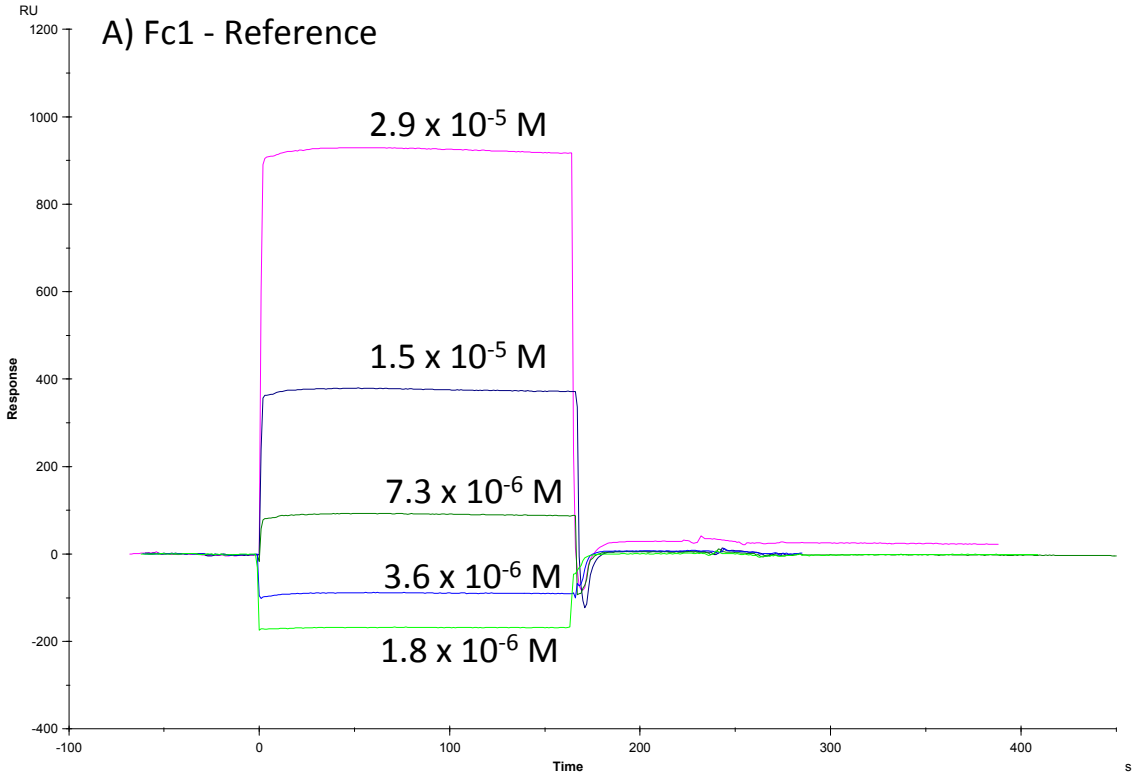

Figure 28. α Trp502Met506 Assay Against Immobilized GST-(β Ser312). A) The sensorgram generated by the injection of peptides into flow cell 1, the reference cell. B) The sensorgram generated by the injection of peptides into flow cell 2, the analyte cell. C) The sensorgram generated by reference-subtracting the reference sensorgram from the analyte sensorgram.

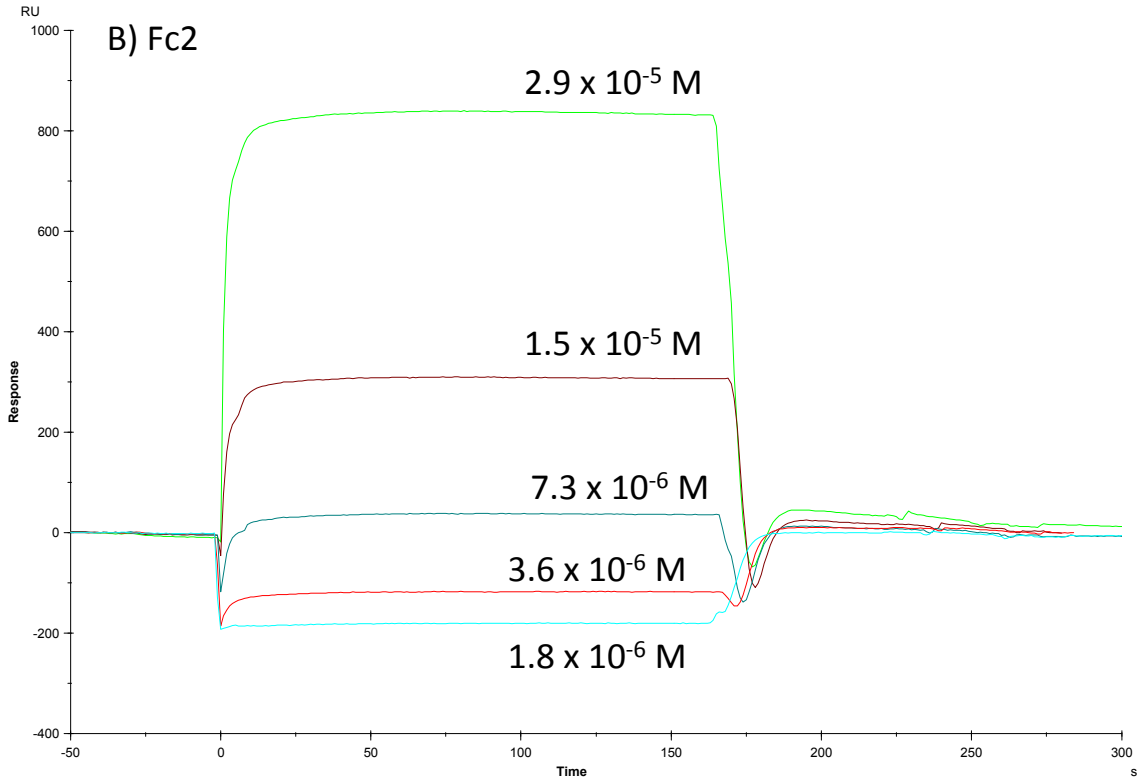

Figure 28, continued.

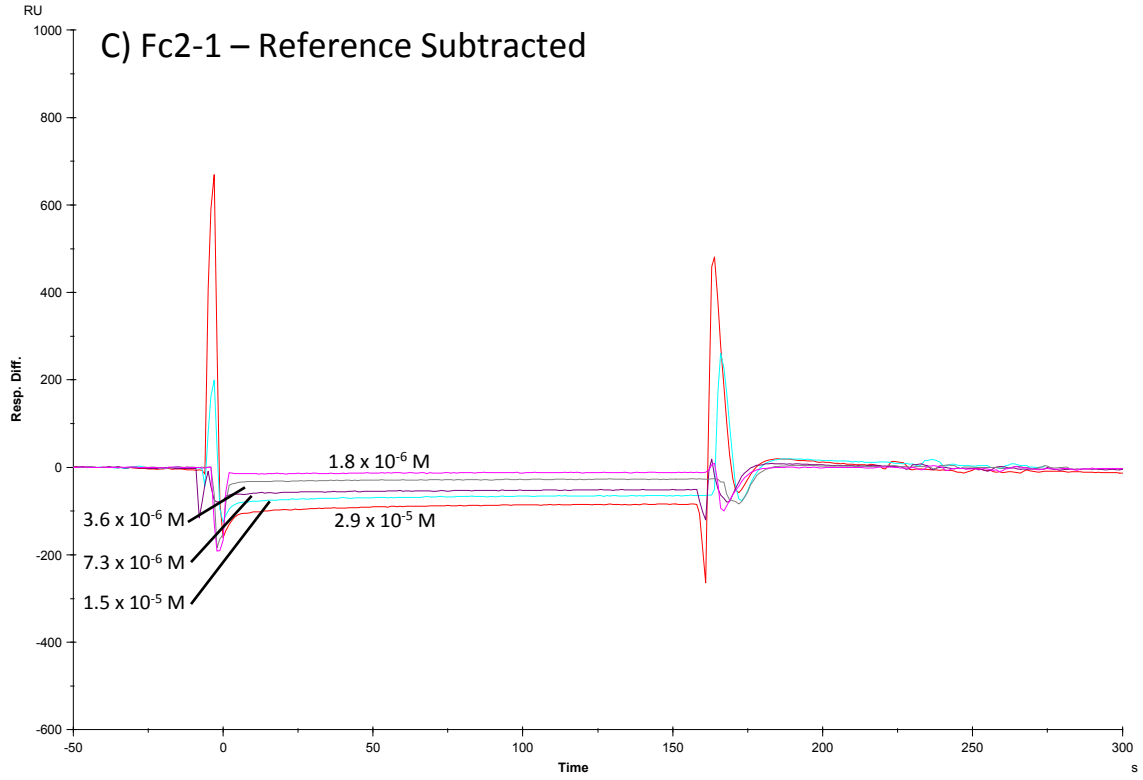

Figure 28, continued.

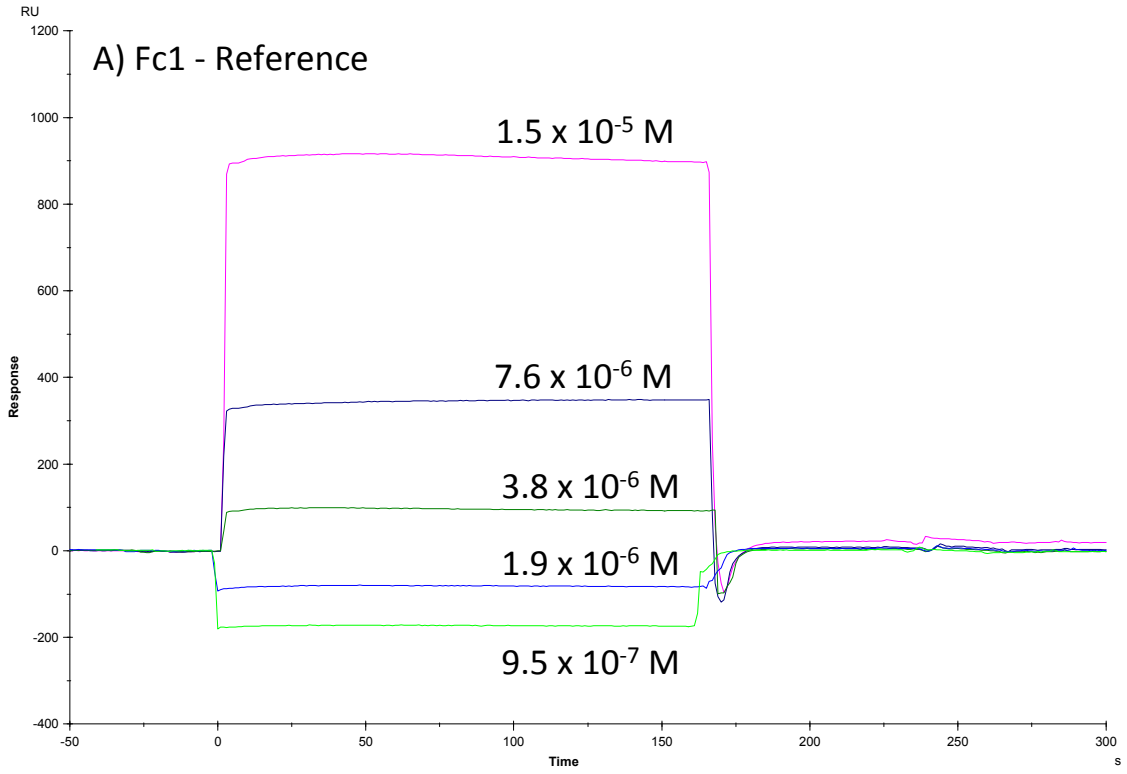

Figure 29. β Ser312 Assay Against Immobilized GST-(β Ser312). A) The sensorgram generated by the injection of peptides into flow cell 1, the reference cell. B) The sensorgram generated by the injection of peptides into flow cell 2, the analyte cell. C) The sensorgram generated by reference-subtracting the reference sensorgram from the analyte sensorgram.

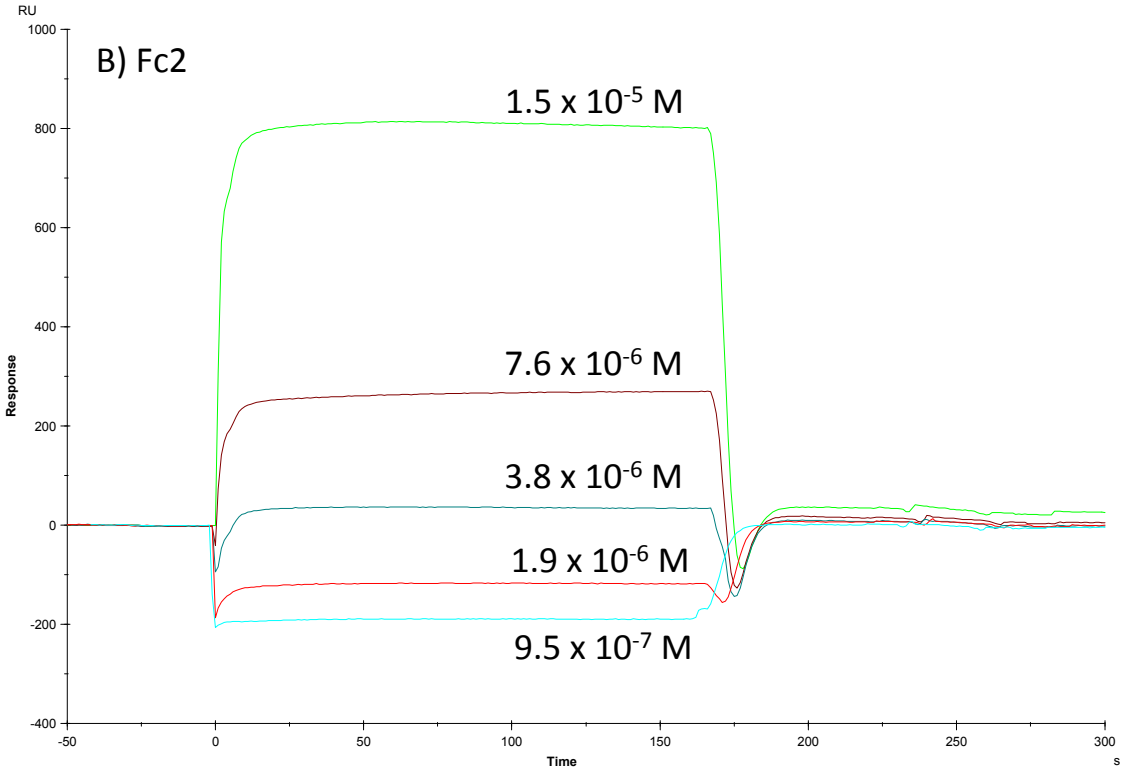

Figure 29, continued.

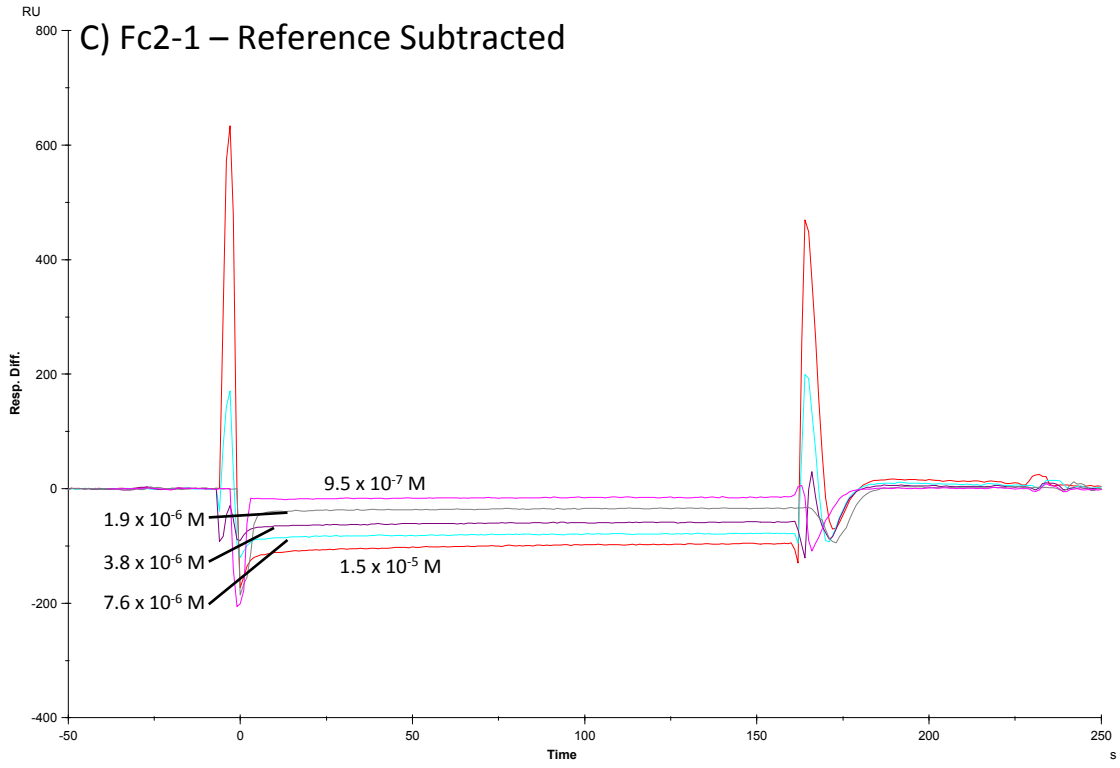

Figure 29, continued.

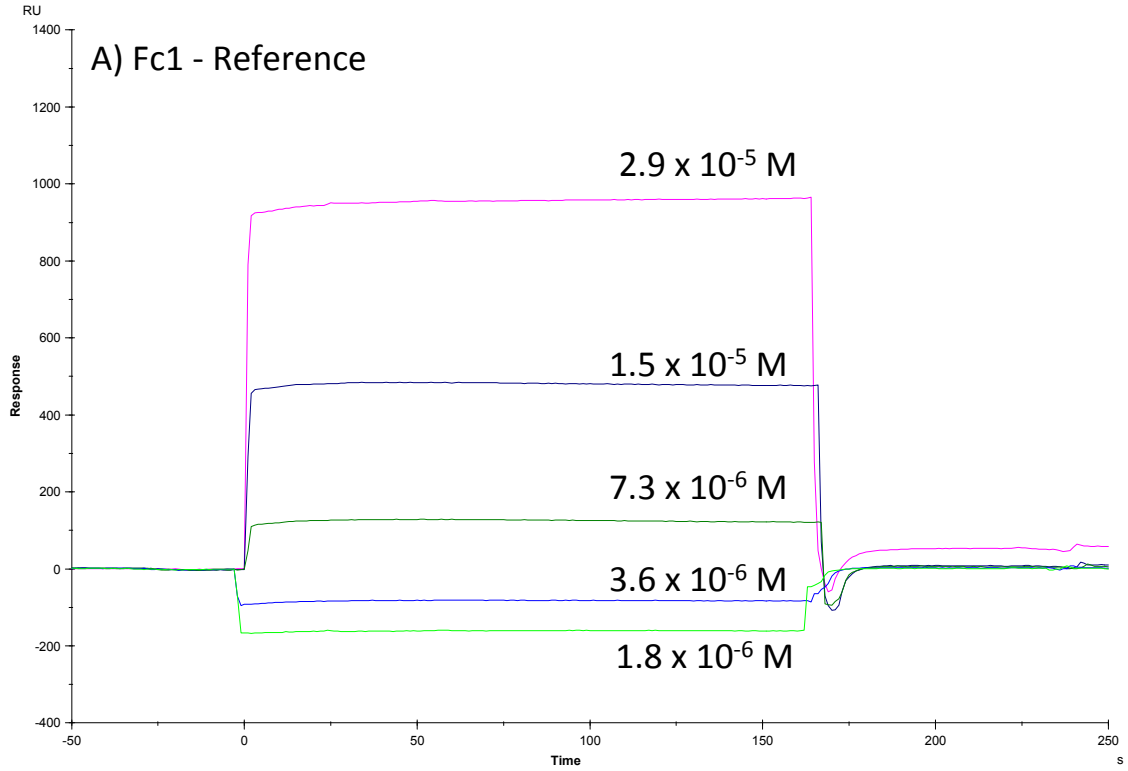

Figure 30. α Trp502Met506 Assay Against Immobilized GST-(γ Lys364). A) The sensorgram generated by the injection of peptides into flow cell 1, the reference cell. B) The sensorgram generated by the injection of peptides into flow cell 2, the analyte cell. C) The sensorgram generated by reference-subtracting the reference sensorgram from the analyte sensorgram.

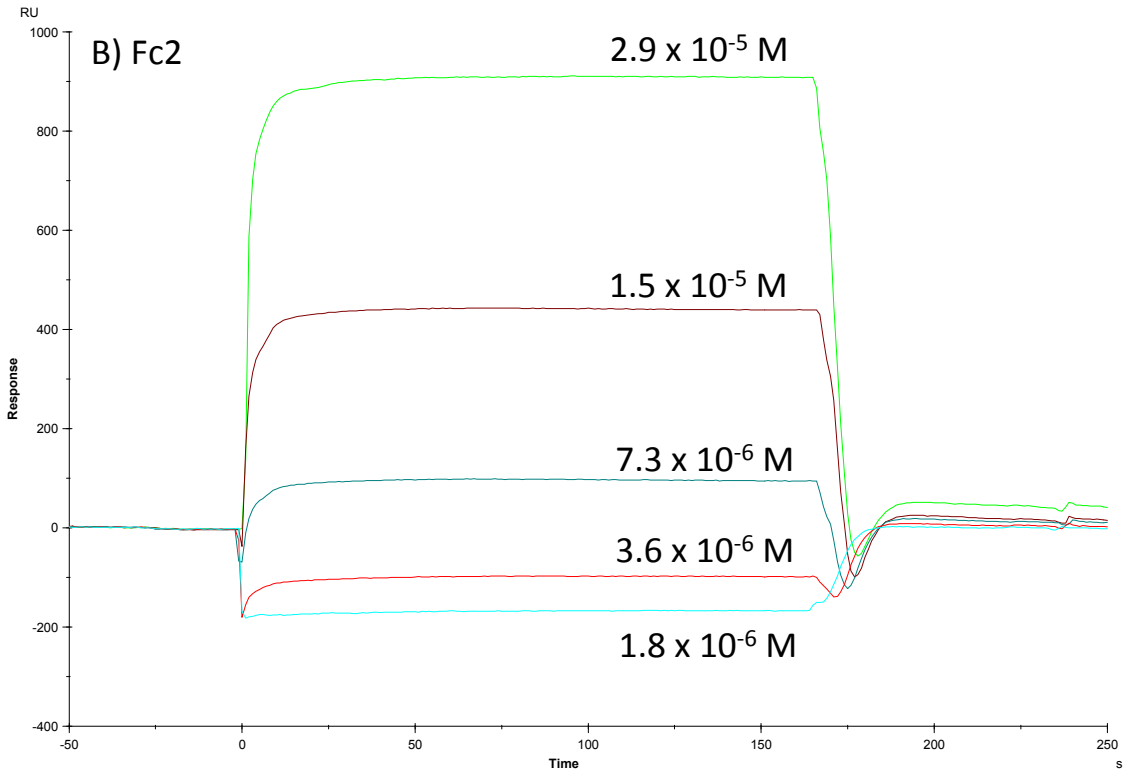

Figure 30, continued.

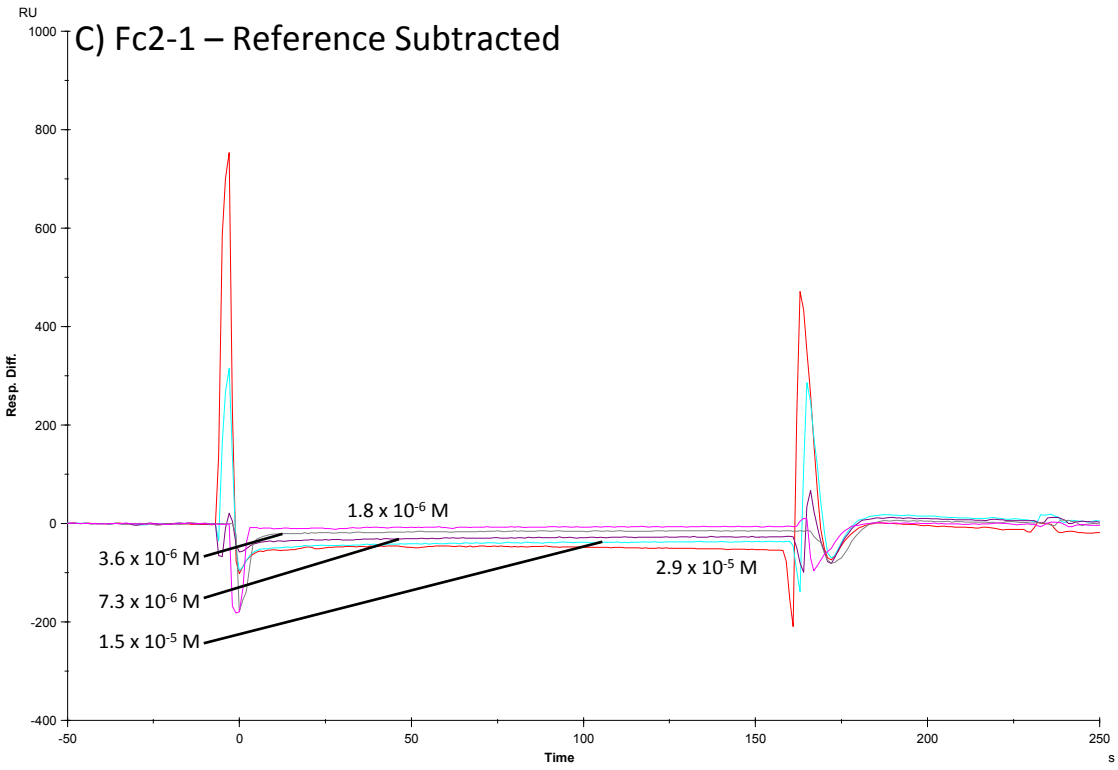

Figure 30, continued.

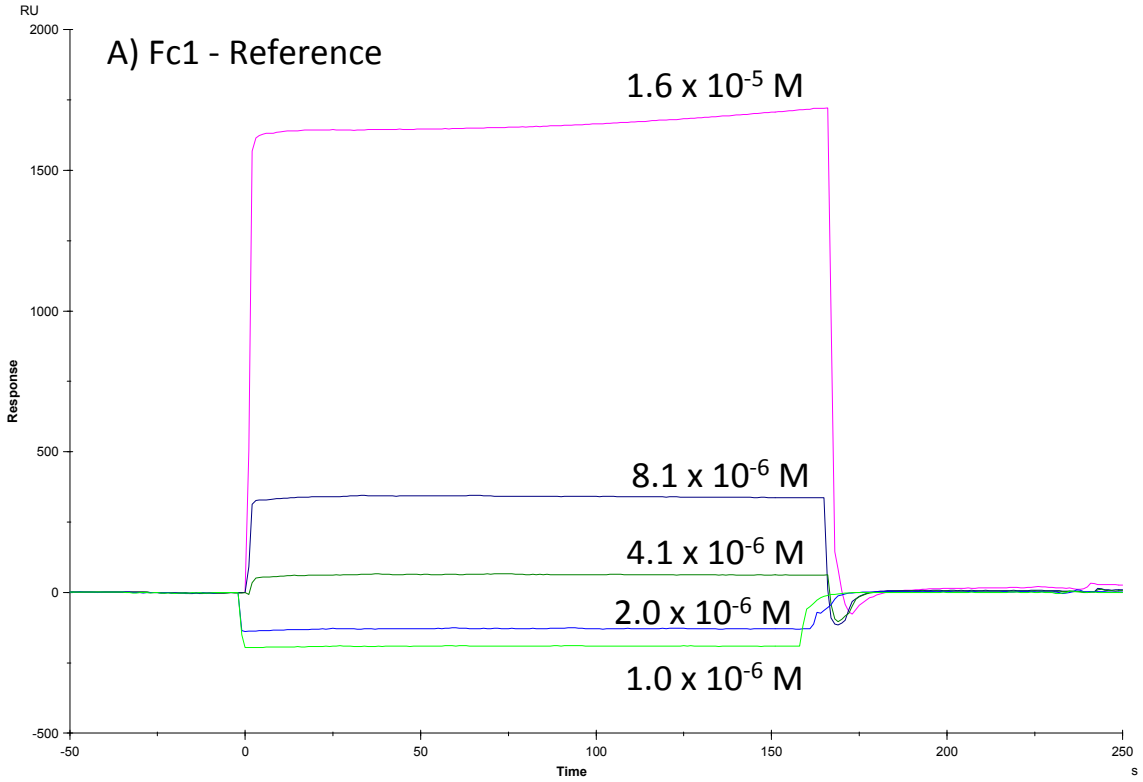

Figure 31. β Ser312 Assay Against Immobilized GST-(γ Lys364). A) The sensorgram generated by the injection of peptides into flow cell 1, the reference cell. B) The sensorgram generated by the injection of peptides into flow cell 2, the analyte cell. C) The sensorgram generated by reference-subtracting the reference sensorgram from the analyte sensorgram.

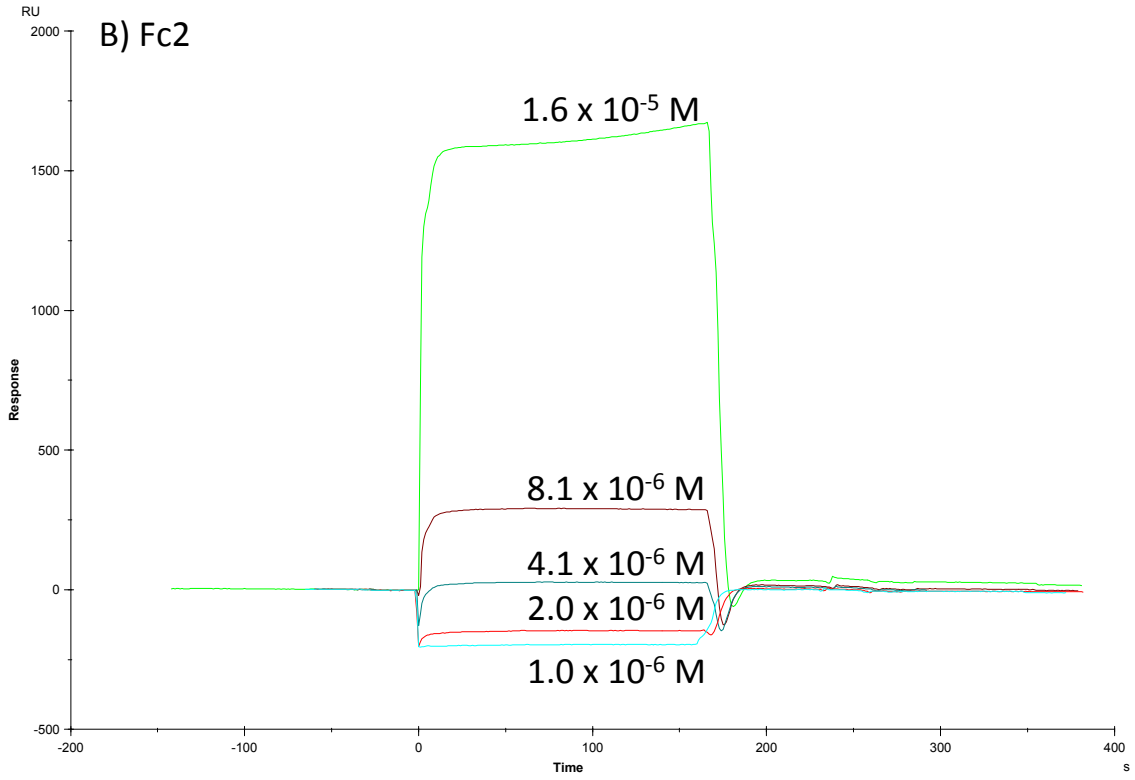

Figure 31, continued.

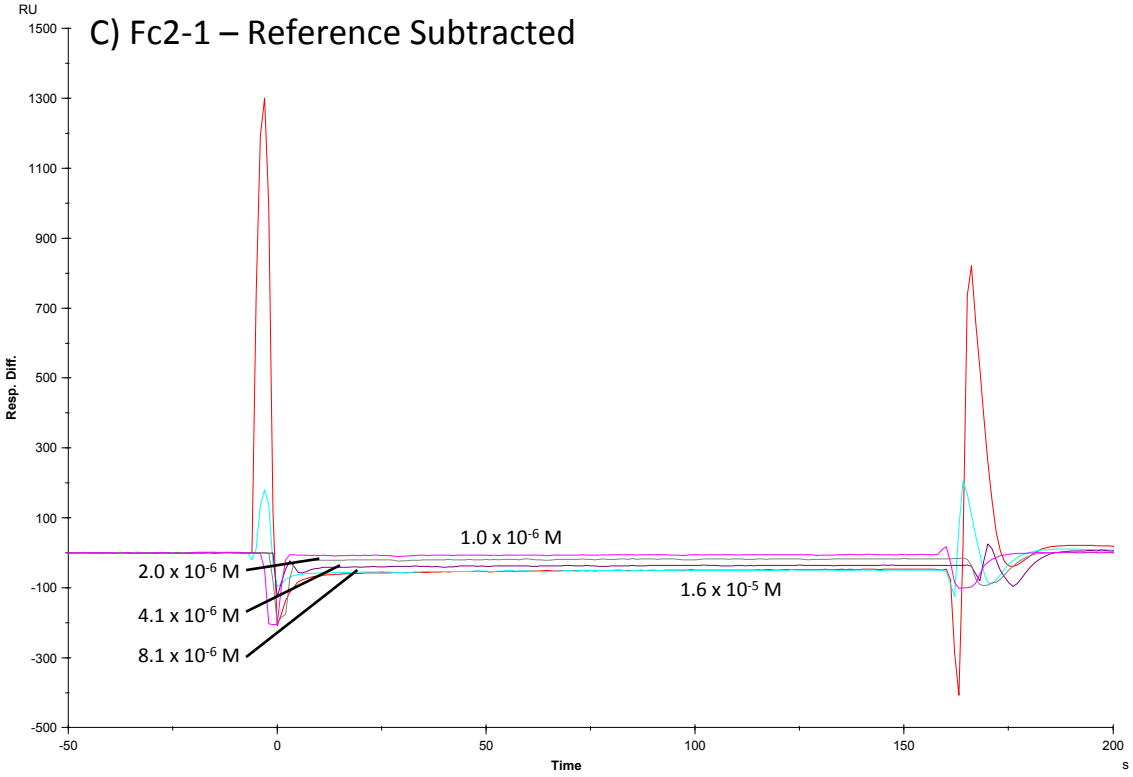

Figure 31, continued.

A second series of assays involved triple injections when immobilizing GST-fusion proteins in the expectations of immobilizing a greater amount of GST-fusion protein onto the sensor chip surface (**Figure 32**). With a greater amount of immobilized GST-fusion protein, interpretable responses were expected when analytes were assayed. Similar to the first series of assays, however, negative changes in reference-subtracted response units were observed (**Figures 33 - 38**). Therefore, analysis of binding kinetics was unobtainable.

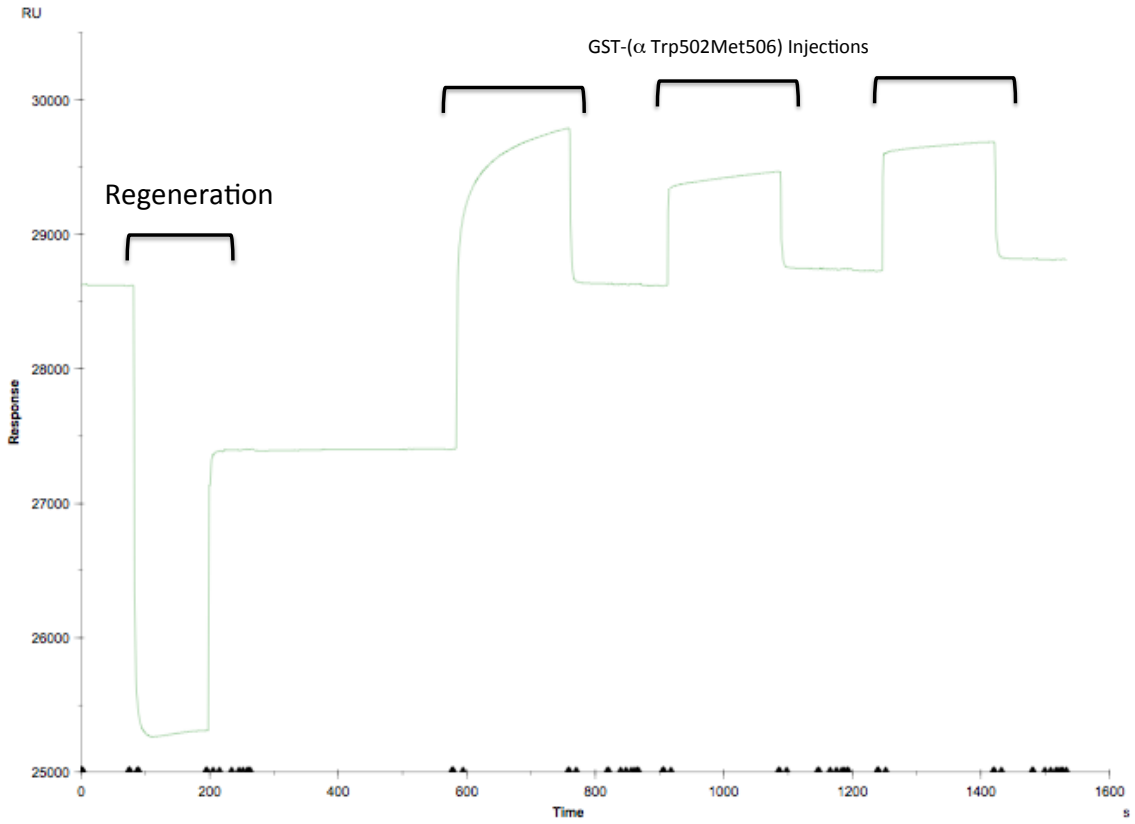

Figure 32. **Regeneration And 3x Injection Of GST-(α Trp502Met506).** This is the sensorgram generated when GST-(α Trp502Met506) fusion proteins were injected 3 times onto the sensor chip for immobilization. Second and third injections caused minimal increase in response units.

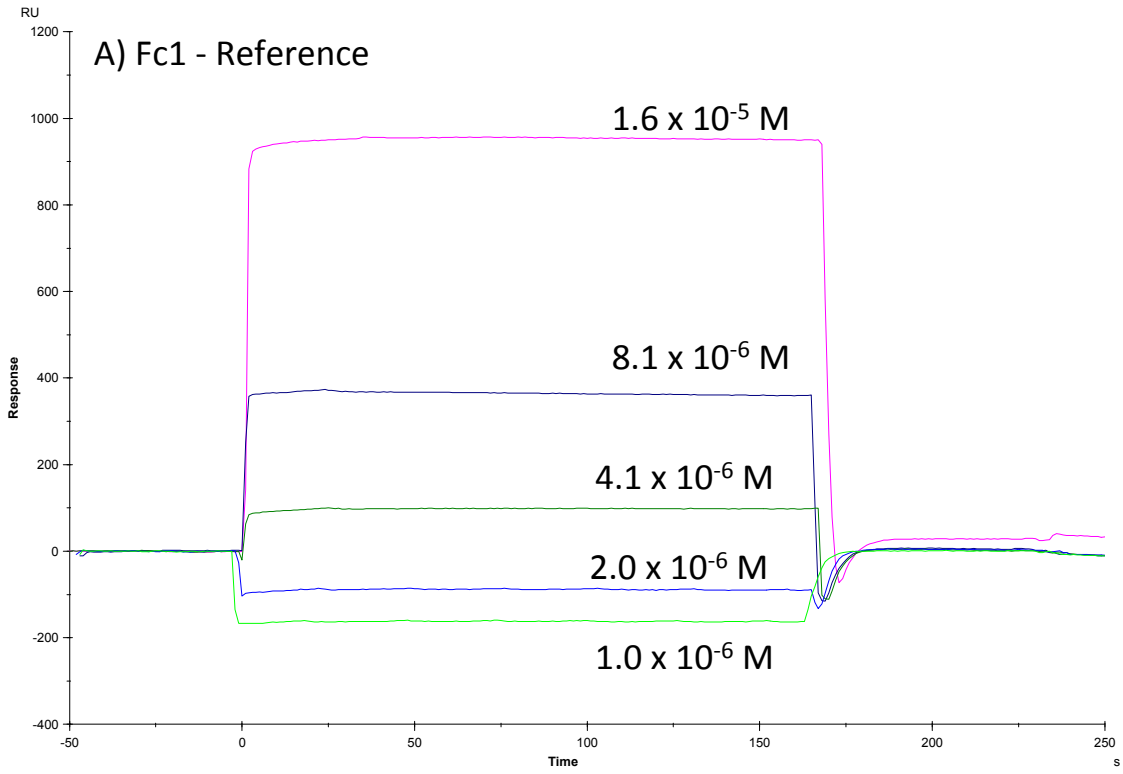

Figure 33. β Ser312 Assay Against 3x-Injected Immobilized GST-(α Trp502Met506). A) The sensorgram generated by the injection of peptides into flow cell 1, the reference cell. B) The sensorgram generated by the injection of peptides into flow cell 2, the analyte cell. C) The sensorgram generated by reference-subtracting the reference sensorgram from the analyte sensorgram.

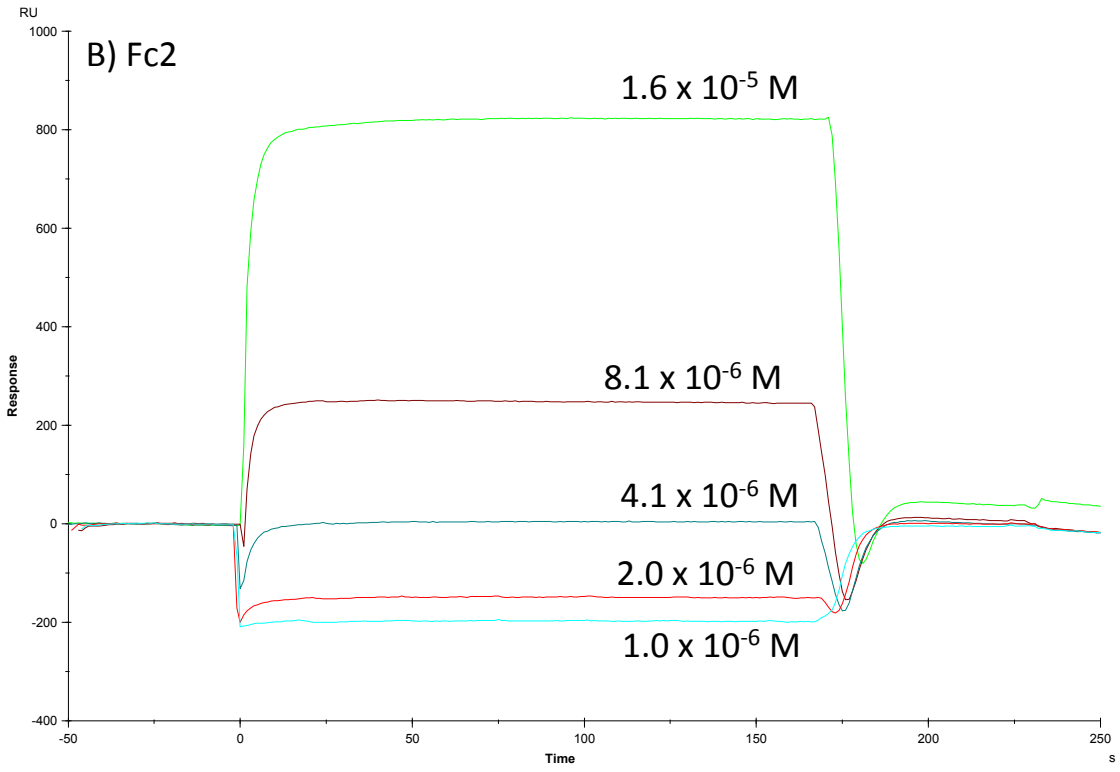

Figure 33, continued.

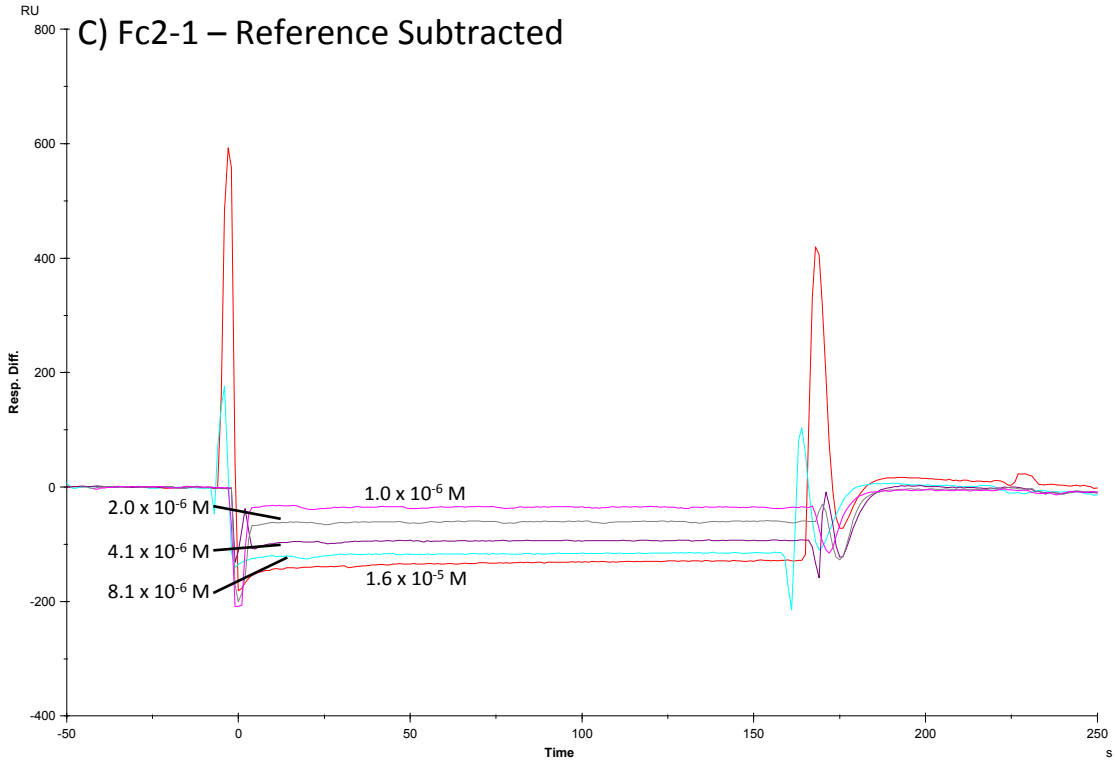

Figure 33, continued.

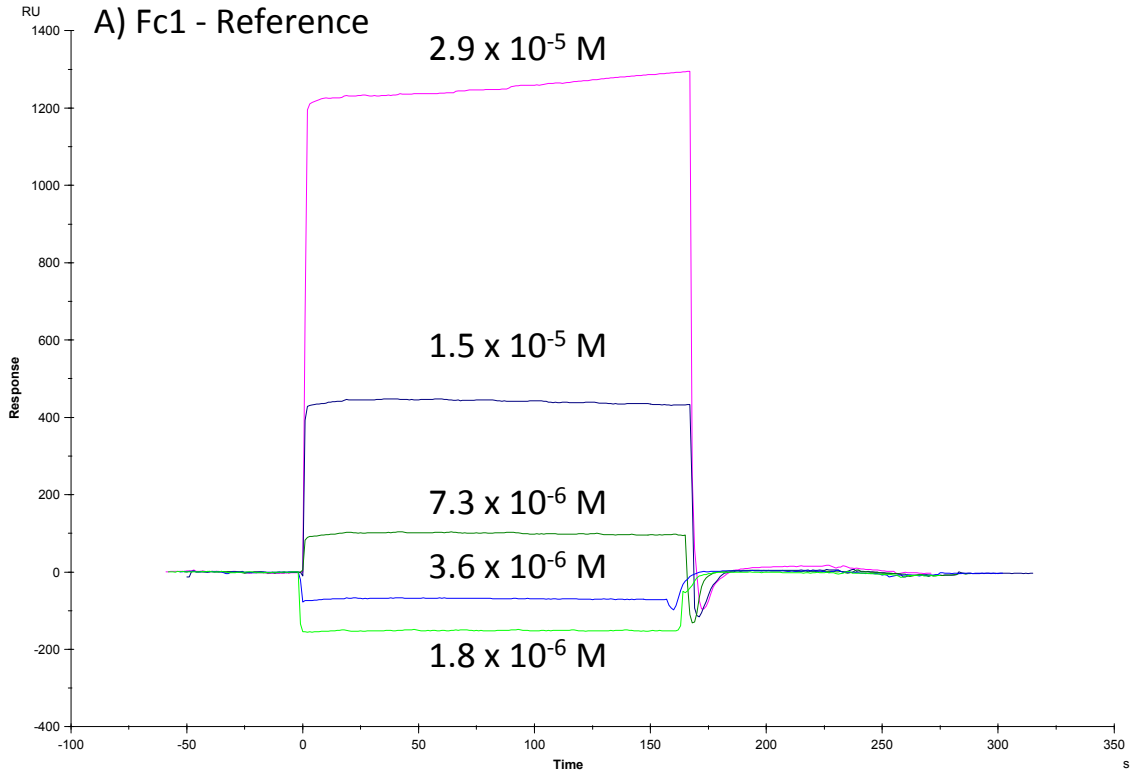

Figure 34. α Trp502Met506 Assay Against 3x-Injected Immobilized GST-(α Trp502Met506). A) The sensorgram generated by the injection of peptides into flow cell 1, the reference cell. B) The sensorgram generated by the injection of peptides into flow cell 2, the analyte cell. C) The sensorgram generated by reference-subtracting the reference sensorgram from the analyte sensorgram.

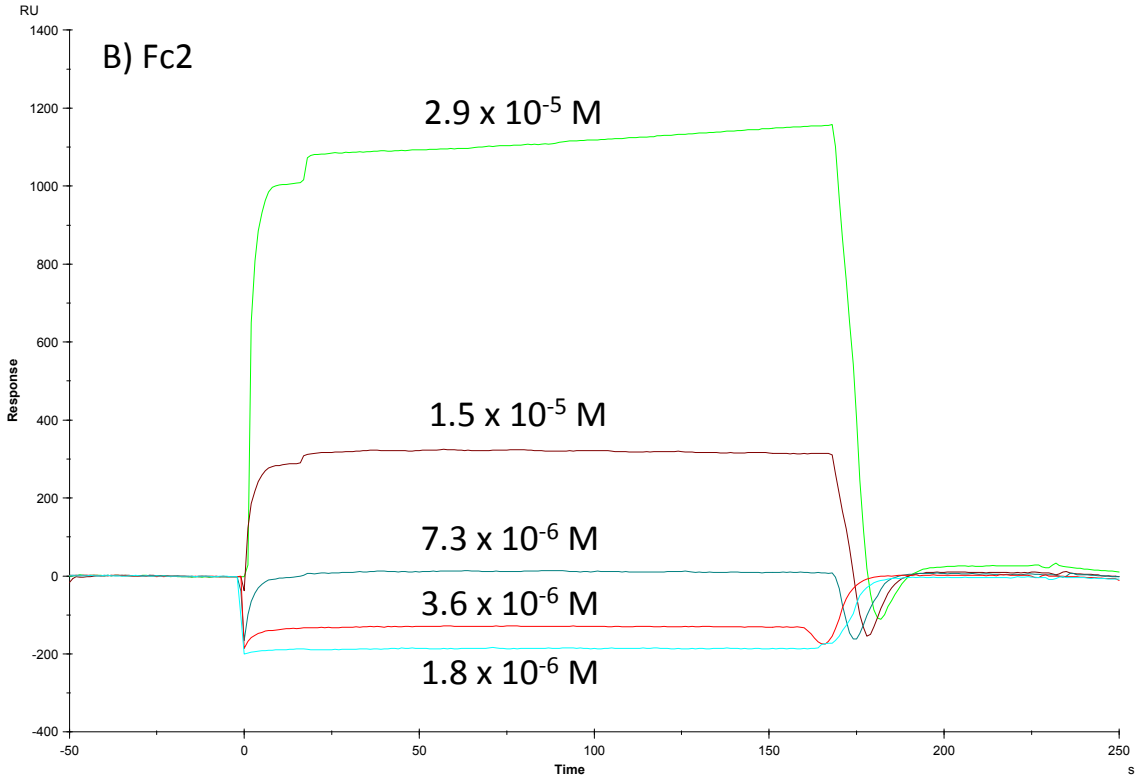

Figure 34, continued.

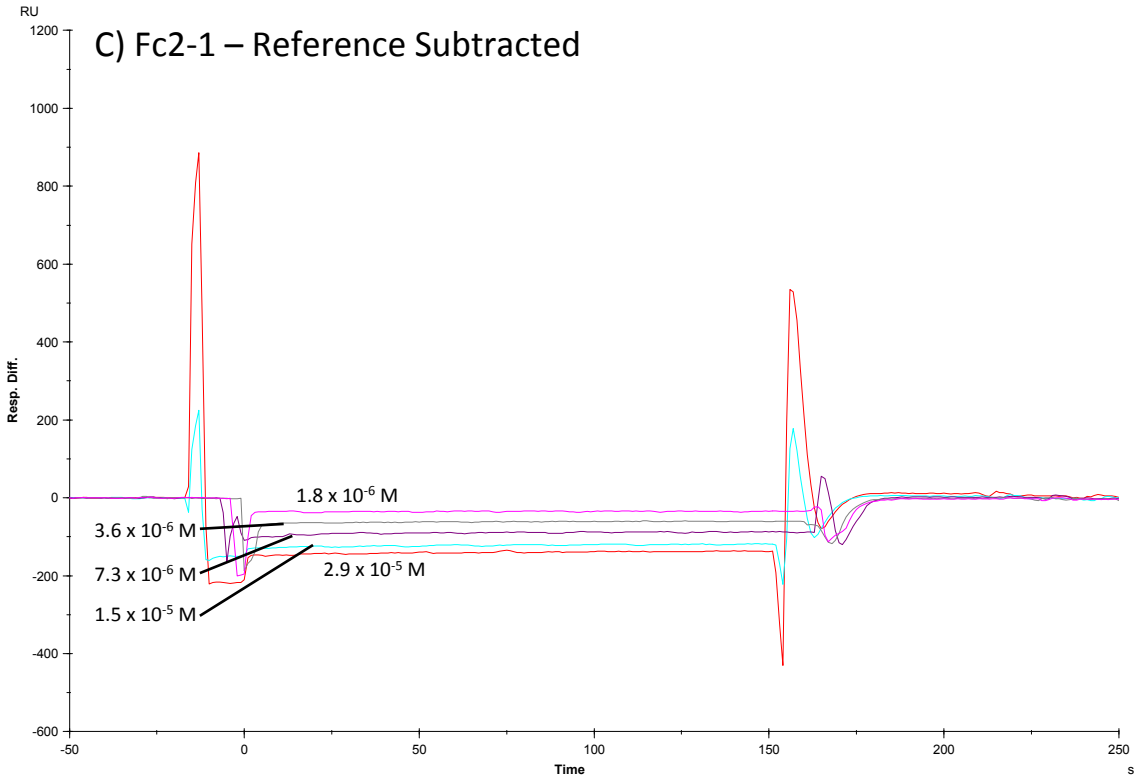

Figure 34, continued.

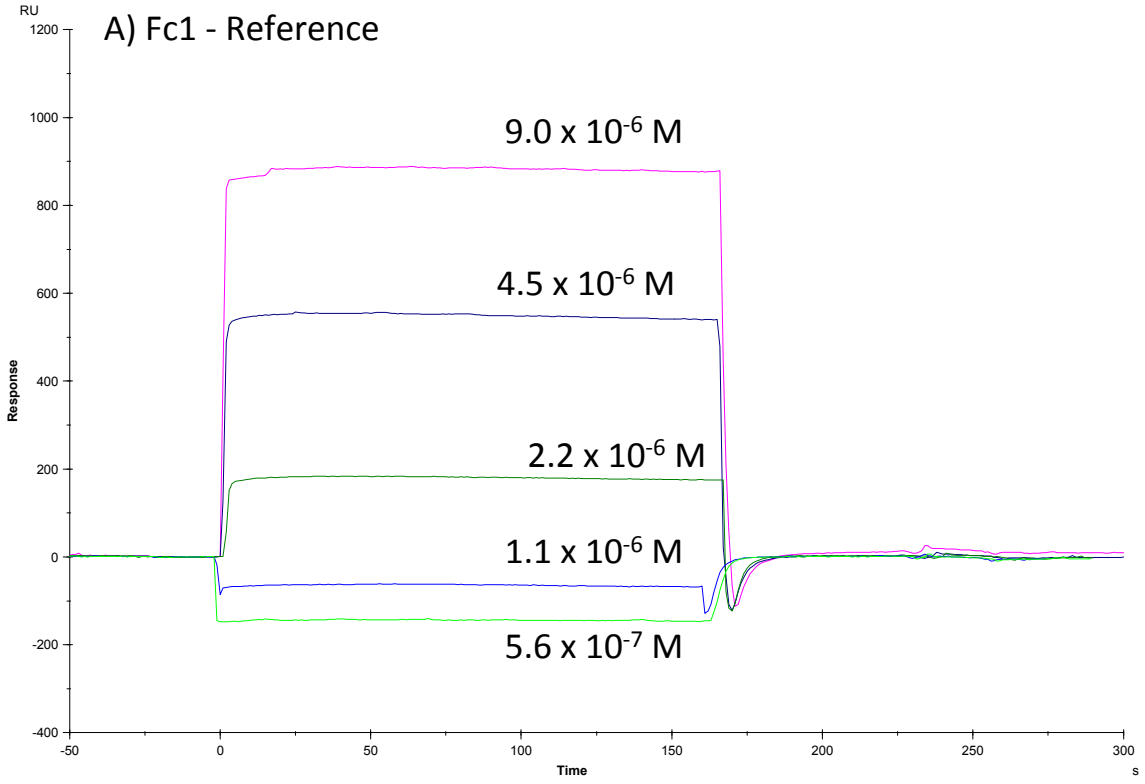

Figure 35. α Trp502Met506 Assay Against 3x-Injected Immobilized GST-(β Ser312). A) The sensorgram generated by the injection of peptides into flow cell 1, the reference cell. B) The sensorgram generated by the injection of peptides into flow cell 2, the analyte cell. C) The sensorgram generated by reference-subtracting the reference sensorgram from the analyte sensorgram.

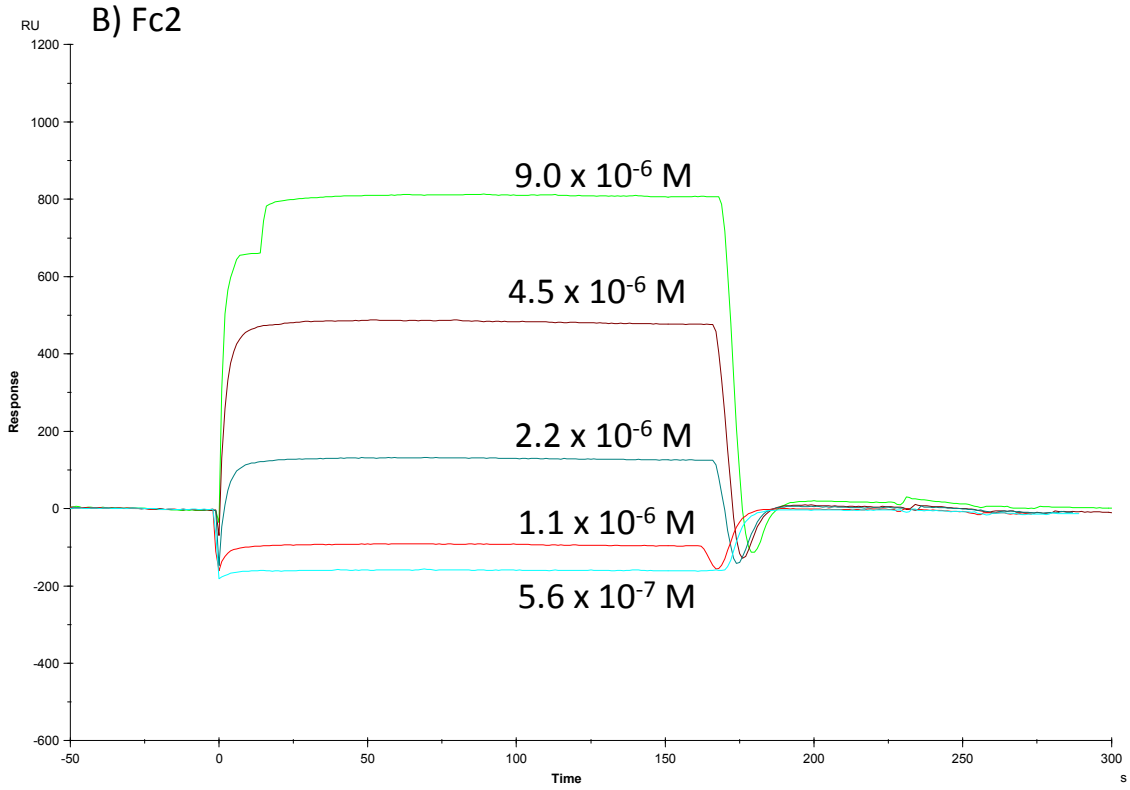

Figure 35, continued.

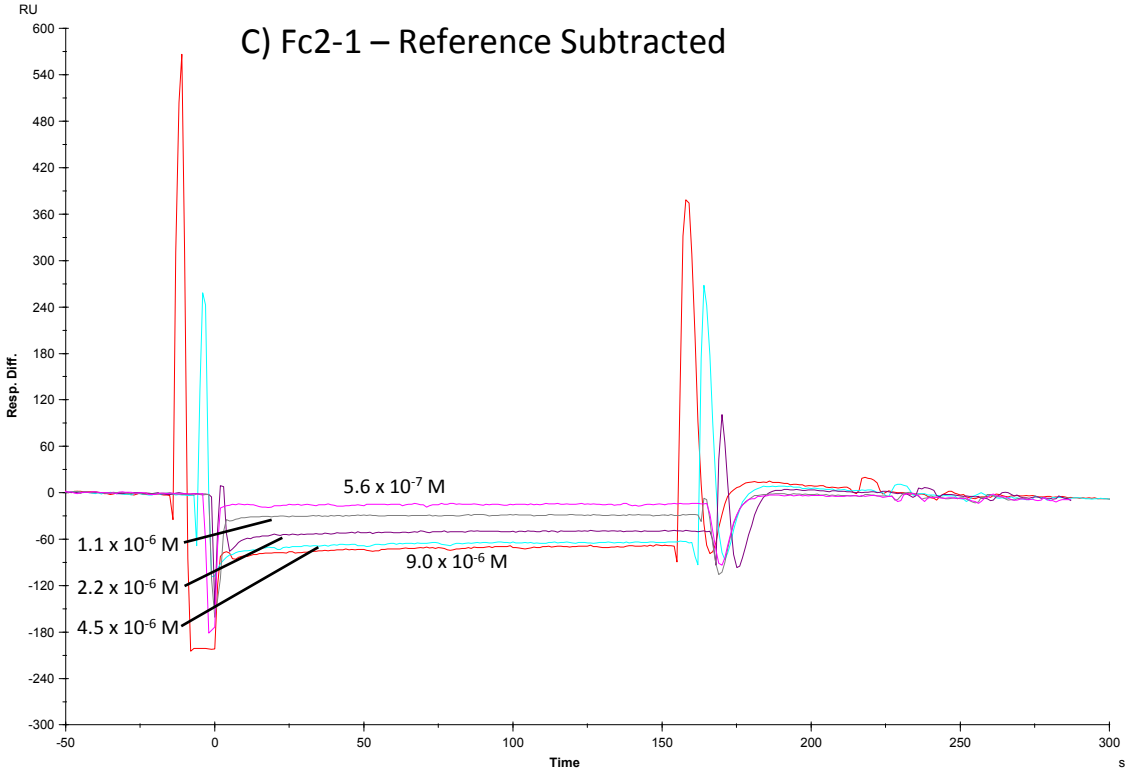

Figure 35, continued.

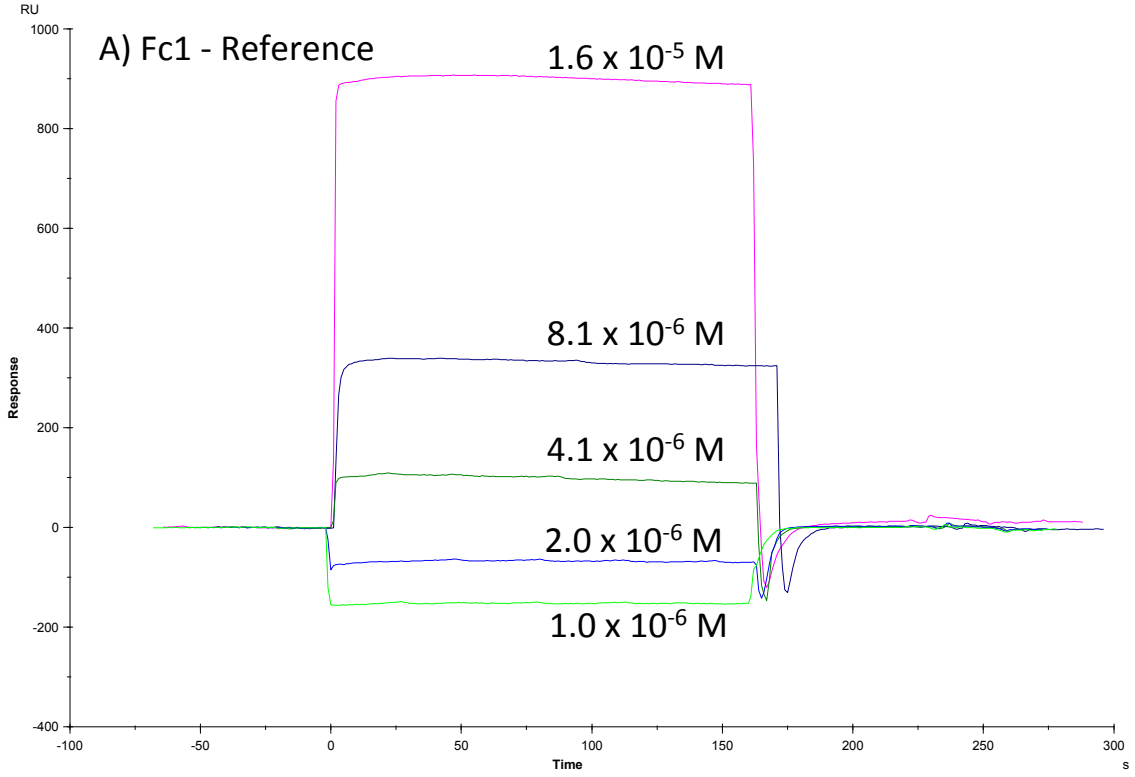

Figure 36. β Ser312 Assay Against 3x-Injected Immobilized GST-(β Ser312). A) The sensorgram generated by the injection of peptides into flow cell 1, the reference cell. B) The sensorgram generated by the injection of peptides into flow cell 2, the analyte cell. C) The sensorgram generated by reference-subtracting the reference sensorgram from the analyte sensorgram.

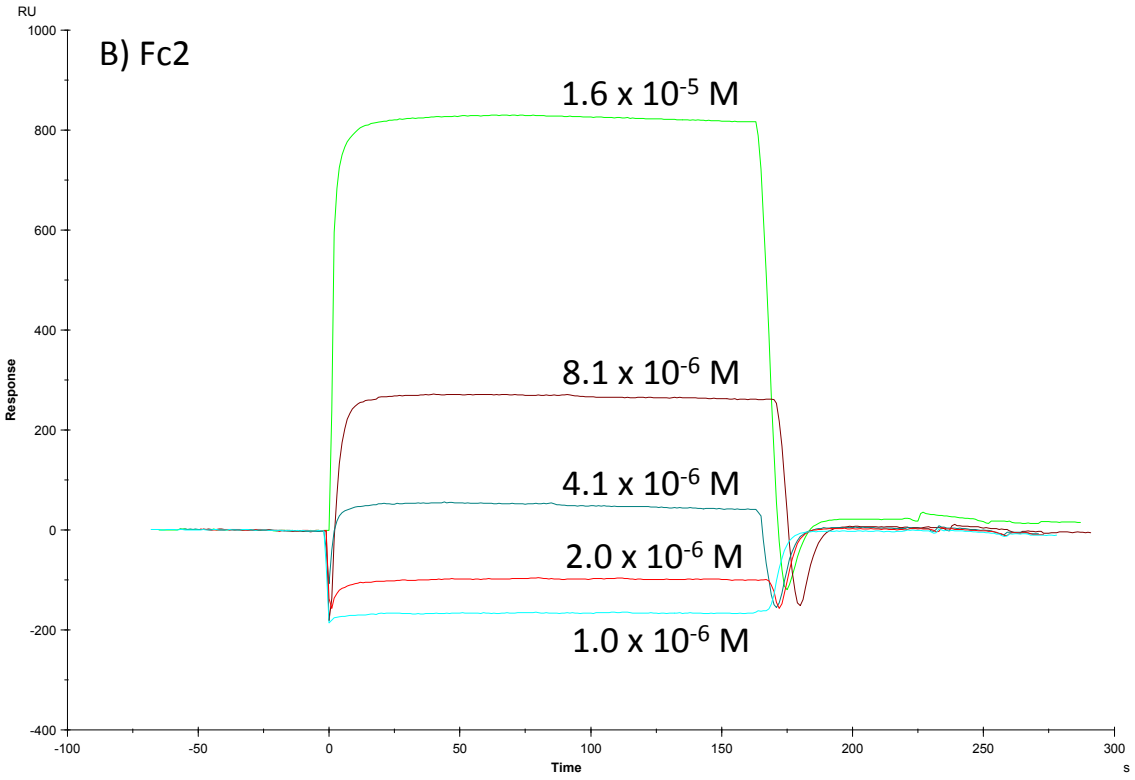

Figure 36, continued.

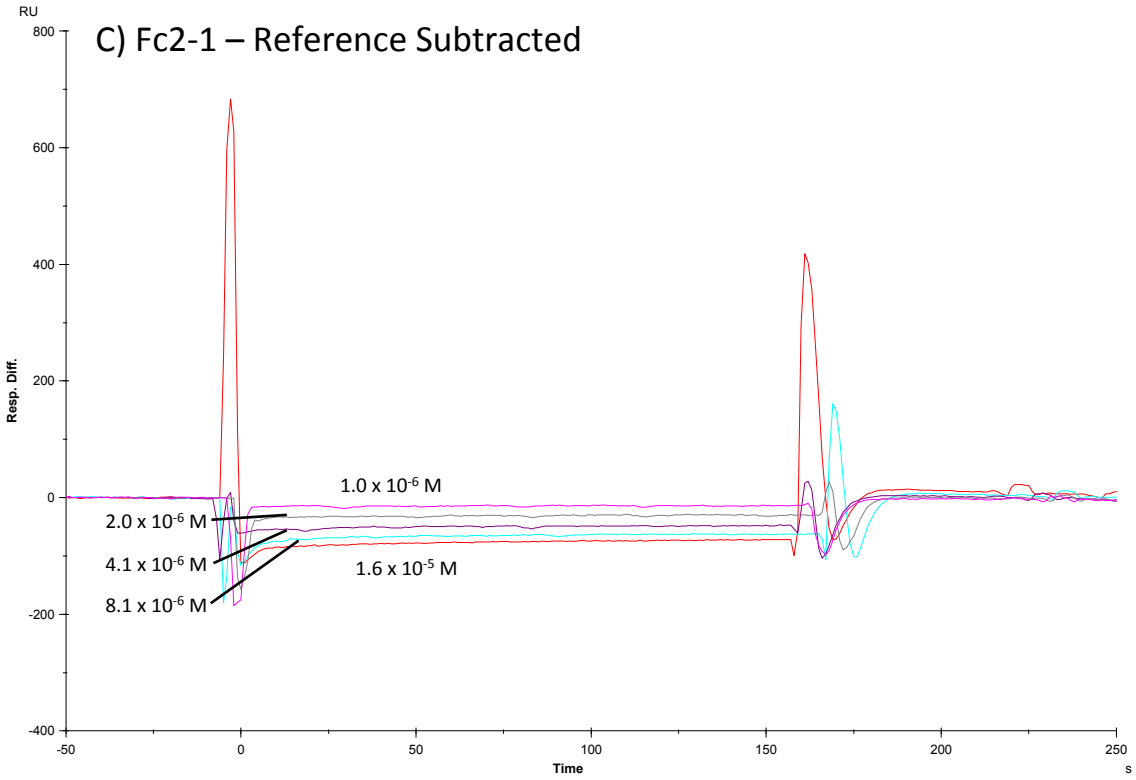

Figure 36, continued.

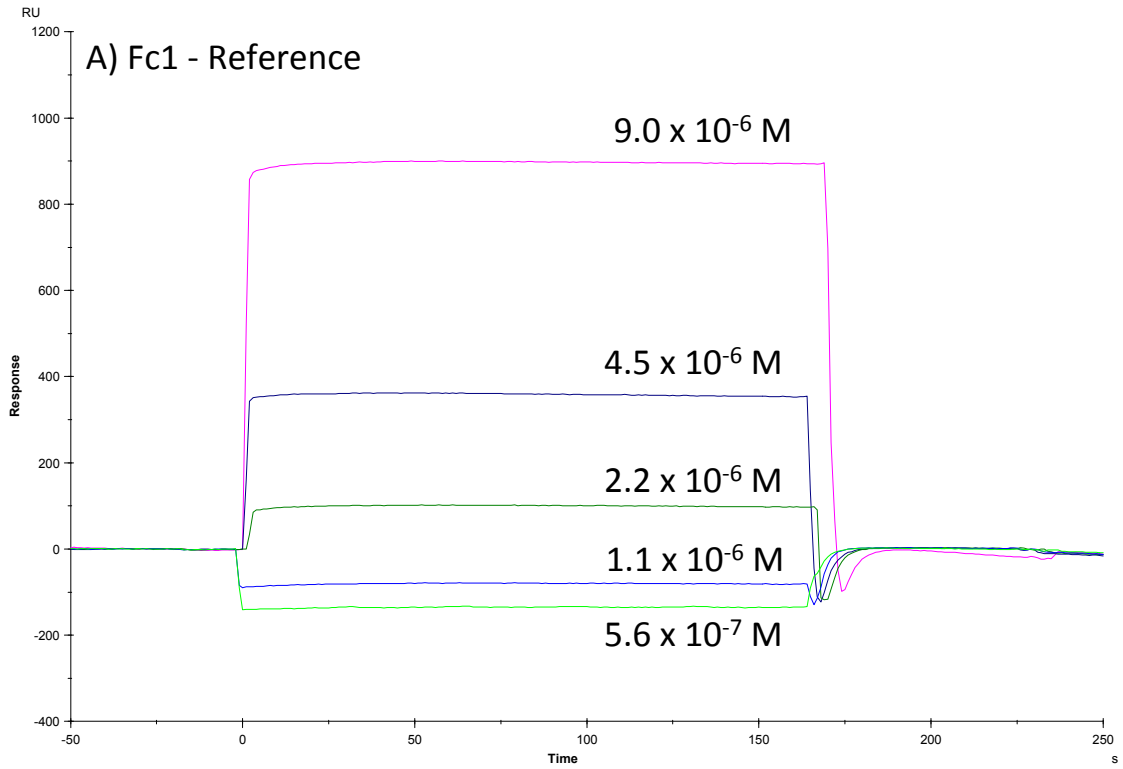

Figure 37. α Trp502Met506 Assay Against 3x-Injected Immobilized GST-(γ Lys364). A) The sensorgram generated by the injection of peptides into flow cell 1, the reference cell. B) The sensorgram generated by the injection of peptides into flow cell 2, the analyte cell. C) The sensorgram generated by reference-subtracting the reference sensorgram from the analyte sensorgram.

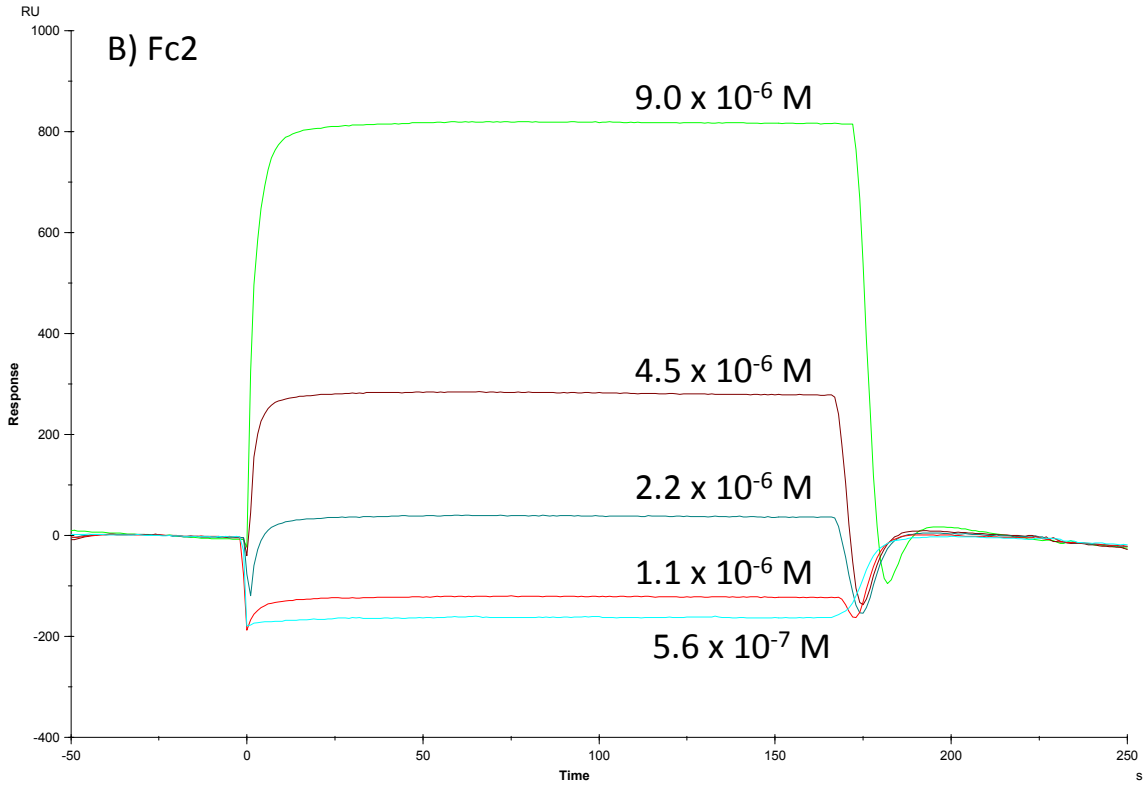

Figure 37, continued.

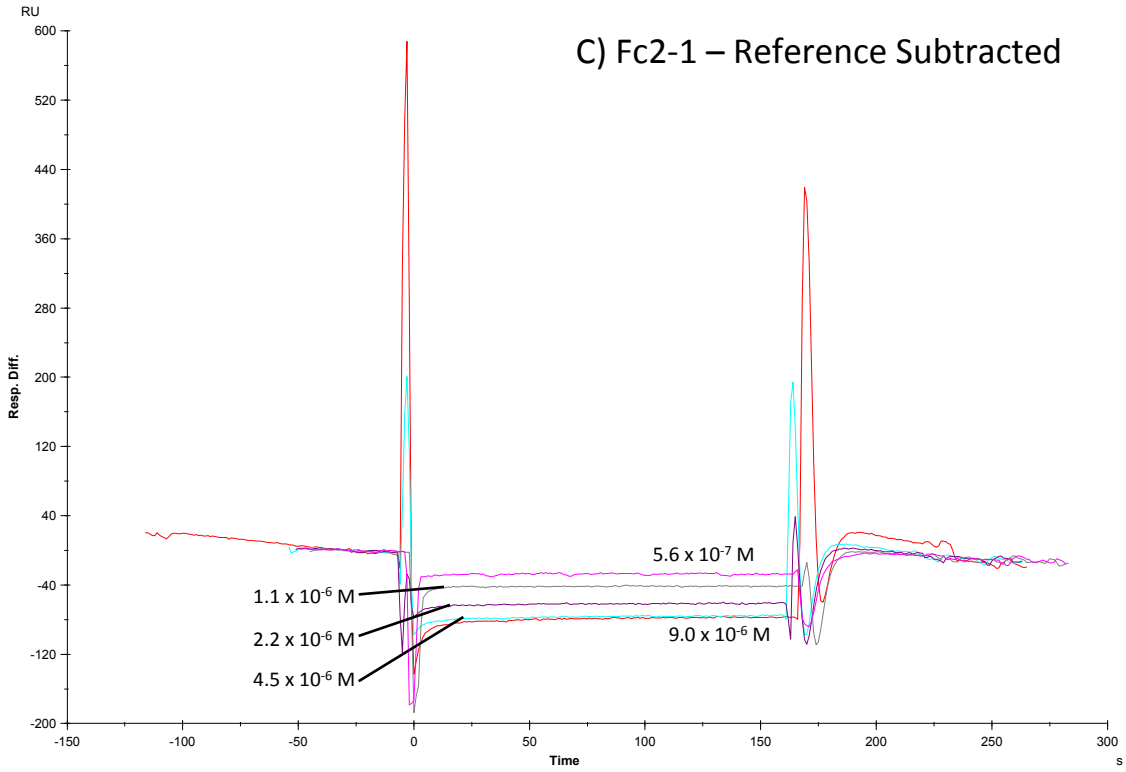

Figure 37, continued.

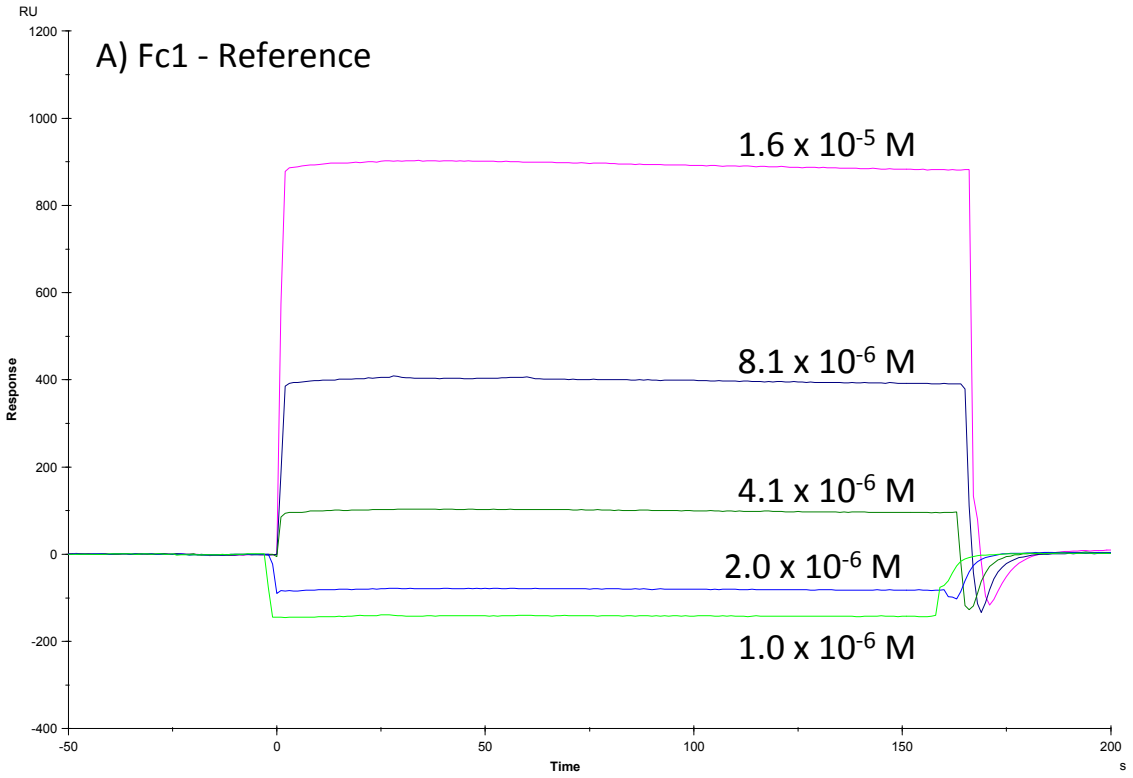

Figure 38. β Ser312 Assay Against 3x-Injected Immobilized GST-(γ Lys364). A) The sensorgram generated by the injection of peptides into flow cell 1, the reference cell. B) The sensorgram generated by the injection of peptides into flow cell 2, the analyte cell. C) The sensorgram generated by reference-subtracting the reference sensorgram from the analyte sensorgram.

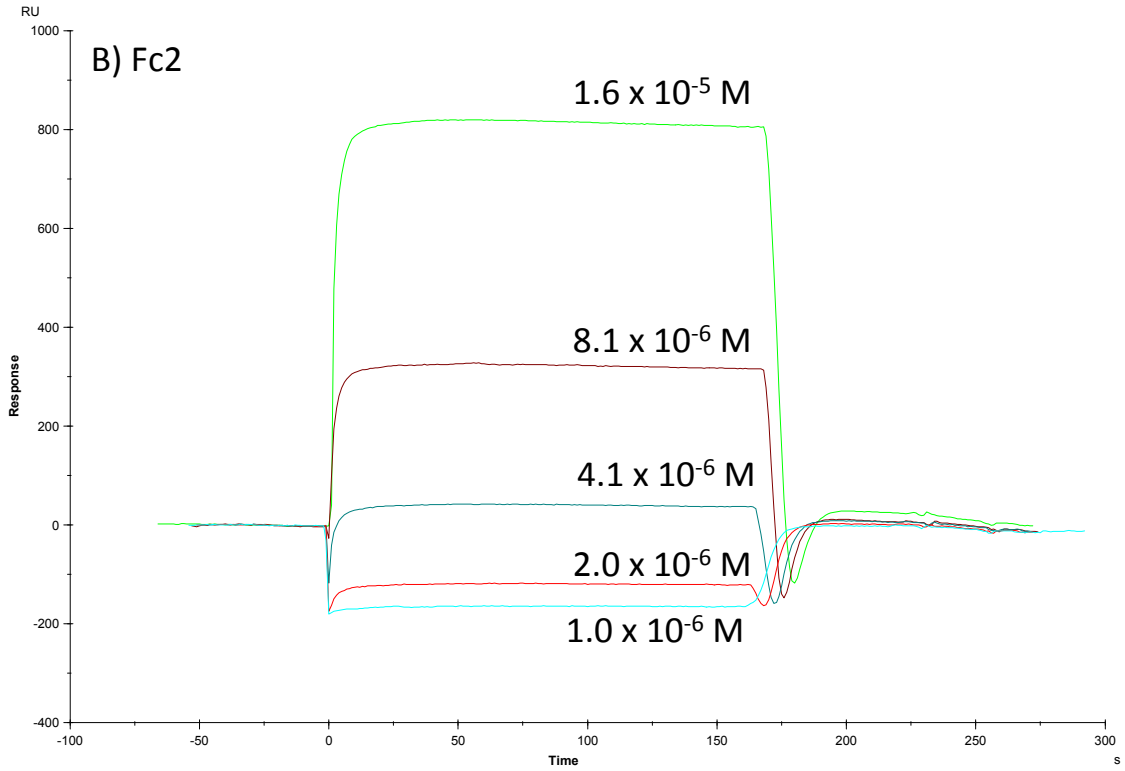

Figure 38, continued.

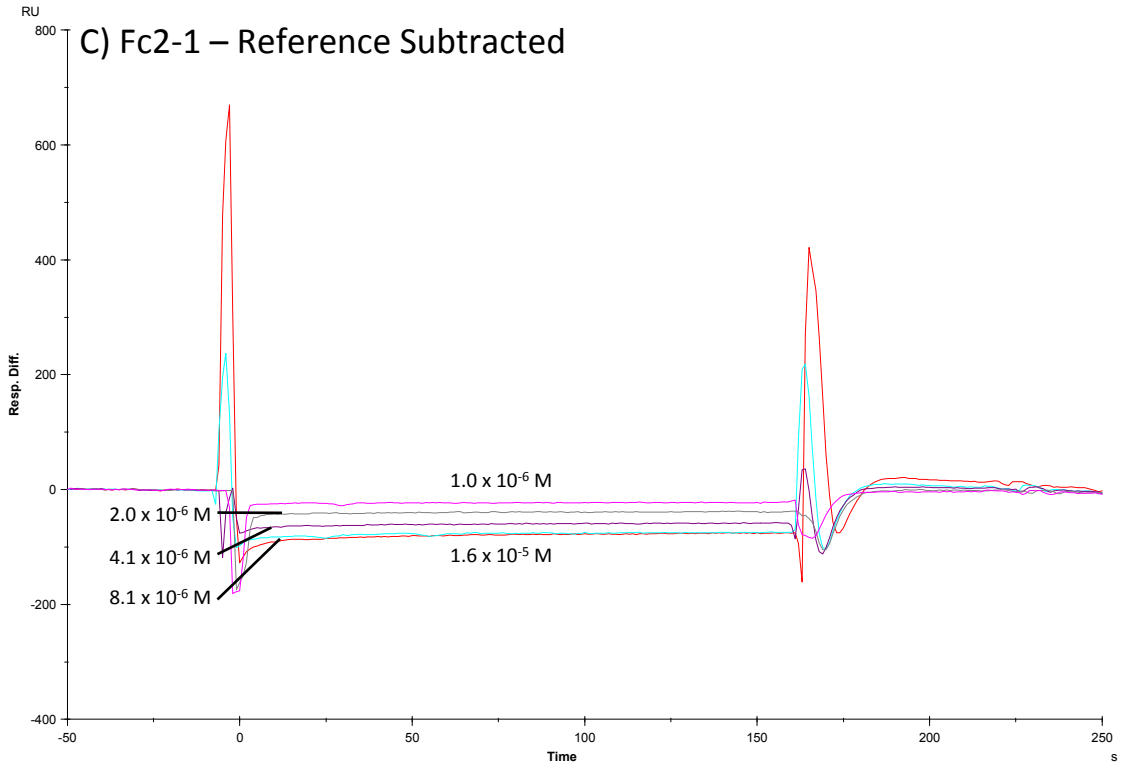

Figure 38, continued.

A third series of assays involved peptides that additionally contained 0.4 M NaCl in solution and running buffer (**Figures 39 - 44**). The addition of salt in the peptide solution appeared to eliminate the greater amount of non-specific interaction previously observed on the reference sensor surface. It can be seen, for example, that when α W502/M506 was assayed against immobilized GST-(β S312), a slight positive change was observed in the reference-subtracted sensorgram for peptides of higher concentrations (**Figure 41**). However, this change in response units was minimal, and the same change can be observed for peptides that were predicted to not interact (i.e. α W502/M506 assayed against immobilized GST-(α W502/M506); **Figure 40**). Thus, interactions in this environment warrant further investigation to elucidate the possibility of obtaining interpretable binding kinetics. It was possible that the peptide concentration in the injections was too low to see weak interactions. Further concentration of the peptides and re-analysis should be done in future studies to follow up on the potential binding interactions evident in some of the sensorgrams (**Figures 42-44**).

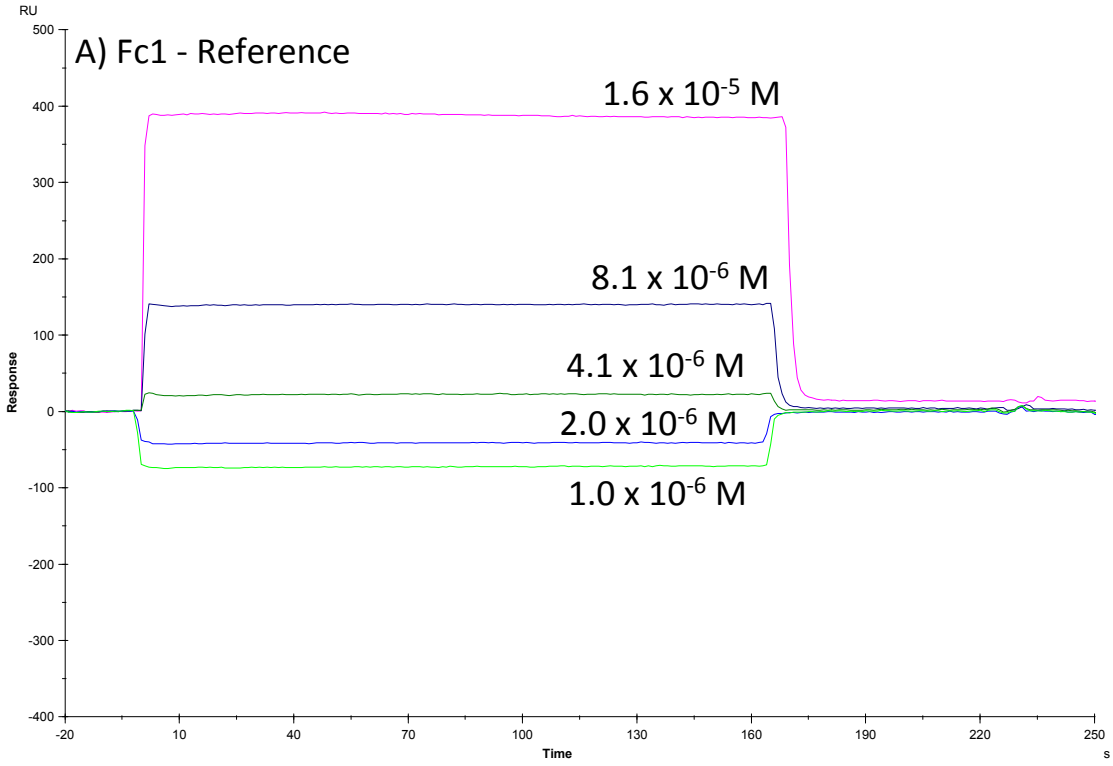

Figure 39. β Ser312 Peptide With 0.4 M NaCl Assay Against 2x-Injected Immobilized GST-(α Trp502Met506). A) The sensorgram generated by the injection of peptides into flow cell 1, the reference cell. B) The sensorgram generated by the injection of peptides into flow cell 2, the analyte cell. C) The sensorgram generated by reference-subtracting the reference sensorgram from the analyte sensorgram.

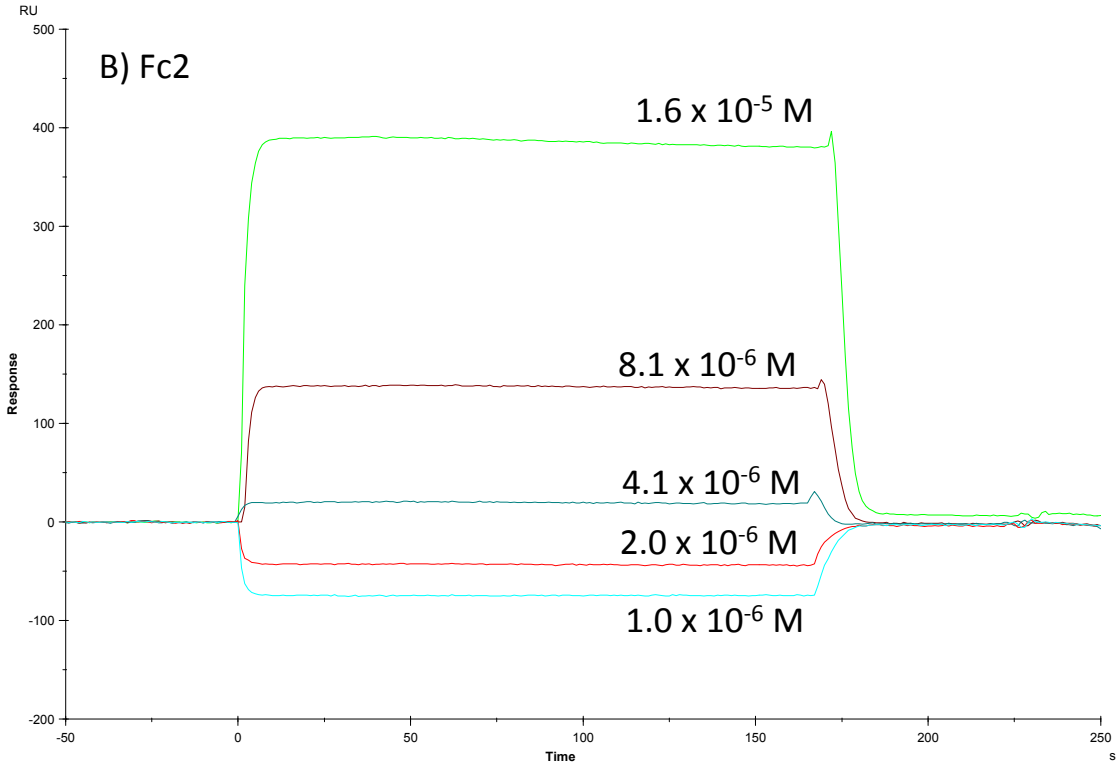

Figure 39, continued.

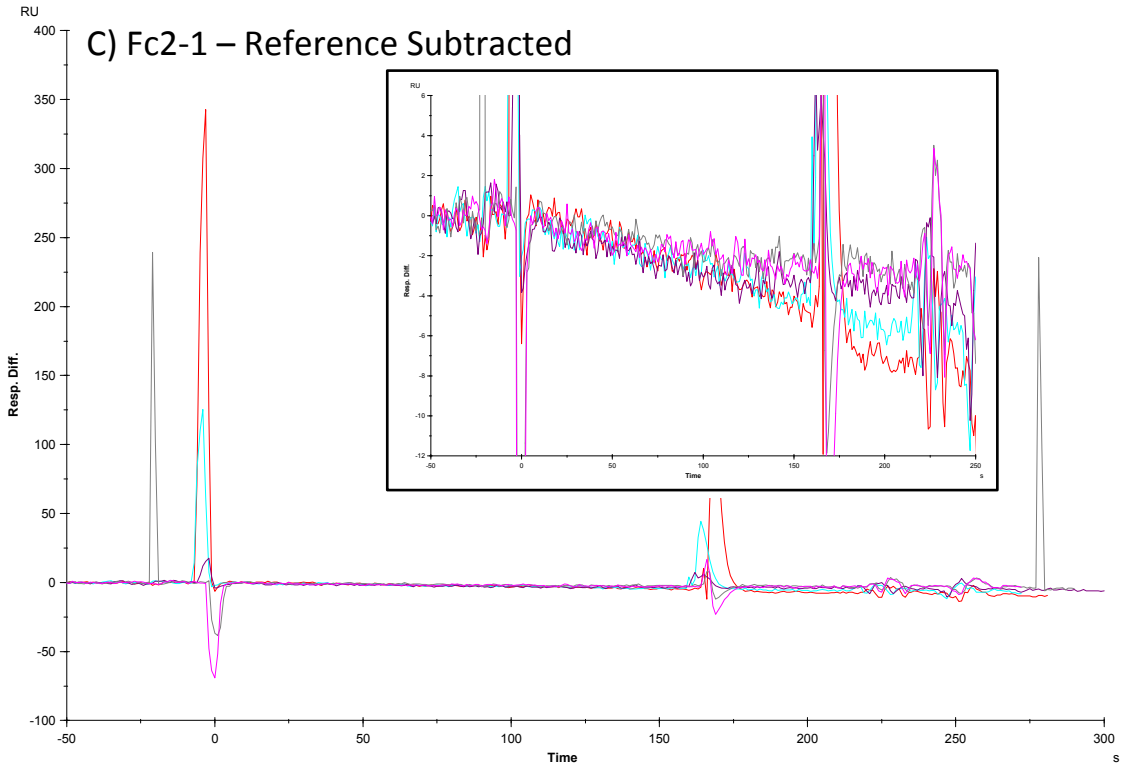

Figure 39, continued.

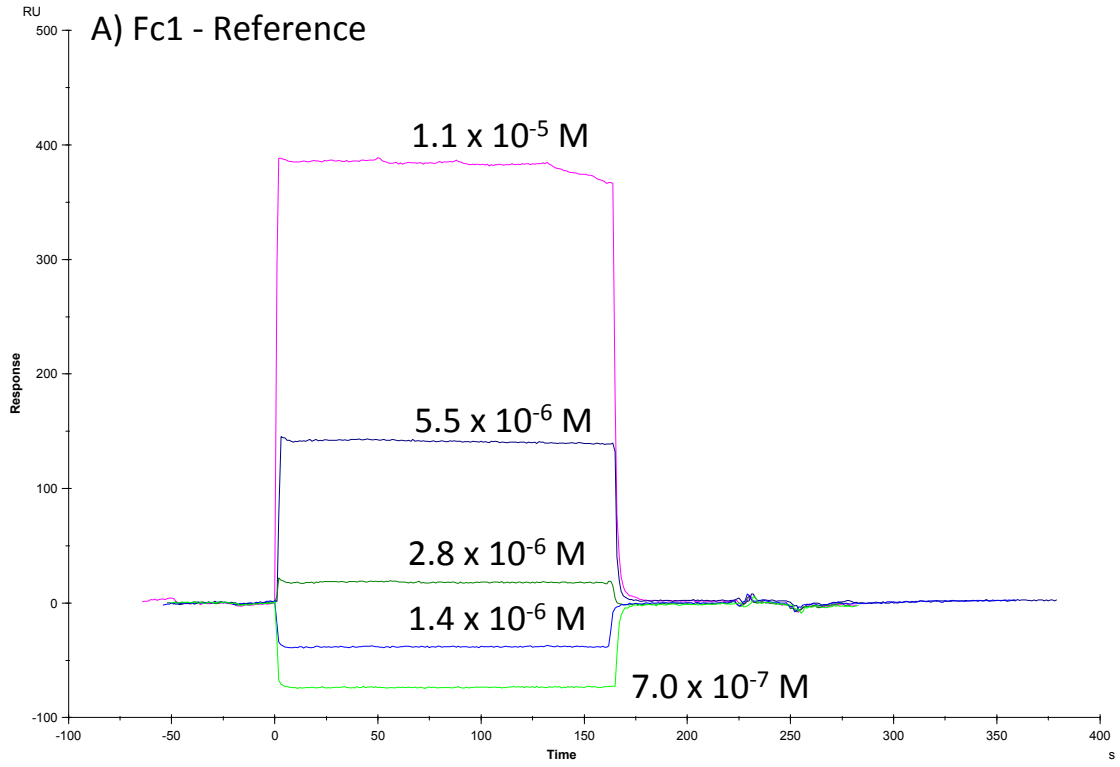

Figure 40. α Trp502Met506 Peptide With 0.4 M NaCl Assay Against 2x-Injected Immobilized GST-(α Trp502Met506). A) The sensorgram generated by the injection of peptides into flow cell 1, the reference cell. B) The sensorgram generated by the injection of peptides into flow cell 2, the analyte cell. C) The sensorgram generated by reference-subtracting the reference sensorgram from the analyte sensorgram.

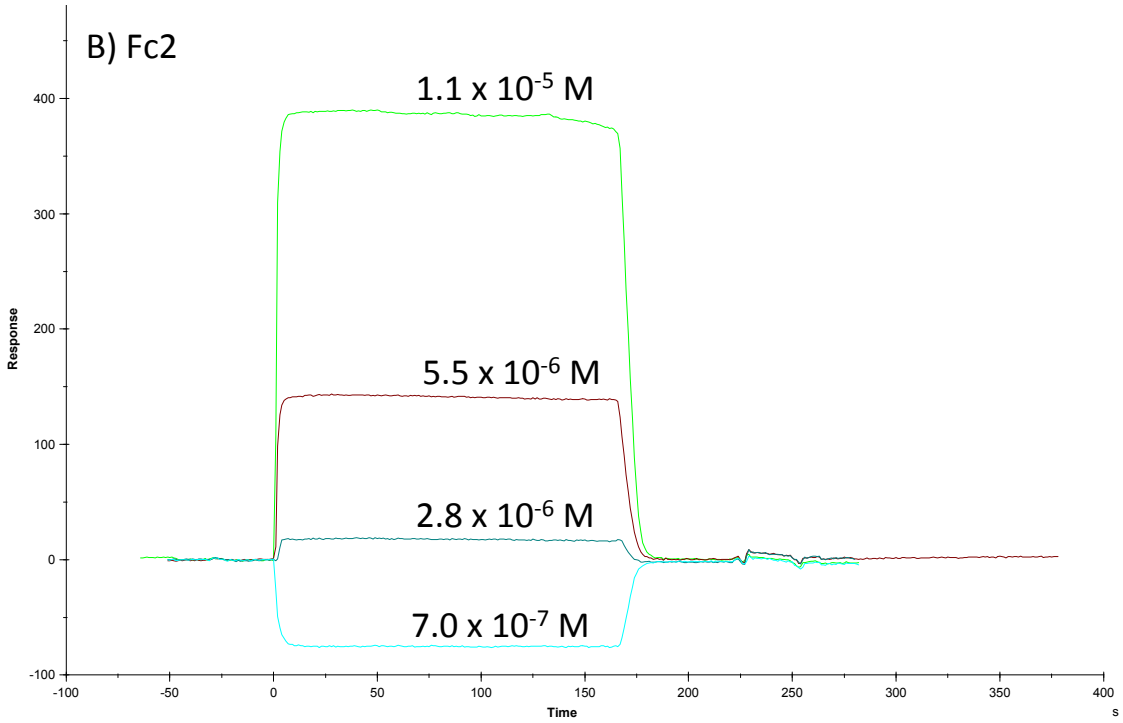

Figure 40, continued.

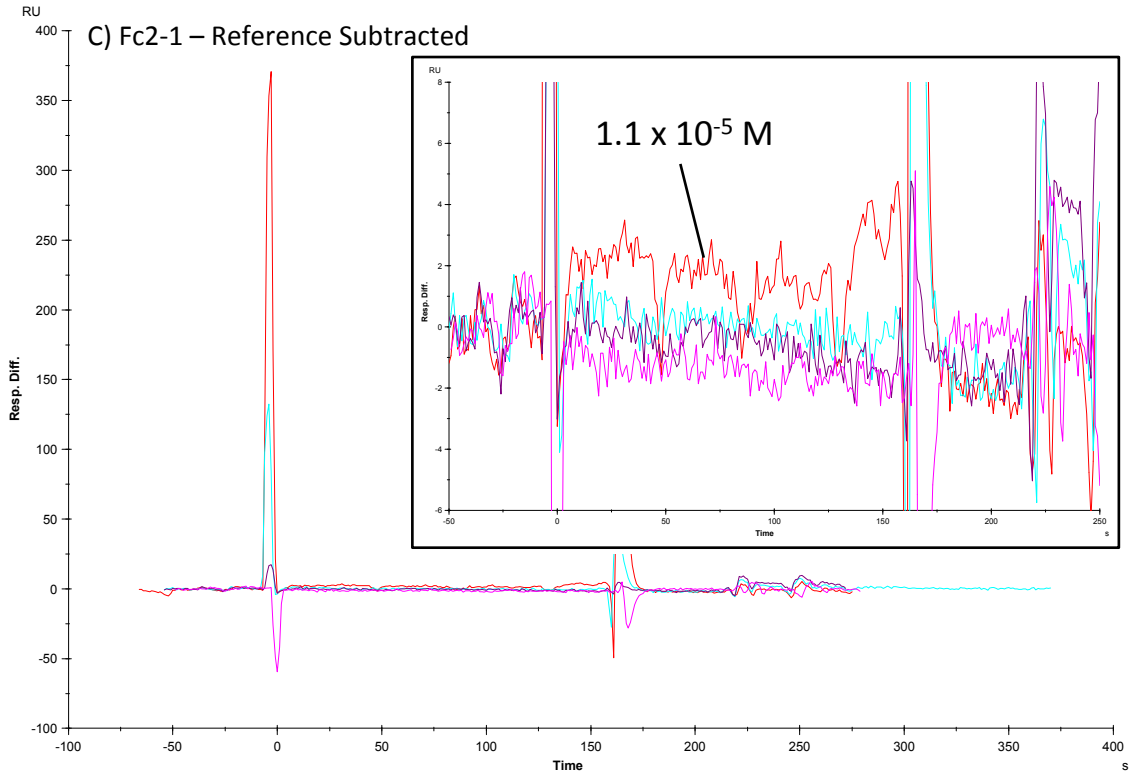

Figure 40, continued.

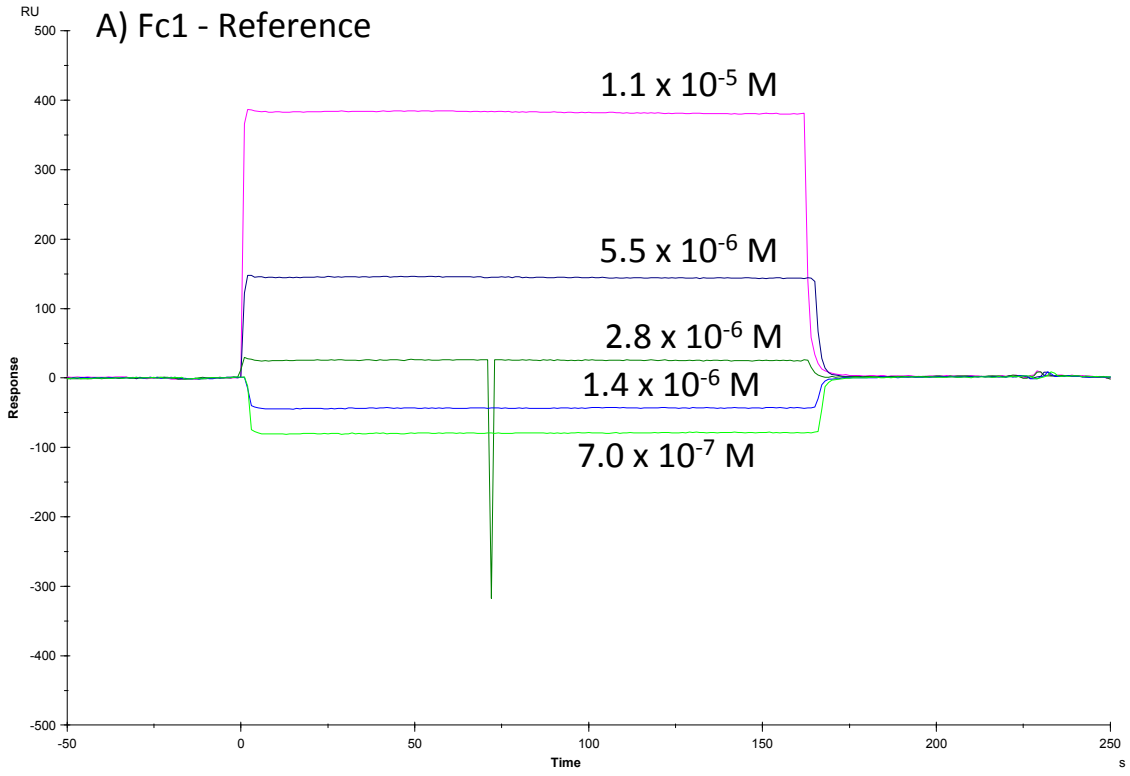

Figure 41. α Trp502Met506 Peptide With 0.4 M NaCl Assay Against 2x-Injected Immobilized GST-(β Ser312). A) The sensorgram generated by the injection of peptides into flow cell 1, the reference cell. B) The sensorgram generated by the injection of peptides into flow cell 2, the analyte cell. C) The sensorgram generated by reference-subtracting the reference sensorgram from the analyte sensorgram.

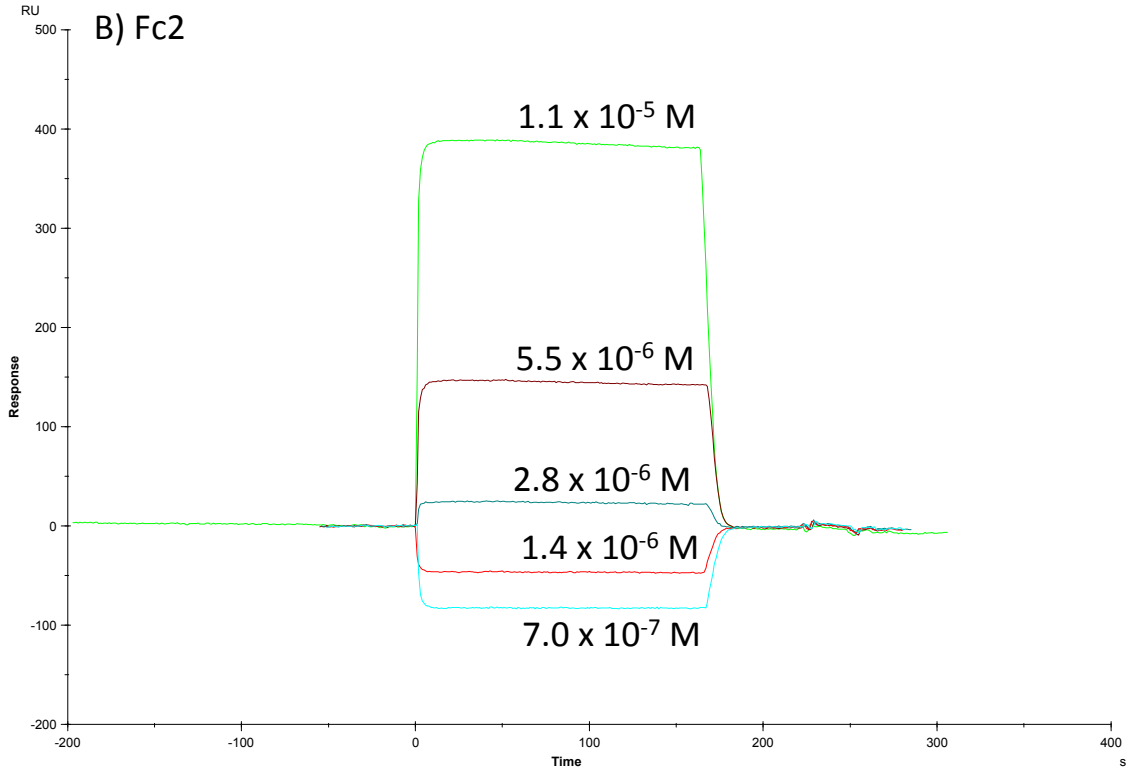

Figure 41, continued.

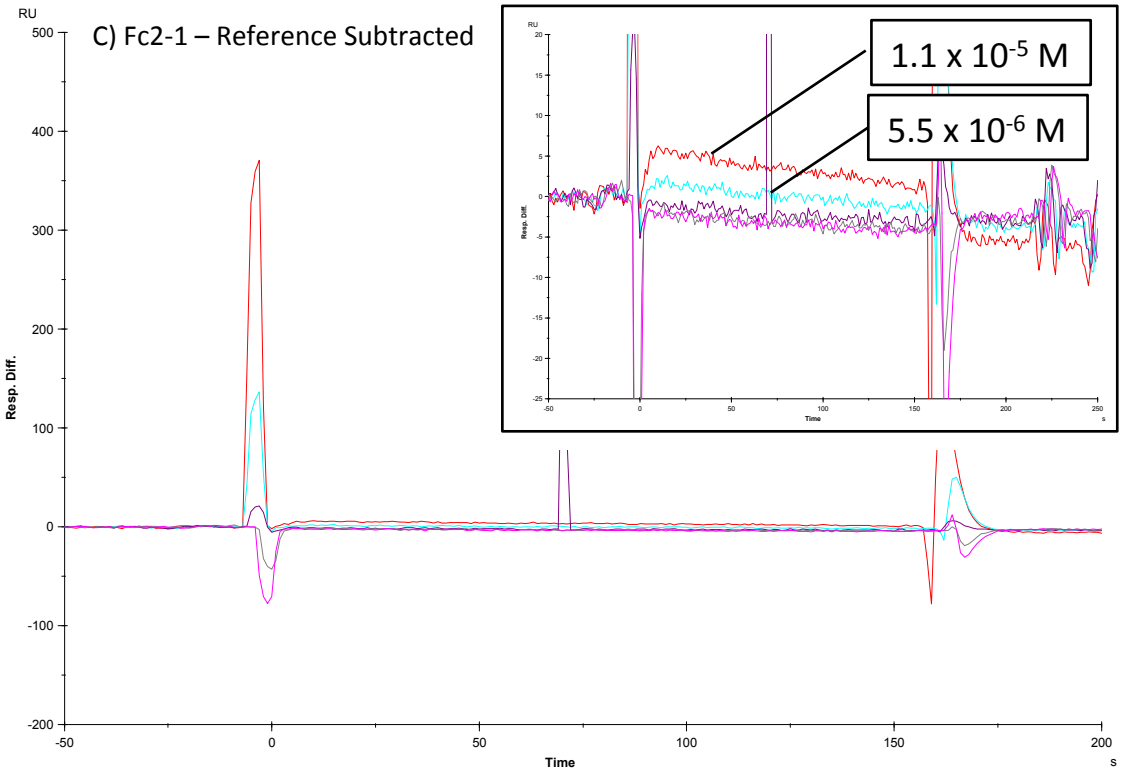

Figure 41, continued.

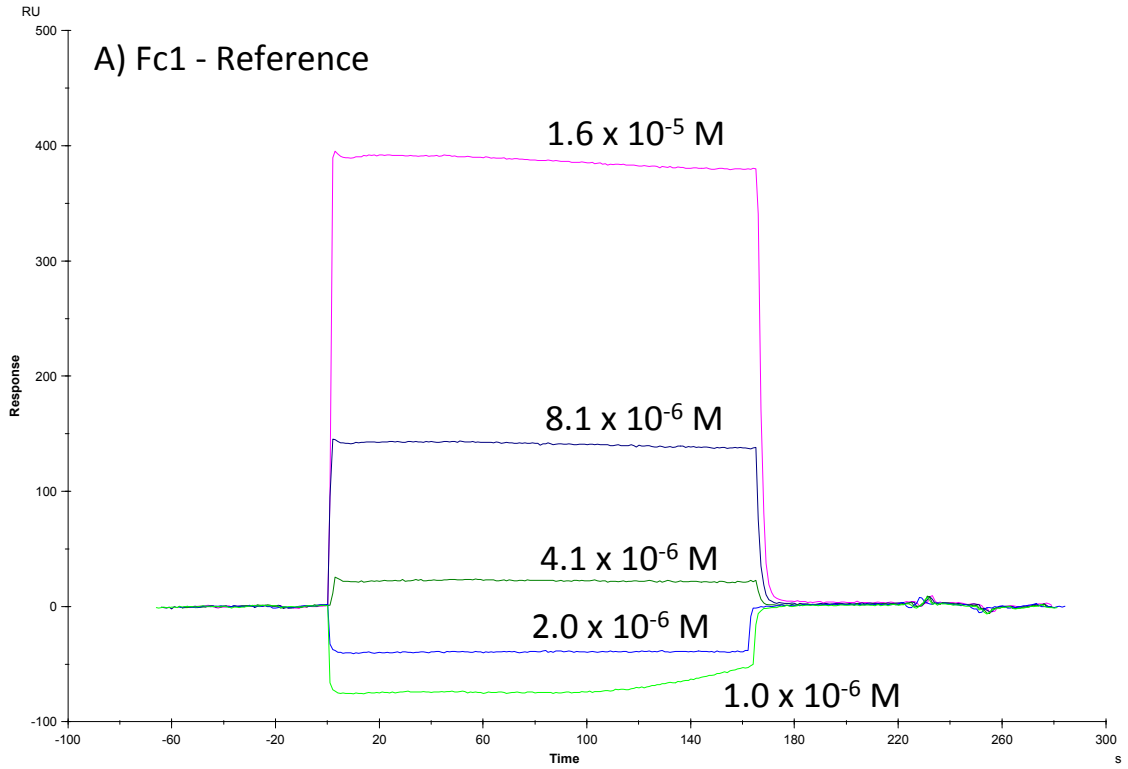

Figure 42. β Ser312 Peptide With 0.4 M NaCl Assay Against 2x-Injected Immobilized GST-(β Ser312). . A) The sensorgram generated by the injection of peptides into flow cell 1, the reference cell. B) The sensorgram generated by the injection of peptides into flow cell 2, the analyte cell. C) The sensorgram generated by reference-subtracting the reference sensorgram from the analyte sensorgram.

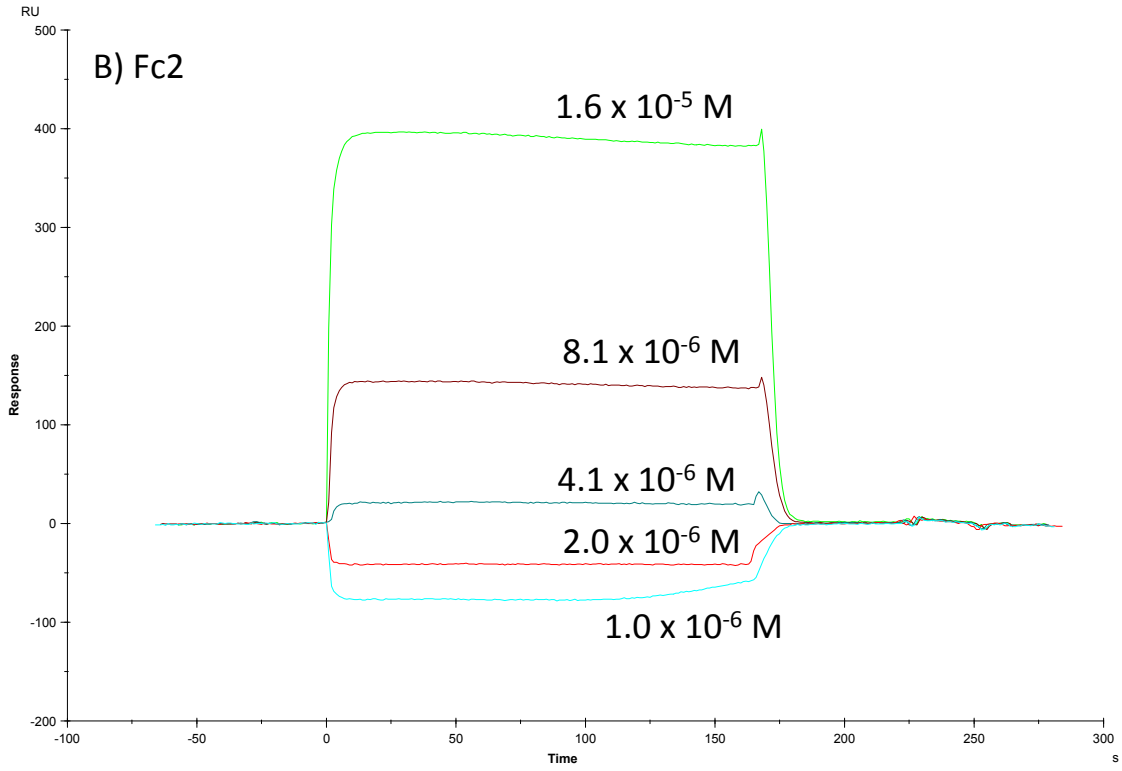

Figure 42, continued.

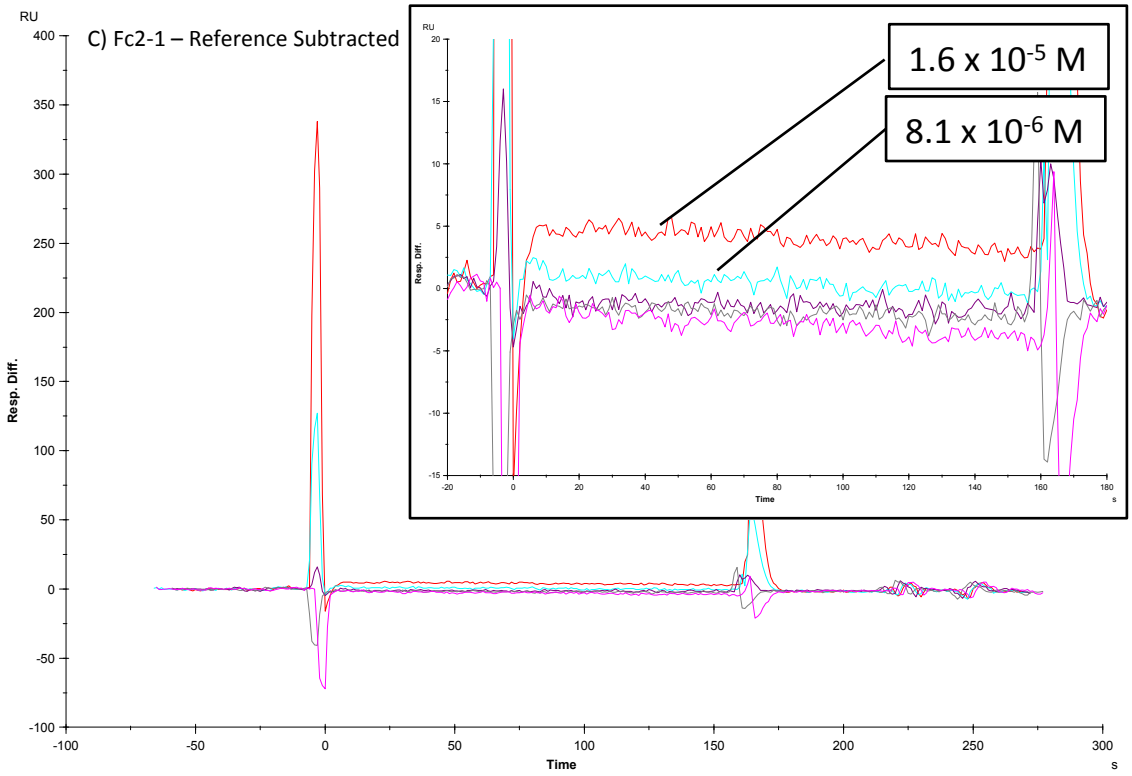

Figure 42, continued.

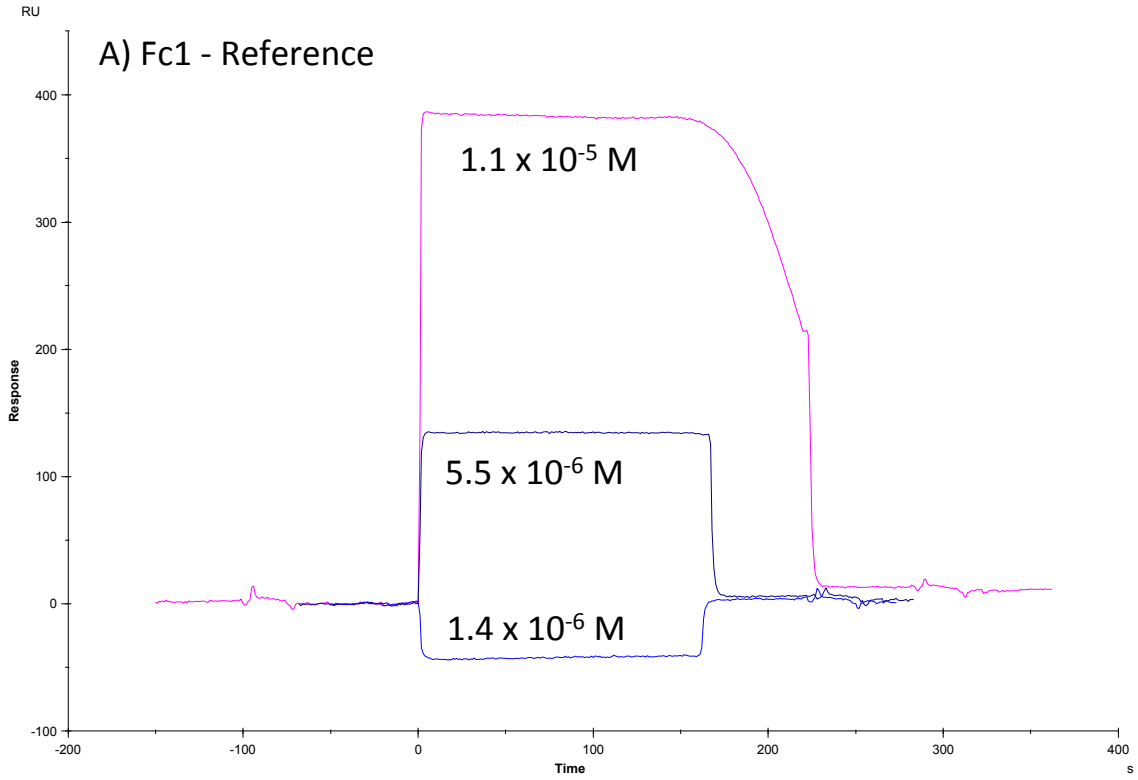

Figure 43. α Trp502Met506 Peptide With 0.4 M NaCl Assay Against 2x-Injected Immobilized GST-(γ Lys364). A) The sensorgram generated by the injection of peptides into flow cell 1, the reference cell. B) The sensorgram generated by the injection of peptides into flow cell 2, the analyte cell. C) The sensorgram generated by reference-subtracting the reference sensorgram from the analyte sensorgram.

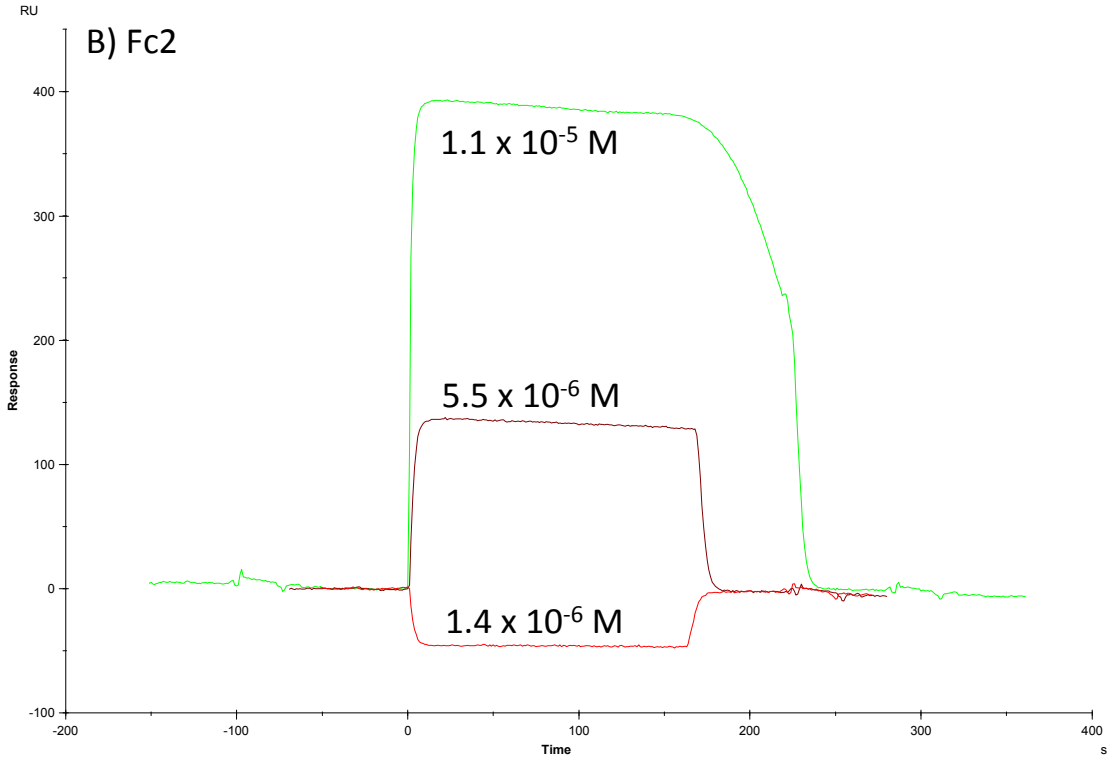

Figure 43, continued.

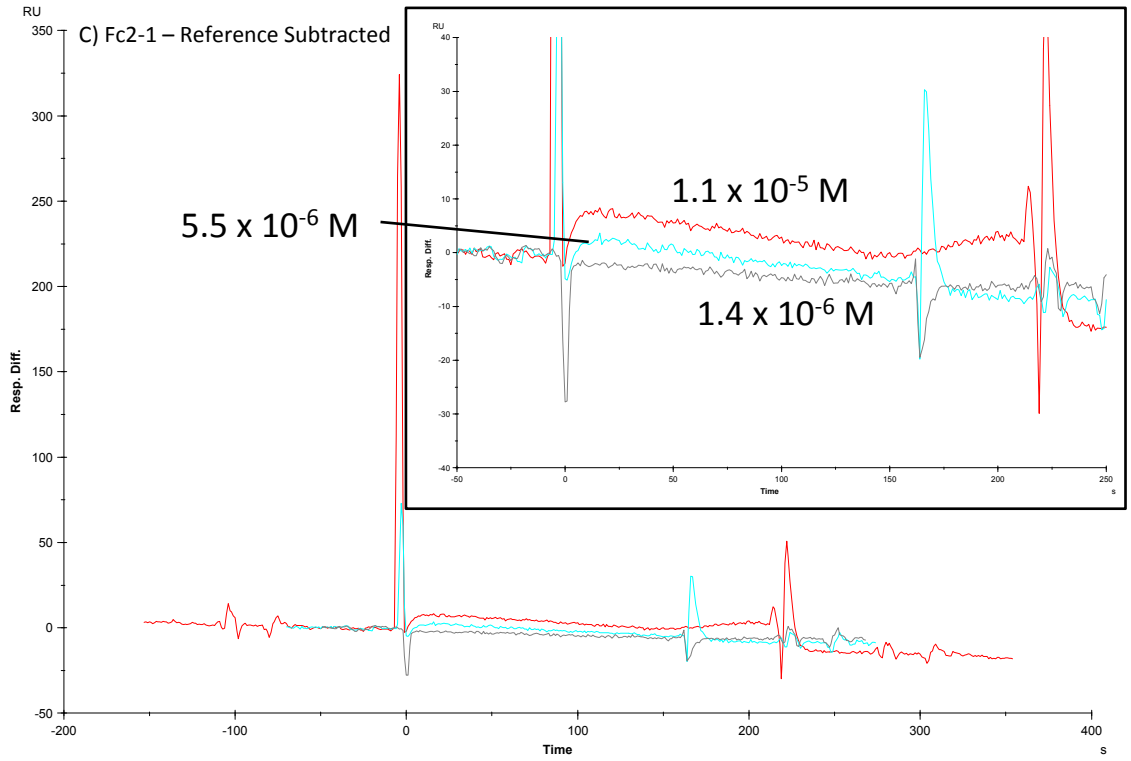

Figure 43, continued.

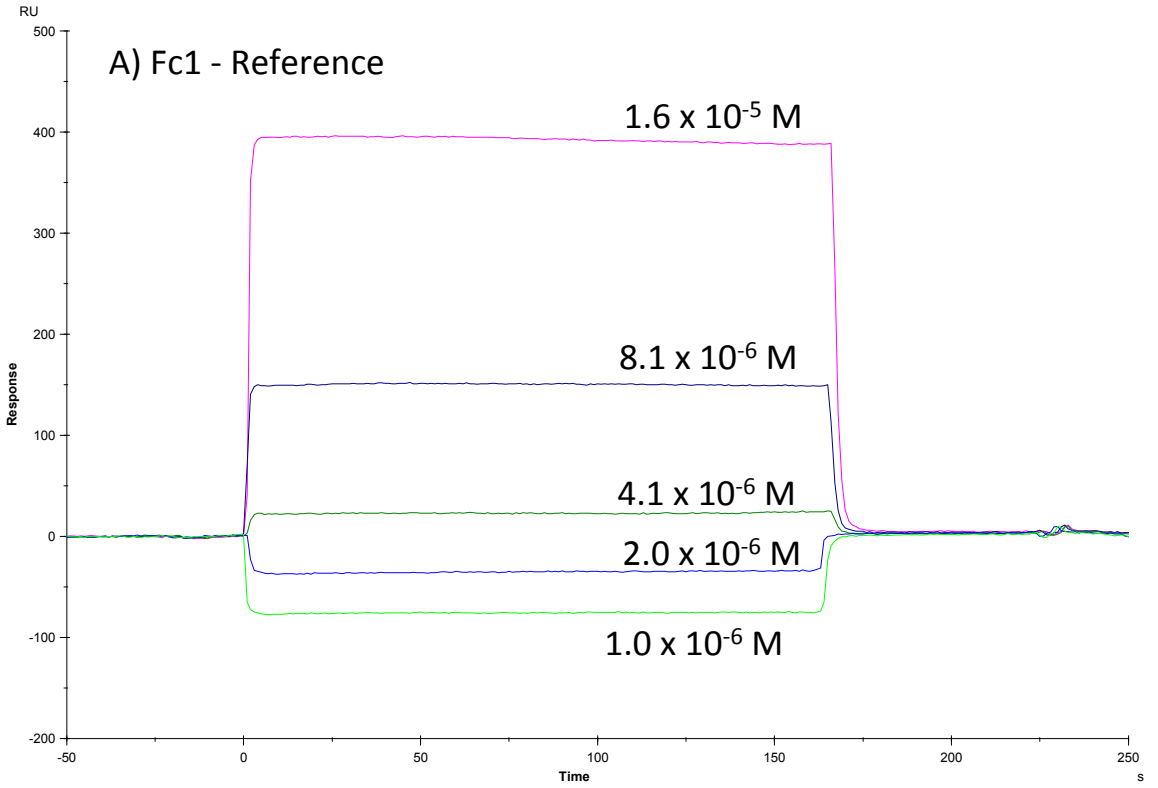

Figure 44. β Ser312 Peptide With 0.4 M NaCl Assay Against 2x-Injected Immobilized GST-(γ Lys364). A) The sensorgram generated by the injection of peptides into flow cell 1, the reference cell. B) The sensorgram generated by the injection of peptides into flow cell 2, the analyte cell. C) The sensorgram generated by reference-subtracting the reference sensorgram from the analyte sensorgram.

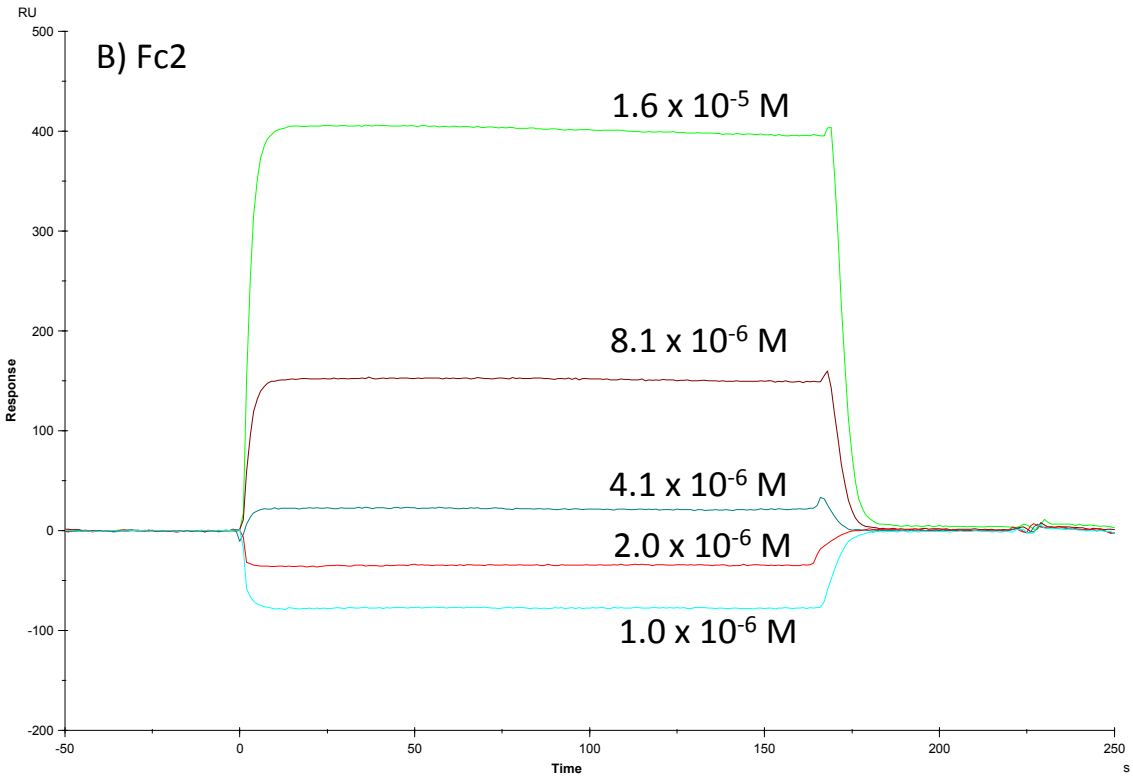

Figure 44, continued.

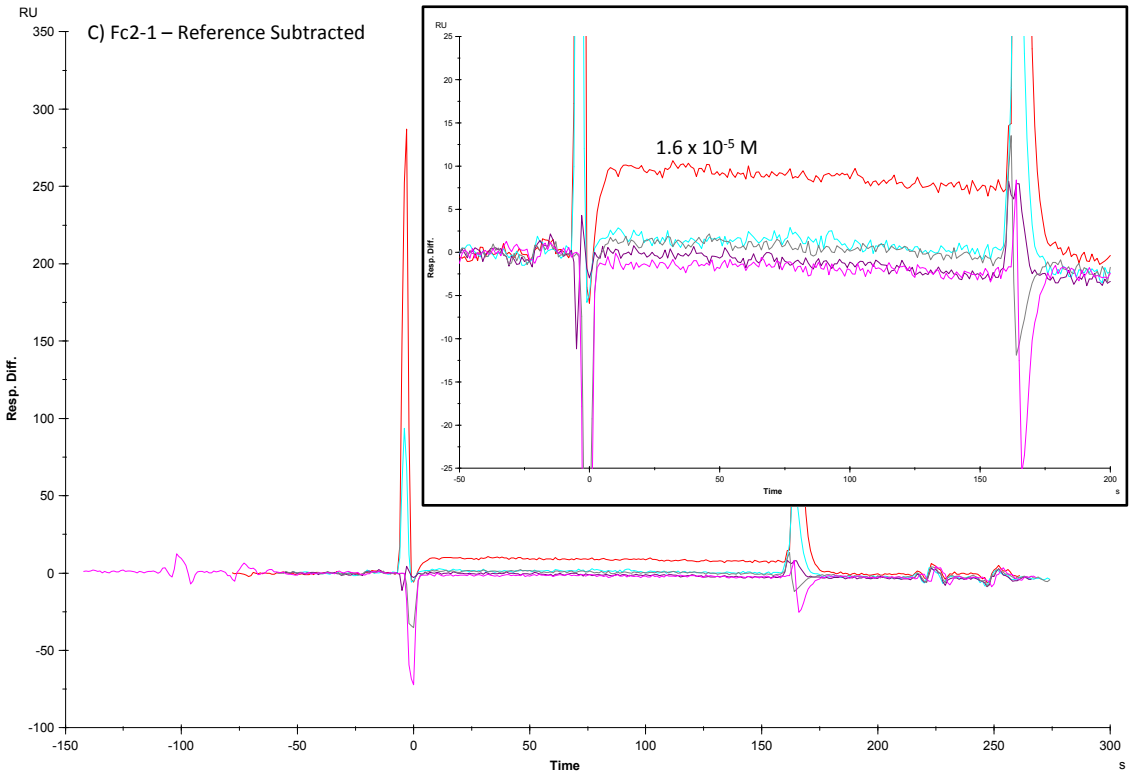

Figure 44, continued.

As a means of providing positive controls, Recombinant GST was assayed against immobilized Anti-GST. In order to insure a proper reference flow cell, recombinant GST was first injected into the reference until no further change in response units was observed. Flow cell 2 was then regenerated and recombinant GST was assayed at various concentrations. A correlation was also observed, with higher concentrations of injected recombinant GST corresponding to a greater positive change in response units (**Figure 45**).

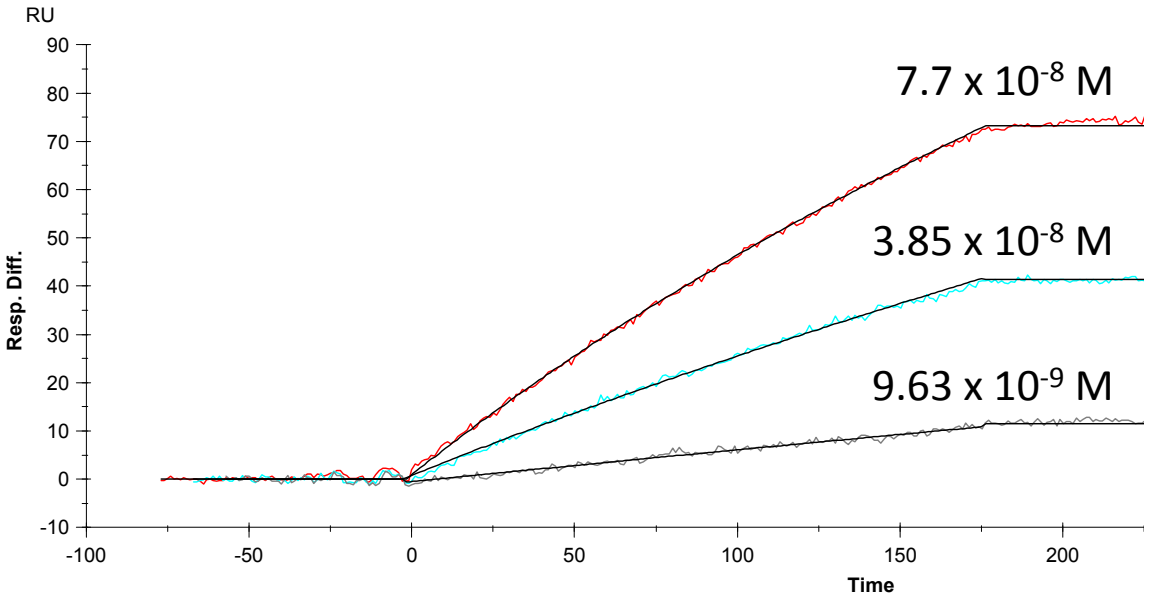

Figure 45. Analysis Of The Interaction Between Anti-GST And GST. Shown above is the reference-subtracted sensorgram generated when immobilized Anti-GST antibody was assayed with Recombinant GST at various concentrations. Higher concentrations correlated with a higher change in response units, indicating the successful capture of recombinant GST on the sensor chip surface. As can be noted, dissociation is negligible, for recombinant GST exhibits strong-specific interactions with immobilized anti-GST antibody.

This positive change in response units within the reference-subtracted sensorgram is indicative of an interaction that is taking place at a stronger magnitude within the regenerated flow cell than that of the reference cell, and this follows what was initially

expected because most, if not all, of the available recombinant GST binding sites within the reference cell were already bound. Kinetic analysis via BIAevaluation software led to a binding constant of 7.34×10^{12}, indicating that a strong non-covalent interaction was taking place (**Table 4**). In this case, any dissociation constant would be considered negligible due to the fact that, when injected, recombinant GST is actively "captured" onto the sensor chip. In other words, there is no observable dissociation taking place when immobilizing recombinant GST and/or GST-fusion proteins. This analysis was carried out in order to obtain measurable kinetics from a positive control.

Table 4. Kinetic Constants Of The Interactions Between Anti-GST And Recombinant GST. With the data taken from **Figure 45**, kinetic constants were established for a "heterogeneous ligand – parallel reaction interaction" model between Anti-GST and assayed recombinant GST. In this reaction, dissociation constants are deemed negligible due to the fact that recombinant GST is captured onto the sensor surface via the immobilized Anti-GST antibodies.

k_a (1/Ms)	k_d (1/s)	K_A (1/M)	Chi^2
9.14×10^{4}	1.24×10^{-8}	7.34×10^{12}	0.297

CHAPTER IV

CONCLUSIONS

Through previous research, peptide regions predicted to be critical for interaction between ENaC α, β, and γ subunits were identified [50] (**Table 1**). In this study, the interactions between the α-knuckle W502/M506 amino acid residue and β-finger S312 amino acid residue were assayed via Surface Plasmon Resonance. Additionally, both the α-W502/M506 and β-S312 residues were assayed against the γ-Wrist/Thumb K364 amino acid residue. Although the γ-K364 peptide region was predicted to be an interactive partner with the β-Wrist/Palm S84 peptide region, and not with either of the α-W502/M506 and β-S312 peptide regions, it was predicted that the β-S312 peptide would exhibit a stronger interaction with the γ-K364 peptide due to their possible electrostatic interactions. All three of the aforementioned amino acids were expressed within peptide segments located along the C-terminus of a GST-fusion protein. For BIAcore studies that involved using the peptides as analytes, GST was cleaved off of the GST-fusion protein with a thrombin treatment, leaving the sole peptide as the analyte.

Anti-GST was successfully immobilized onto the CM5 sensor chip within the BIAcore X, and this was the interpretation of a permanent increase in response units within the sensorgram generated during anti-GST immobilization (**Figure 23**). Subsequent recombinant GST was also captured onto the chip on both flow cells within the BIAcore, and regeneration of flow cell 2 allowed for the capture of the previously expressed GST-fusion proteins, leaving flow cell 1 as a reference cell that contained GST without peptide on the sensor chip surface.

When β-S312 peptide was assayed against immobilized GST-(α W502/M506), changes in response units within the sensorgram were observed in both flow cells respective of the injected peptide's concentration, indicating the possibility of nonspecific interactions with both recombinant GST and the immobilized GST-(α W502/M506). When the data was reference subtracted, overall negative changes were observed in the sensorgram, indicating that there was most likely a stronger response in the reference cell than there was in the flow cell used for analysis. This pattern was also seen among assays that involved immobilized GST-(β-S312) and immobilized GST-(γ-K364). As a result, no binding kinetics could be interpreted.

A second assay was performed in which immobilization of GST-fusion proteins was carried out with triple-injections. This opened the possibility of observing a more appreciable response within the analysis flow cell. However, the pattern seen in the first assay was also observed. Binding kinetics could not be interpreted.

A third assay involved spiking samples with 0.4 M NaCl. Previous research had indicated that samples analyzed in the presence of salt exhibited interpretable binding kinetics [50]. However, such was not this case in this study. Interactions between analyte and both the reference cell and GST-peptide immobilized flow cell were virtually equalized. A slight, minor interaction was observed for peptides that contained the highest concentration, but the same response was observed for the negative controls. Therefore, interactions in this environment warrant further investigation to elucidate the possibility of obtaining interpretable binding kinetics.

LITERATURE CITED

Articles:

[1] Anantharam, Arun, Yuan Tian, and Lawrence G. Palmer. "Open Probability of the Epithelial Sodium Channel is Regulated by Intracellular Sodium." Journal of Physiology-London 574.2 (2006): 333-47. Web.

[2] Asher, C., A. Chigaev, and H. Garty. "Characterization of Interactions between Nedd4 and Beta and Gamma ENaC using Surface Plasmon Resonance." Biochemical and biophysical research communications 286.5 (2001): 1228-31. Web.

[3] Asher, C., I. Sinha, and H. Garty. "Characterization of the Interactions between Nedd4-2, ENaC, and Sgk-1 using Surface Plasmon Resonance." Biochimica Et Biophysica Acta-Biomembranes 1612.1 (2003): 59-64. Web.

[4] Auberson, M., et al. "Epithelial Na+ Channel Mutants Causing Liddle's Syndrome Retain Ability to Respond to Aldosterone and Vasopressin." American Journal of Physiology-Renal Physiology 285.3 (2003): F459-71. Web.

[5] Bertog, Marko, et al. "Aldosterone Responsiveness of the Epithelial Sodium Channel (ENaC) in Colon is Increased in a Mouse Model for Liddle's Syndrome." Journal of Physiology-London 586.2 (2008): 459-75. Web.

[6] Bhalla, V., et al. "Serum- and Glucocorticoid-Regulated Kinase 1 Regulates Ubiquitin Ligase Neural Precursor Cell-Expressed, Developmentally Down-Regulated Protein 4-2 by Inducing Interaction with 14-3-3." Molecular Endocrinology 19.12 (2005): 3073-84. Web.

[7] Booth, R. E., and J. D. Stockand. "Targeted Degradation of ENaC in Response to PKC Activation of the ERK1/2 Cascade." American Journal of Physiology-Renal Physiology 284.5 (2003): F938-47. Web.

[8] Booth, R. E., et al. "A Region Directly Following the Second Transmembrane Domain in Gamma ENaC is Required for Normal Channel Gating." Journal of Biological Chemistry 278.42 (2003): 41367-79. Web.

[9] Butterworth, Michael B. "Regulation of the Epithelial Sodium Channel (ENaC) by Membrane Trafficking." Biochimica Et Biophysica Acta-Molecular Basis of Disease 1802.12 (2010): 1166-77. Web.

[10] Canessa, C. M., et al. "Amiloride-Sensitive Epithelial Na+ Channel is made of 3 Homologous Subunits." Nature 367.6462 (1994): 463-7. Web.

[11] Chraibi, A., and A. D. Horisberger. "Na Self Inhibition of Human Epithelial Na Channel: Temperature Dependence and Effect of Extracellular Proteases." Journal of General Physiology 120.2 (2002): 133-45. Web.

[12] Eaton, Douglas C., et al. "Regulation of Epithelial Sodium Channel Trafficking by Ubiquitination." Proceedings of the American Thoracic Society 7.1 (2010): 54-64. Web.

[13] Fakitsas, Panagiotis, et al. "Early Aldosterone-Induced Gene Product Regulates the Epithelial Sodium Channel by Deubiquitylation." Journal of the American Society of Nephrology 18.4 (2007): 1084-92. Web.

[14] Fejes-Toth, Geza, et al. "Epithelial Na(+) Channel Activation and Processing in Mice Lacking SGK1." American Journal of Physiology-Renal Physiology 294.6 (2008): F1298-305. Web.

[15] Firsov, D., et al. "Cell Surface Expression of the Epithelial Na Channel and a Mutant Causing Liddle Syndrome: A Quantitative Approach." Proceedings of the National Academy of Sciences of the United States of America 93.26 (1996): 15370-5. Web.

[16] Frindt, G., and L. G. Palmer. "Na Channels in the Rat Connecting Tubule." American Journal of Physiology-Renal Physiology 286.4 (2004): F669-74. Web.

[17] Frindt, Gustavo, Zuhal Ergonul, and Lawrence G. Palmer. "Surface Expression of Epithelial Na Channel Protein in Rat Kidney." Journal of General Physiology 131.6 (2008): 617-27. Web.

[18] Gonzales, Eric B., Toshimitsu Kawate, and Eric Gouaux. "Pore Architecture and Ion Sites in Acid-Sensing Ion Channels and P2X Receptors." Nature 460.7255 (2009): 599-U62. Web.

[19] Grunder, S., et al. "A Mutation Causing Pseudohypoaldosteronism Type 1 Identifies a Conserved Glycine that is Involved in the Gating of the Epithelial Sodium Channel." Embo Journal 16.5 (1997): 899-907. Web.

[20] Hendron, E., et al. "Identification of Cytoplasmic Domains within the Epithelial Na+ Channel Reactive at the Plasma Membrane." Journal of Biological Chemistry 277.37 (2002): 34480-8. Web.

[21] Hughey, R. P., et al. "Maturation of the Epithelial Na+ Channel Involves Proteolytic Processing of the Alpha- and Gamma-Subunits." Journal of Biological Chemistry 278.39 (2003): 37073-82. Web.

[22] Kamynina, E., et al. "A Novel Mouse Nedd4 Protein Suppresses the Activity of the Epithelial Na+ Channel." Faseb Journal 15.1 (2001): 204-14. Web.

[23] Kellenberger, S., and L. Schild. "Epithelial Sodium channel/degenerin Family of Ion Channels: A Variety of Functions for a Shared Structure." Physiological Reviews 82.3 (2002): 735-67. Web.

[24] Lifton, R. P., A. G. Gharavi, and D. S. Geller. "Molecular Mechanisms of Human Hypertension." Cell 104.4 (2001): 545-56. Web.

[25] Loffing, J., and B. Kaissling. "Sodium and Calcium Transport Pathways Along the Mammalian Distal Nephron: From Rabbit to Human." American Journal of Physiology-Renal Physiology 284.4 (2003): F628-43. Web.

[26] Loffing, J., et al. "Differential Subcellular Localization of ENaC Subunits in Mouse Kidney in Response to High- and Low-Na Diets." American Journal of Physiology-Renal Physiology 279.2 (2000): F252-8. Web.

[27] Lott, J. S., et al. "A Single WW Domain is the Predominant Mediator of the Interaction between the Human Ubiquitin-Protein Ligase Nedd4 and the Human Epithelial Sodium Channel." Biochemical Journal 361 (2002): 481-8. Web.

[28] Lu, Chen, et al. "The PY Motif of ENaC, Mutated in Liddle Syndrome, Regulates Channel Internalization, Sorting and Mobilization from Subapical Pool." Traffic 8.9 (2007): 1246-64. Web.

[29] Masilamani, S., et al. "Aldosterone-Mediated Regulation of ENaC Alpha,Beta, and Gamma Subunit Proteins in Rat Kidney." Journal of Clinical Investigation 104.7 (1999): R19-23. Web.

[30] Palmer, Lawrence G., and Olaf S. Andersen. "The Two-Membrane Model of Epithelial Transport: Koefoed-Johnsen and Ussing (1958)." Journal of General Physiology 132.6 (2008): 607-12. Web.

[31] Pradervand, S., et al. "A Mouse Model for Liddle's Syndrome." Journal of the American Society of Nephrology 10.12 (1999): 2527-33. Web.

[32] Rossier, Bernard C., and M. Jackson Stutts. "Activation of the Epithelial Sodium Channel (ENaC) by Serine Proteases." Annual Review of Physiology 71 (2009): 361-79. Web.

[33] Rotin, D., V. Kanelis, and L. Schild. "Trafficking and Cell Surface Stability of ENaC. (Vol 281, Pg 391, 2001)." American Journal of Physiology-Renal Physiology 281.6 (2001)Web.

[34] Ruffieux-Daidie, Dorothee, et al. "Deubiquitylation Regulates Activation and Proteolytic Cleavage of ENaC." Journal of the American Society of Nephrology 19.11 (2008): 2170-80. Web.

[35] Schild, L., et al. "A Mutation in the Epithelial Sodium-Channel Causing Liddle Disease Increases Channel Activity in the Xenopus-Laevis Oocyte Expression System." Proceedings of the National Academy of Sciences of the United States of America 92.12 (1995): 5699-703. Web.

[36] Schild, L., et al. "Identification of a PY Motif in the Epithelial Na Channel Subunits as a Target Sequence for Mutations Causing Channel Activation found in Liddle Syndrome." Embo Journal 15.10 (1996): 2381-7. Web.

[37] Schild, L., et al. "Identification of Amino Acid Residues in the Alpha, Beta, and Gamma Subunits of the Epithelial Sodium Channel (ENaC) Involved in Amiloride Block and Ion Permeation." Journal of General Physiology 109.1 (1997): 15-26. Web.

[38] Schild, Laurent. "The Epithelial Sodium Channel and the Control of Sodium Balance." Biochimica Et Biophysica Acta-Molecular Basis of Disease 1802.12 (2010): 1159-65. Web.

[39] Shi, H. K., et al. "Interactions of Beta and Gamma ENaC with Nedd4 can be Facilitated by an ERK-Mediated Phosphorylation." Journal of Biological Chemistry 277.16 (2002): 13539-47. Web.

[40] Snyder, P. M., et al. "CAMP and Serum and Glucocorticoid-Inducible Kinase (SGK) Regulate the Epithelial Na+ Channel through Convergent Phosphorylation of Nedd4-2." Journal of Biological Chemistry 279.44 (2004): 45753-8. Web.

[41] Staruschenko, A., et al. "Epithelial Na+ Channel Subunit Stoichiometry." Biophysical journal 88.6 (2005): 3966-75. Web.

[42] Staruschenko, A., et al. "Fluorescence Resonance Energy Transfer Analysis of Subunit Stoichiometry of the Epithelial Na+ Channel." Journal of Biological Chemistry 279.26 (2004): 27729-34. Web.

[43] Staruschenko, A., O. Pochynyuk, and J. D. Stockand. "Regulation of Epithelial Na+ Channel Activity by Conserved serine/threonine Switches within Sorting Signals." Journal of Biological Chemistry 280.47 (2005): 39161-7. Web.

[44] Staruschenko, Alexander, et al. "Functional Reconstitution of the Human Epithelial Na+ Channel in a Mammalian Expression System." Methods in Molecular Biology 337 (2006): 3-13. Web.

[45] Stockand, James D., et al. "Insight Toward Epithelial Na+ Channel Mechanism Revealed by the Acid-Sensing Ion Channel 1 Structure." IUBMB life 60.9 (2008): 620-8. Web.

[46] Tong, Q. S., et al. "Regulation of Na(+) Transport by Aldosterone: Signaling Convergence and Cross Talk between the PI3-K and MAPK1/2 Cascades." American Journal of Physiology-Renal Physiology 286.6 (2004): F1232-8. Web.

[47] Tong, Q. S., A. G. Menon, and J. D. Stockand. "Functional Polymorphisms in the Alpha-Subunit of the Human Epithelial Na+ Channel Increase Activity." American Journal of Physiology-Renal Physiology 290.4 (2006): F821-7. Web.

Texts:

[48] Sheehan, David. "Surface Plasmon Resonance." *Physical Biochemistry: Principles and Applications*. The Atrium, Southern Gate, Chichester, West Sussex, PO19 8SQ, UK: John Wiley & Sons, Ltd, 2009. 103-110. Print.

Websites:

[49] Biosensing Instrument – Surface Plasmon Resonance http://www.biosensingusa.com/biosensing_instrument_technology.html (accessed March 17, 2014)

Prior Thesis Documentation:

[50] Peltier GC. (2012) Determining Critical Residues For Intersubunit Binding Of The Human Epithelial Sodium Channel. M.S. Thesis, Texas State University, San Marcos, TX

[51] Whisenant T. (2011) Identification of Residues Critical for Epithelial Sodium Channel Assembly. M.S. Thesis, Texas State University, San Marcos, TX